

All-order momentum correlations of three ultracold bosonic atoms confined in triple-well traps: Signatures of emergent many-body quantum phase transitions and analogies with three-photon quantum-optics interference

Constantine Yannouleas^{*} and Uzi Landman[†]*School of Physics, Georgia Institute of Technology, Atlanta, Georgia 30332-0430, USA*

(Received 11 December 2019; accepted 13 May 2020; published 11 June 2020)

All-order momentum correlation functions associated with the time-of-flight spectroscopy of three spinless ultracold bosonic interacting neutral atoms confined in a linear three-well optical trap are presented. The underlying Hamiltonian employed for the interacting atoms is an augmented three-site Hubbard model. Our investigations target matter-wave interference of massive particles, aiming at the establishment of experimental protocols for characterizing the quantum states of trapped attractively or repulsively interacting ultracold particles, with variable interaction strength. The advantages and physical insights that can be gained from the results of our study for a comprehensive understanding of the nature of the quantum states of interacting many-particle systems, via analysis of the all-order (that is, first, second, and third) momentum correlation functions for three bosonic atoms in a three-well confinement, are illustrated in the context of time-of-flight interferometric interrogations of the interaction-strength-induced emergent quantum phase transition from the Mott insulating phase to the superfluid one. Furthermore, our interferometric interrogations establish strong analogies with the quantum-optics interference of three photons, including the aspects of genuine three-photon interference, which are important to explorations targeting the development and implementation of quantum information applications and quantum computing.

DOI: [10.1103/PhysRevA.101.063614](https://doi.org/10.1103/PhysRevA.101.063614)

I. INTRODUCTION

Theoretical and experimental access to many-body correlations is essential in elucidating the properties and underlying physics of strongly interacting systems [1,2]. In the framework of ultracold atoms, the quantum correlations in momentum space associated with bosonic or fermionic neutral atoms trapped in optical tweezers (with a finite number N of particles [3–5]) or in extended optical lattices (with control of one-, two-, or three-dimensionality [6–10]) are currently attracting significant experimental attention, empowered [3–5,9–11] by advances in single-atom-resolved detection methods [12].

In this paper, we derive explicit analytic expressions for the third-, second-, and first-order momentum correlations of three ultracold bosonic atoms trapped in an optical trap of three wells in a linear arrangement (denoted as 3b-3w). Compared to the case of two particles in two wells (2p-2w) [13–16], a complete Hubbard-model treatment of momentum correlations (as a function of the interparticle interaction) for the 3b-3w case increases the complexity and effort involved, by an order of magnitude, because of the larger Hilbert space and the larger number of states, i.e., a total of 10 states instead of 4, including the excited states which are long lived [17] for trapped ultracold atoms. Therefore, demonstrating that this complexity of the theoretical treatment can be handled in an efficient manner through the use of algebraic computer languages constitutes an important step toward the implementation of the bottom-up approach for simulating many-body

physics with ultracold atoms. In this respect, the statement above parallels earlier observations that three-particle entanglement extends two-particle entanglement in a nontrivial way [18–20].

Compared to the standard numerical treatments [21–25] of the Hubbard model, the advantage of our algebraic treatment is the ability to produce in closed analytic form cosinusoidal and/or sinusoidal expressions of the many-body wave function and the associated momentum correlations of all orders; see for example Eqs. (29), (31), and (36), which codify the main results of our paper. Due to recent experimental advances in tunability and control of a system of a few ultracold atoms trapped in finite optical lattices (also referred to as optical tweezers), such momentum correlations can be measured directly in time-of-flight experiments [3–5] and their experimental cosinusoidal diffraction patterns reveal direct analogies with the quantum optics of massless photons [4,14,15].

In this context, this paper is aimed at researchers actively engaged in experimental and theoretical investigations of the properties of (finite) quantum few-body systems, as well as those intending to understand many-body quantum systems through bottom-up hierarchical modeling of trapped finite ultracold-atom assemblies with deterministically controllable increased size and complexity; see, e.g., Refs. [3–5,17,26–29]. Indeed, we target researchers in these fields by providing fingerprint characteristics to aid the design, diagnostics, and interpretation of experiments as well as by giving benchmark results [30] for comparisons with future theoretical treatments. We foresee these as important merits that will contribute to future impact of our work.

^{*}Constantine.Yannouleas@physics.gatech.edu[†]Uzi.Landman@physics.gatech.edu

In addition, the availability of the complete analytic set of momentum correlations enabled us to reveal and explore two major physical aspects of the 3b-3w ultracold-atom system, namely (i) signatures of an emergent quantum phase transition [31], from a superfluid phase to a Mott-insulator phase; here the designation “emergent” is used to indicate the gradual emergence of a phase transition in a finite system as the system size is increased to infinity [31], alternatively termed “interphase crossover,” and (ii) analogies between the interference properties of three trapped ultracold atom systems with quantum-optics three-photon interference. These aspects are elaborated in some detail immediately below.

A. Signatures of emergent superfluid to Mott transition

The sharp superfluid-to-Mott transition has been observed in extended optical lattices with trapped ultracold bosonic alkali atoms (^{87}Rb) [6], as well as with excited $^4\text{He}^*$ bosonic atoms [9]. In these experiments, after a time-of-flight (TOF) expansion, the single-particle momentum (spm) density (first-order momentum correlation) was recorded. An oscillating spm density provides a hallmark of a superfluid phase, associated with a maximum uncertainty regarding a particle’s site occupation; this happens for the noninteracting case when the particles are fully delocalized. On the other hand, a featureless spm density is the hallmark of being deeply in the Mott-insulator phase when all particles are fully localized on the lattice sites, exhibiting no fluctuations in the site occupancies.

Here, we show that the first-order momentum correlations for the 3b-3w system vary smoothly, alternating as a function of the Hubbard U between a featureless profile and that resulting from the sum of two cosine terms; such profile alternations may provide signatures of an emerging superfluid to Mott-insulator phase crossing. The periods of the cosine terms depend on the inverse of the lattice constant d and its double $2d$ (d being the nearest-neighbor interwell distance). We note that for extended lattices only the $\cos(dk)$ term has been theoretically specified [8,32,33] with perturbative $1/U$ approaches, and that our nonperturbative results suggest that all cosine terms with all possible interwell distances in the argument should in general contribute.

Furthermore, we show that the correspondence between the featureless profiles and the interaction strength is not a one-to-one correspondence. Indeed, we show that a featureless spm density can correspond to different strengths of the interaction, depending on the sign of the interaction (repulsive versus attractive) and the precise Hubbard state under consideration (ground state or one of the excited states). For a unique characterization of a phase regime, both the second- and third-order momentum correlations beyond the spm density are required.

B. Analogies with quantum-optics three-photon interference

Recent experimental [4,5,34–38] and theoretical [13–16,20,39,40] advances have ushered in a new research direction regarding investigations of higher order quantum interference resolved at the level of the intrinsic microscopic variables that constitute the single-particle wave packet of the interfering particles. These intrinsic variables are pairwise conjugated; they are the single-particle momenta (k ’s) and

mutual distances (d ’s) for massive localized particles [4,5,13–16,20,39] and the frequencies (ω ’s) and relative time delays (τ ’s) for massless photons [34–38,40].

For the case of two fermionic or bosonic ultracold atoms, we investigated in Ref. [15] this correspondence in detail and we proceeded to establish a complete analogy between the cosinusoidal patterns (with arguments $\propto kd$ or $\propto \omega\tau$) of the second-order (k_1, k_2) correlation maps for the two trapped atoms (determined experimentally through TOF measurements [4,5]) with the landscapes of the two-photon (ω_1, ω_2) interferograms [35,36,38]. In addition, we demonstrated that the Hong-Ou-Mandel (HOM) [41] single-occupancy coincidence probability at the detectors, P_{11} (which relates to the celebrated HOM dip for total destructive interference, i.e., when $P_{11} = 0$), corresponds to a double integral over the momentum variables (k_1, k_2) of a specific term contributing to the full correlation map, in full analogy with the treatment of the optical (ω_1, ω_2) interferograms in Ref. [35]. Because of this summation over the intrinsic momentum (or frequency for photons) variables, the information contained in the HOM dip is limited compared to the full correlation map. Precise analogs of the original optical HOM dip (with P_{11} varying as a function of relative time delay or separation between particles) have also been experimentally realized using the interference of massive particles, i.e., two colliding electrons [42–44] or two colliding ^4He atoms [45]. For the case of two ultracold atoms trapped in two optical tweezers, analogs of the P_{11} coincidence probability can be determined via *in situ* measurements, as a function of the time evolution of the system [15,26] or the interparticle interaction [14,15].

In this paper, we establish for the 3b-3w case the full range of analogies between the TOF spectroscopy [46], as well as the *in situ* measurements, of localized massive particles and the multiphoton interference in linear optical networks [37,38,40,47], paying attention in particular to the mutual interparticle interactions which are absent for photons. These analogies encompass extensions of the 2p-2w analogies mentioned above, i.e., correlation maps dependent on three momentum variables (k_1, k_2, k_3) for massive particles versus interferograms with three frequency variables $(\omega_1, \omega_2, \omega_3)$ for massless photons, and the HOM P_{111} coincidence probability for three particles versus that for three photons. Most importantly, however, these analogies include highly nontrivial aspects beyond the reach of two-photon (or two-particle) and one-photon (or one-particle) interferences, such as genuine three-photon interference [48,49], which cannot be determined from the knowledge solely of the lower two-photon and one-photon interferences.

C. Plan of paper

Following the introductory section where we defined the aims of this work, we introduce in Sec. II the linear three-site Hubbard model and its analytic solution for three spinless ultracold bosonic atoms. We display the spectrum of the ten bosonic eigenvalues of the Hubbard model for both attractive and repulsive interatomic interactions (Fig. 1) and discuss in detail (1) the infinite repulsive or attractive interaction limit and (2) the noninteracting limit. In Sec. III, we outline the general definition and relations pertaining to higher order correlations in momentum space.

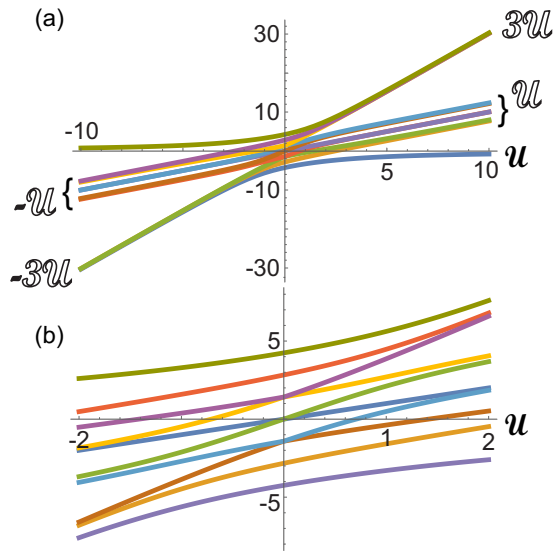


FIG. 1. Spectrum of the ten bosonic eigenvalues in Eq. (4) as a function of U (horizontal axis). (a) This frame (with the extended $-10 \leq U \leq 10$ scale) illustrates the convergence to the three values of zero [ground state ($U > 0$) or highest excited state ($U < 0$)], $\pm|U|$ (six excited states), and $\pm 3|U|$ (ground state and two excited states for $U < 0$). (b) A more detailed view in the range $-2 \leq U \leq 2$. Taking into consideration the three energy crossings at $U = 0$, the corresponding eigenstates are labeled in ascending energy order as $i = 1, 2, 3r(4l), 4r(3l), 5r(6l), 6r(5l), 7r(8l), 8r(7l), 9, 10$, where “r” means “right” for the region of positive U and “l” means “left” for the region of negative U .

In the following several sections, we give explicit analytic results and graphical illustrations pertaining to momentum correlation functions of the various orders, starting from the third order, since the lower order are obtained from the third-order one by integration over the unresolved momentum variables [see, e.g., Eq. (30) for the second-order momentum correlation]. The third-order momentum correlations for three bosons in three wells, with explicit discussion of the infinite-interaction (repulsive or attractive) limit is given in Sec. IV (see Fig. 2), followed by explicit results for the noninteracting limit in Sec. V. Section VI is devoted to a presentation and discussion of results for the third-order momentum correlations for three bosons in three wells as a function of the strength of the interatom interaction over the whole range, from highly attractive to highly repulsive (see momentum correlation maps in Fig. 4). Next we discuss in Sec. VII the second-order momentum correlation as a function of the interparticle interaction; see momentum correlation maps for the whole interaction range in Fig. 6.

The first-order momentum correlation, obtained via integration of the second-order one over the momentum of one of the atoms, is discussed as a function of interatom interaction strength in Sec. VIII, with a graphic illustration in Fig. 8 for the first-excited state of three bosons in three wells, illustrating transition as a function of interaction strength from localized (Mott insulator) to superfluid behavior. Section IX is devoted to a detailed study of the quantum phase transition from localized to superfluid behavior, as deduced from inspection of the first-order correlation function for the ground

state of three bosons in three wells (Fig. 9, top row), and further elucidated and elaborated with the use of second-order (Fig. 9, middle row), and third-order (Fig. 9, bottom row) momentum correlation maps. Further discussion of the quantum phase transition through analysis of site occupancies and their fluctuations for the ground and first-excited states as a function of the interparticle interactions, illuminating the connection between the quantum phase-transition from superfluid (phase coherent) to localized (incoherent) states, and the phase-number (site occupancy) uncertainty principle, is illustrated in Fig. 10.

Section X expounds on analogies with three-photon interference in quantum optics, including *genuine* three-photon interference. We summarize the contents of the paper in Sec. XI, closing with a comment concerning the expected relevance of the all-order momentum-space correlations for the three bosons in three wells as an alternative route to exploration with massive particles of aspects pertaining to the boson sampling problem [50] and its extensions, which are serving as a major topic (see, e.g., Refs. [51–55]) in quantum-optics investigations as an intermediate step towards the implementation of a quantum computer.

Appendixes A and B complement Secs. II A and II B, respectively, by listing the Hubbard eigenvectors of the remaining eight excited states not discussed in the main text (where, as previously mentioned, we focus on the ground and first-excited states). In addition, regarding again the remaining eight excited states not discussed in the main text, Appendixes C and D complement Secs. IV and V, respectively, by listing the corresponding three-body wave functions. Specifically, Appendixes A and C focus on the limit of infinite repulsive or attractive interaction, whereas Appendixes B and D focus on the noninteracting case. The last three Appendixes give details of the all-order correlation functions as a function of the interaction strength for the remaining eight states not discussed in the main text.

II. THE LINEAR THREE-SITE HUBBARD MODEL AND ITS ANALYTIC SOLUTION FOR THREE SPINLESS ULTRACOLD BOSONIC ATOMS

Numerical solutions for small Hubbard clusters are readily available in the literature. Here we present a compact analytic exposition for all the 10 eigenvalues and eigenstates of the linear three-boson three-site Hubbard Hamiltonian. Such analytic solutions, involving both the ground and excited states, are needed to further obtain the characteristic cosinusoidal or sinusoidal expressions for the associated third-, second-, and first-order momentum correlations.

The following *ten* primitive kets form a basis that spans the many-body Hilbert space of three spinless bosonic atoms distributed over three trapping wells:

$$\begin{aligned}
 1 &\rightarrow |111\rangle, \\
 2 &\rightarrow |210\rangle, \quad 3 \rightarrow |201\rangle, \quad 4 \rightarrow |120\rangle, \\
 5 &\rightarrow |021\rangle, \quad 6 \rightarrow |102\rangle, \quad 7 \rightarrow |012\rangle, \\
 8 &\rightarrow |300\rangle, \quad 9 \rightarrow |030\rangle, \quad 10 \rightarrow |003\rangle.
 \end{aligned} \tag{1}$$

The kets used above are of a general notation $|n_1, n_2, n_3\rangle$, where n_i (with $i = 1, 2, 3$) denotes the particle occupancy at

the i th well. We note that there is only one primitive ket (no. 1) with all three wells being singly occupied. The case of doubly occupied wells is represented by six primitive kets (nos. 2–7). Finally, there are three primitive kets (nos. 8–10) that represent triply occupied wells.

The Bose-Hubbard Hamiltonian for three spinless bosons trapped in three wells in a linear arrangement is given by

$$H_B = -J(\hat{b}_1^\dagger \hat{b}_2 + \hat{b}_2^\dagger \hat{b}_3 + \text{H.c.}) + \frac{U}{2} \sum_{i=1}^3 n_i(n_i - 1), \quad (2)$$

$$H_b = \begin{pmatrix} 0 & 0 & -\sqrt{2}J & -\sqrt{2}J & -\sqrt{2}J & -\sqrt{2}J & 0 & 0 & 0 & 0 \\ 0 & U & -J & -2J & 0 & 0 & 0 & -\sqrt{3}J & 0 & 0 \\ -\sqrt{2}J & -J & U & 0 & 0 & 0 & 0 & 0 & 0 & 0 \\ -\sqrt{2}J & -2J & 0 & U & 0 & 0 & 0 & 0 & -\sqrt{3}J & 0 \\ -\sqrt{2}J & 0 & 0 & 0 & U & 0 & -2J & 0 & -\sqrt{3}J & 0 \\ -\sqrt{2}J & 0 & 0 & 0 & 0 & U & -J & 0 & 0 & 0 \\ 0 & 0 & 0 & 0 & -2J & -J & U & 0 & 0 & -\sqrt{3}J \\ 0 & -\sqrt{3}J & 0 & 0 & 0 & 0 & 0 & 3U & 0 & 0 \\ 0 & 0 & 0 & -\sqrt{3}J & -\sqrt{3}J & 0 & 0 & 0 & 3U & 0 \\ 0 & 0 & 0 & 0 & 0 & 0 & -\sqrt{3}J & 0 & 0 & 3U \end{pmatrix}. \quad (3)$$

The eigenvalues (in units of J) of the bosonic matrix Hamiltonian in Eq. (3) are

$$\begin{aligned} E_1 &= {}^6\mathcal{R}_1^b, & E_6 &= {}^3\mathcal{R}_2^b(\mathcal{U}), \\ E_2 &= {}^3\mathcal{R}_1^b, & E_7 &= {}^6\mathcal{R}_4^b, \\ E_3 &= {}^6\mathcal{R}_2^b, & E_8 &= {}^6\mathcal{R}_5^b, \\ E_4 &= {}^6\mathcal{R}_3^b, & E_9 &= {}^3\mathcal{R}_3^b, \\ E_5 &= \mathcal{U}({}^3\mathcal{R}_2^b), & E_{10} &= {}^6\mathcal{R}_6^b, \end{aligned} \quad (4)$$

where $\mathcal{U} = U/J$. For E_5 and E_6 , the quantities without parentheses apply for $\mathcal{U} > 0$ and those within parentheses for $\mathcal{U} < 0$. The expressions for the remaining eigenvalues apply for any \mathcal{U} , negative or positive. ${}^6\mathcal{R}_i^b$, $i = 1, \dots, 6$ denote in ascending order (for any \mathcal{U} , negative or positive) the six real roots of the sixth-order polynomial

$$\begin{aligned} P_6^b(x) &= x^6 - 9\mathcal{U}x^5 + (30\mathcal{U}^2 - 22)x^4 + (144\mathcal{U} - 46\mathcal{U}^3)x^3 \\ &+ (76 - 314\mathcal{U}^2 + 33\mathcal{U}^4)x^2 - (252\mathcal{U} - 264\mathcal{U}^3) \\ &+ 9\mathcal{U}^5)x - (72 - 180\mathcal{U}^2 + 72\mathcal{U}^4), \end{aligned} \quad (5)$$

and ${}^3\mathcal{R}_i^b$, $i = 1, 2, 3$ denote in ascending order (for any \mathcal{U} , negative or positive) the three real roots of the third-order polynomial

$$P_3^b(x) = x^3 - 5\mathcal{U}x^2 + (7\mathcal{U}^2 - 8)x + 18\mathcal{U} - 3\mathcal{U}^3. \quad (6)$$

At $\mathcal{U} = 0$, a smooth crossing of eigenvalues implies the correspondence displayed in Table I, associated with the double degeneracies $E_3(\mathcal{U} = 0) = E_4(\mathcal{U} = 0)$, $E_5(\mathcal{U} = 0) = E_6(\mathcal{U} = 0)$, and $E_7(\mathcal{U} = 0) = E_8(\mathcal{U} = 0)$. These remarks are reflected in the choice of online colors (or shading in the

where $n_i = \hat{b}_i^\dagger \hat{b}_i$ is the occupation operator per site. J is the hopping (tunneling) parameter and the Hubbard U can be positive (repulsive interaction), vanishing (noninteracting), or negative (attractive interaction).

Using the capabilities of the SNEG [56] program in conjunction with the MATHEMATICA [57] algebraic language, one can write the following matrix Hamiltonian for the spinless three-boson Hubbard problem:

print grayscale version) for the $\mathcal{U} > 0$ and $\mathcal{U} < 0$ segments of the curves in Fig. 1, where the bosonic eigenvalues listed in Eq. (4) are plotted as a function of \mathcal{U} . Note further that the ordering between E_4 and E_5 is interchanged for $|\mathcal{U}| \geq 3\sqrt{2} = 4.24264$ [not visible in Fig. 1(a) due to the scale of the figure]. In the following, the corresponding Hubbard eigenstates are labeled in ascending energy order as $i = 1, 2, 3r(4l), 4r(3l), 5r(6l), 6r(5l), 7r(8l), 8r(7l), 9, 10$, where “ r ” means “right” for the region of positive \mathcal{U} and “ l ” means “left” for the region of negative \mathcal{U} .

The 10 normalized eigenvectors $\phi_i^b(\mathcal{U})$, with $i = 1, \dots, 10$, of the bosonic matrix Hamiltonian in Eq. (3) have the general form

$$\begin{aligned} \phi_i^b(\mathcal{U}) &= \{\mathbf{c}_{111}(\mathcal{U}), \mathbf{c}_{210}(\mathcal{U}), \mathbf{c}_{201}(\mathcal{U}), \mathbf{c}_{120}(\mathcal{U}), \mathbf{c}_{021}(\mathcal{U}), \\ &\mathbf{c}_{102}(\mathcal{U}), \mathbf{c}_{012}(\mathcal{U}), \mathbf{c}_{300}(\mathcal{U}), \mathbf{c}_{030}(\mathcal{U}), \mathbf{c}_{003}(\mathcal{U})\}. \end{aligned} \quad (7)$$

Because the algebraic expressions for the \mathbf{c}_{ijk} ’s for an arbitrary \mathcal{U} are very long and complicated, we explicitly list in this paper the Hubbard eigenvectors only for the characteristic limits of infinite repulsive and attractive interaction ($\mathcal{U} \rightarrow \pm\infty$) and for the noninteracting case ($\mathcal{U} = 0$). Specifically, for the reader’s convenience, we list in the main text

TABLE I. Correspondence of the energy eigenvalues of the Hubbard matrix Hamiltonian [Eq. (3)] at the double degeneracies at $\mathcal{U} = 0$; see Fig. 1.

$E_3(\mathcal{U} > 0)$	\iff	$E_4(\mathcal{U} < 0)$,	$E_4(\mathcal{U} > 0)$	\iff	$E_3(\mathcal{U} < 0)$
$E_5(\mathcal{U} > 0)$	\iff	$E_6(\mathcal{U} < 0)$,	$E_6(\mathcal{U} > 0)$	\iff	$E_5(\mathcal{U} < 0)$
$E_7(\mathcal{U} > 0)$	\iff	$E_8(\mathcal{U} < 0)$,	$E_8(\mathcal{U} > 0)$	\iff	$E_7(\mathcal{U} < 0)$

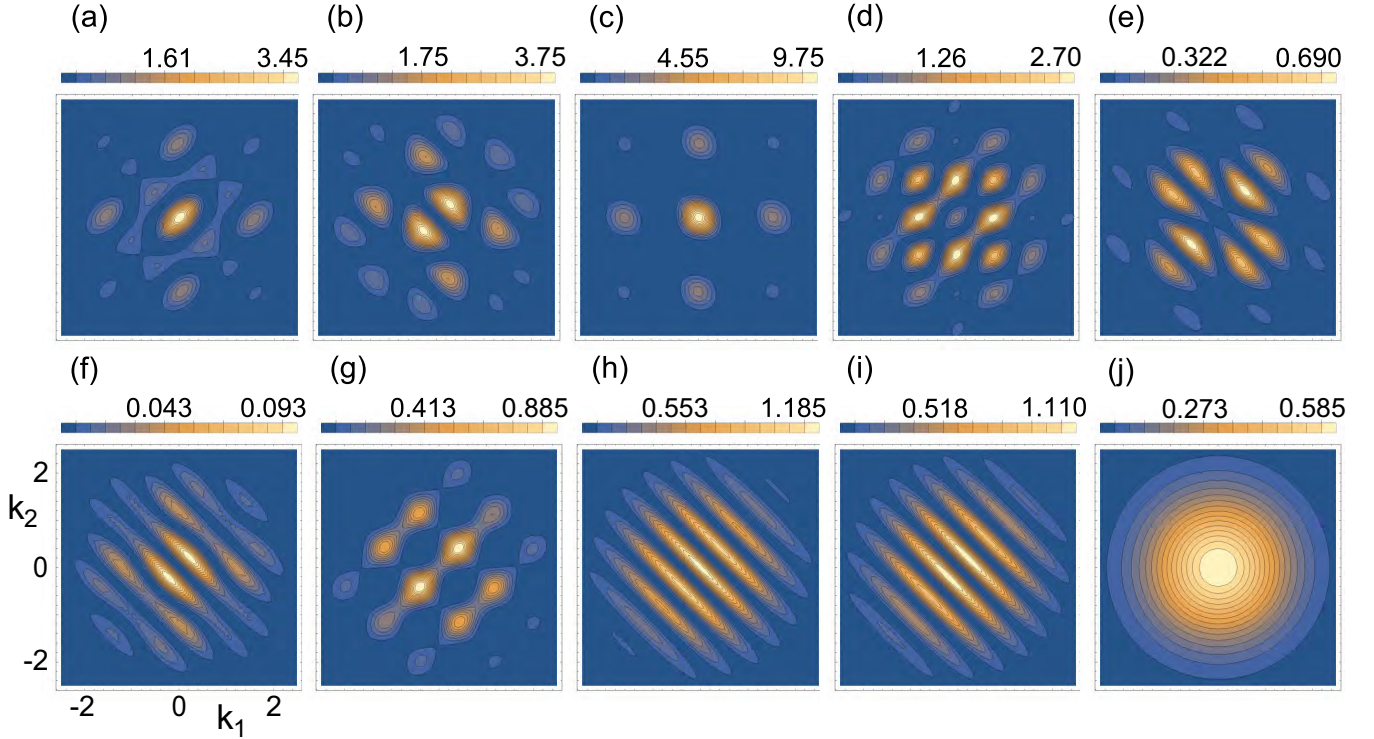


FIG. 2. Cuts ($k_3 = 0$) of third-order momentum correlation maps, ${}^3\mathcal{G}_i^{b,+\infty} = \Phi_i^{b,+\infty} \Phi_i^{b,+\infty,*}$, corresponding to the momentum-space wave functions for three bosons in three wells [see Eqs. (23) and (24) and Eqs. (C1)–(C8), top expressions]. (a) Ground state ($i = 1$). (b) First-excited state ($i = 2$). (c) Second-excited state ($i = 3$). (d) Third-excited state ($i = 4$). (e) Fourth-excited state ($i = 5$). (f) Fifth-excited state ($i = 6$). (g) Sixth-excited state ($i = 7$). (h) Seventh-excited state ($i = 8$). (i) Eighth-excited state ($i = 9$). (j) Ninth-excited state ($i = 10$). Parameters are interwell distance $d = 3.8 \mu\text{m}$ and spectral width of single-particle distribution in momentum space [see Eq. (20)] being the inverse of $s = 0.5 \mu\text{m}$. The correlation functions ${}^3\mathcal{G}_i^{b,+\infty}(k_1, k_2, k_3 = 0)$ (map landscapes) are given in units of μm^3 according to the color bars on top of each panel, and the momenta k_1 and k_2 are in units of $1/\mu\text{m}$. The value of the plotted correlation functions was multiplied by a factor of 10 to achieve better contrast for the map features. Third-order momentum correlation maps for the infinite attractive limit are not explicitly plotted due to the equalities between pairs of the Hubbard eigenvectors at $\mathcal{U} \rightarrow -\infty$ and $\mathcal{U} \rightarrow +\infty$; see Eq. (11) for the detailed association of states.

only the Hubbard eigenvectors for the ground and first-excited states; see Secs. II A and II B. The eigenvectors for the remaining eight excited states are given in Appendix A (for $\mathcal{U} \rightarrow \pm\infty$) and Appendix B (for $\mathcal{U} = 0$).

A. The infinite repulsive or attractive interaction ($\mathcal{U} \rightarrow \pm\infty$) limit

For large values of $|\mathcal{U}|$ ($\mathcal{U} \rightarrow \pm\infty$), the ten bosonic eigenvalues in Eq. (4) (in units of J) are well approximated by the simpler expressions:

$$\begin{aligned}
 E_1^{+\infty}(E_{10}^{-\infty}) &= -8/\mathcal{U} + 20/\mathcal{U}^3, \\
 E_2^{+\infty}(E_9^{-\infty}) &= \mathcal{U} \mp \sqrt{5} - 3/(4\mathcal{U}), \\
 E_3^{+\infty}(E_8^{-\infty}) &= \mathcal{U} \mp \sqrt{5} + 33/(20\mathcal{U}), \\
 E_4^{+\infty}(E_7^{-\infty}) &= \mathcal{U} + 1/(5\mathcal{U}), \\
 E_5^{+\infty}(E_6^{-\infty}) &= \mathcal{U}, \\
 E_6^{+\infty}(E_5^{-\infty}) &= \mathcal{U} \pm \sqrt{5} - 3/(4\mathcal{U}), \\
 E_7^{+\infty}(E_4^{-\infty}) &= \mathcal{U} \pm \sqrt{5} + 33/(20\mathcal{U}), \\
 E_8^{+\infty}(E_3^{-\infty}) &= 3\mathcal{U} + 3/(2\mathcal{U}) - 9/(4\mathcal{U}^3),
 \end{aligned}$$

$$\begin{aligned}
 E_9^{+\infty}(E_2^{-\infty}) &= 3\mathcal{U} + 3/(2\mathcal{U}) + 3/(4\mathcal{U}^3), \\
 E_{10}^{+\infty}(E_1^{-\infty}) &= 3\mathcal{U} + 3/\mathcal{U} + 7/(2\mathcal{U}^3),
 \end{aligned} \tag{8}$$

where symbols $E_i^{+\infty}$ without parentheses and the upper signs in \mp and \pm refer to the positive limit $\mathcal{U} \rightarrow +\infty$, and those ($E_i^{-\infty}$) within parentheses and the lower signs in \mp and \pm refer to the negative limit $\mathcal{U} \rightarrow -\infty$.

From the above, one sees that for large $\pm|\mathcal{U}|$ the bosonic eigenvalues are organized in three groups: a high-energy (low-energy) group of three eigenvalues around $\pm 3|\mathcal{U}|$ (triply occupied sites, see below), a middle-energy group of six eigenvalues around $\pm|\mathcal{U}|$ (doubly occupied sites, see below), and a single negative and lowest (positive and highest) eigenvalue approaching zero (singly occupied sites, see below). Figure 1 illustrates this behavior.

The corresponding eigenvectors at $\mathcal{U} \rightarrow +\infty$ and $\mathcal{U} \rightarrow -\infty$ for the ground and first-excited states are given by

$$\begin{aligned}
 \phi_1^{b,+\infty} &= \{1, 0, 0, 0, 0, 0, 0, 0, 0, 0\}, \\
 \phi_1^{b,-\infty} &= \{0, 0, 0, 0, 0, 0, 0, 0, 1, 0\}, \\
 \phi_2^{b,+\infty} &= \left\{0, -\frac{1}{2}, -\frac{1}{2\sqrt{5}}, -\frac{1}{\sqrt{5}}, \frac{1}{\sqrt{5}}, \frac{1}{2\sqrt{5}}, \frac{1}{2}, 0, 0, 0\right\},
 \end{aligned} \tag{9}$$

$$\phi_2^{b,-\infty} = \left\{ 0, 0, 0, 0, 0, 0, 0, -\frac{1}{\sqrt{2}}, 0, \frac{1}{\sqrt{2}} \right\}, \quad (10)$$

The eigenvectors for the remaining eight excited states are listed in Appendix A. Note that the eigenvectors in Eqs. (9) and (10) and in Appendix A are grouped in pairs (+ ∞ , - ∞), which are displayed using a common equation number.

Note that the eigenvectors at $\mathcal{U} \rightarrow +\infty$ and $\mathcal{U} \rightarrow -\infty$ are pairwise related as follows:

$$\begin{aligned} \phi_1^{b,+\infty} &= -\phi_{10}^{b,-\infty}, & \phi_6^{b,+\infty} &= -\phi_9^{b,-\infty}, \\ \phi_2^{b,+\infty} &= -\phi_5^{b,-\infty}, & \phi_7^{b,+\infty} &= -\phi_8^{b,-\infty}, \\ \phi_3^{b,+\infty} &= -\phi_4^{b,-\infty}, & \phi_8^{b,+\infty} &= \phi_3^{b,-\infty}, \\ \phi_4^{b,+\infty} &= \phi_7^{b,-\infty}, & \phi_9^{b,+\infty} &= \phi_2^{b,-\infty}, \\ \phi_5^{b,+\infty} &= \phi_6^{b,-\infty}, & \phi_{10}^{b,+\infty} &= \phi_1^{b,-\infty}. \end{aligned} \quad (11)$$

The pairs in Eq. (11) correspond to states with the same absolute eigenvalues $|E_i^{+\infty}|$ and $|E_j^{-\infty}|$ (with $i, j = 1, \dots, 10$) given in Eq. (8).

B. The noninteracting ($\mathcal{U} = 0$) limit

When $\mathcal{U} = 0$, the polynomial-root eigenvalues listed in Eq. (4) simplify to

$$\begin{aligned} E_1 &= -3\sqrt{2}, & E_6 &= 0, \\ E_2 &= -2\sqrt{2}, & E_7 &= \sqrt{2}, \\ E_3 &= -\sqrt{2}, & E_8 &= \sqrt{2}, \\ E_4 &= -\sqrt{2}, & E_9 &= 2\sqrt{2}, \\ E_5 &= 0, & E_{10} &= 3\sqrt{2}. \end{aligned} \quad (12)$$

The $\mathcal{U} = 0$ Hubbard ground-state eigenvector is given by

$$\phi_1^{b,\mathcal{U}=0} = \left\{ \frac{\sqrt{3}}{4}, \frac{\sqrt{\frac{3}{2}}}{4}, \frac{\sqrt{3}}{8}, \frac{\sqrt{3}}{4}, \frac{\sqrt{3}}{4}, \frac{\sqrt{3}}{8}, \frac{\sqrt{\frac{3}{2}}}{4}, \frac{1}{8}, \frac{1}{2\sqrt{2}}, \frac{1}{8} \right\}, \quad (13)$$

whereas the first-excited state is represented by the eigenvector

$$\phi_2^{b,\mathcal{U}=0} = \left\{ 0, -\frac{1}{2}, -\frac{1}{4\sqrt{2}}, -\frac{1}{2\sqrt{2}}, \frac{1}{2\sqrt{2}}, \frac{1}{4\sqrt{2}}, \frac{1}{2}, -\frac{\sqrt{\frac{3}{2}}}{4}, 0, \frac{\sqrt{\frac{3}{2}}}{4} \right\}. \quad (14)$$

The eigenvectors for the remaining eight excited states are listed in Appendix B.

III. HIGHER ORDER CORRELATIONS IN MOMENTUM SPACE: OUTLINE OF GENERAL DEFINITIONS

To motivate our discussion about momentum-space correlation functions, it is convenient to recall that, usually, a configuration-interaction (CI) calculation (or other exact diagonalization schemes used for solution of the microscopic many-body Hamiltonian) yields a many-body wave function expressed in position coordinates. Then the N th-order *real space* density, $\rho(x_1, x'_1, x_2, x'_2, \dots, x_N, x'_N)$, for an N -particle system is defined as the product of the many-body

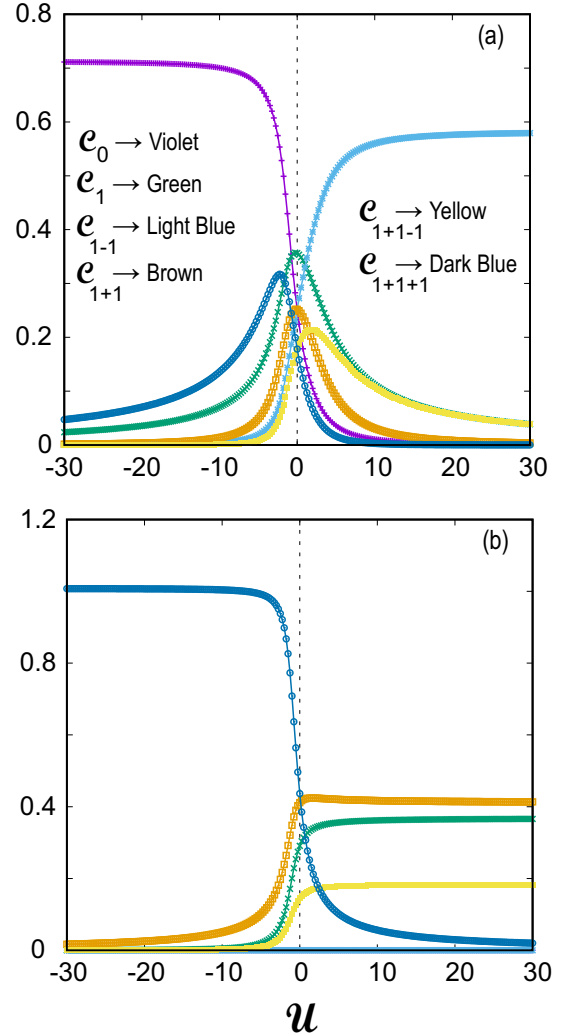


FIG. 3. The six different \mathcal{C} coefficients (dimensionless) [see Eq. (29)] for the two lowest-in-energy eigenstates of three bosons trapped in three linearly arranged wells as a function of \mathcal{U} (dimensionless). (a) Ground state ($i = 1$). (b) First-excited state ($i = 2$). See text for a detailed description. For a description of the remaining eight excited states, see Appendix E. The choice of online colors is as follows: \mathcal{C}_0 , violet; \mathcal{C}_1 , green; \mathcal{C}_{1-1} , light blue; \mathcal{C}_{1+1} , brown; \mathcal{C}_{1+1-1} , yellow; and \mathcal{C}_{1+1+1} , dark blue. For the print grayscale version, the positioning (referred to as # n , with $n = 1, 2, 3, \dots$) of the curves from top to bottom at the point $\mathcal{U} = -6$ is as follows: (a) $\mathcal{C}_0 \rightarrow \#1$; $\mathcal{C}_1 \rightarrow \#3$; $\mathcal{C}_{1-1} \rightarrow \#5$; $\mathcal{C}_{1+1} \rightarrow \#4$; $\mathcal{C}_{1+1-1} \rightarrow \#6$; $\mathcal{C}_{1+1+1} \rightarrow \#2$; and (b) $\mathcal{C}_0 = 0$; $\mathcal{C}_1 \rightarrow \#3$; $\mathcal{C}_{1-1} = 0$; $\mathcal{C}_{1+1} \rightarrow \#2$; $\mathcal{C}_{1+1-1} \rightarrow \#4$; $\mathcal{C}_{1+1+1} \rightarrow \#1$.

wave function $\Psi(x_1, x_2, \dots, x_N)$ and its complex conjugate $\Psi^*(x'_1, x'_2, \dots, x'_N)$ [58]. The i th-order density function (with $i \leq N$) is defined as an integral over ρ taken over the coordinates x_{i+1}, \dots, x_N of $N - i$ particles, i.e.,

$$\begin{aligned} \rho_i(x_1, x'_1, x_2, x'_2, \dots, x_i, x'_i) \\ = \int dx_{i+1} \dots dx_N \rho(x_1, x'_1, \dots, x_i, x'_i, x_{i+1}, x'_{i+1}, \dots, x_N, x'_N). \end{aligned} \quad (15)$$

To obtain the i th-order real space correlation, one simply sets the prime coordinates in Eq. (15) to be equal to the corresponding unprimed ones,

$${}^i\mathcal{G}(x_1, x_2, \dots, x_i) = \rho_i(x_1, x_1, x_2, x_2, \dots, x_i, x_i). \quad (16)$$

Knowing the real-space density, one can obtain the corresponding higher order momentum correlations through a Fourier transform [13–15,59]

$$\begin{aligned} & {}^i\mathcal{G}(k_1, k_2, \dots, k_i) \\ &= \frac{1}{4\pi^2} \int e^{ik_1(x_1-x'_1)} e^{ik_2(x_2-x'_2)} \dots e^{ik_i(x_i-x'_i)} \\ & \times \rho_i(x_1, x'_1, x_2, x'_2, \dots, x_i, x'_i) dx_1 dx'_1 dx_2 dx'_2 \dots dx_i dx'_i, \end{aligned} \quad (17)$$

In this paper, we obtain directly an expression for the momentum-space N -body wave function corresponding to the Hubbard model Hamiltonian. This circumvents the need for the above Fourier transform. Instead, consistent with the Fourier-transform relation [Eq. (17) above], the highest-order N th-order momentum correlation function is given by the modulus square

$${}^N\mathcal{G}(k_1, k_2, \dots, k_N) = |\Phi(k_1, k_2, \dots, k_N)|^2, \quad (18)$$

and, successively, any lower $(N-i)$ th-order (with $i = 1, \dots, N-1$) momentum correlation is obtained through an integration of the higher $(N-i+1)$ th-order correlation over the k_{N-i+1} momentum.

IV. THIRD-ORDER MOMENTUM CORRELATIONS FOR THREE BOSONS IN THREE WELLS: THE INFINITE-INTERACTION LIMIT ($\mathcal{U} \rightarrow \pm\infty$)

To derive the all-order momentum correlations, we augment the finite-site Hubbard model as follows: Each boson in any of the three wells is represented by a single-particle localized orbital having the form of a displaced Gaussian function [13–15,20], which in the real configuration space has the form

$$\psi_j(x) = \frac{1}{(2\pi)^{1/4} \sqrt{s}} \exp\left[-\frac{(x-d_j)^2}{4s^2}\right]. \quad (19)$$

In Eq. (19), d_j ($j = 1, 2, 3$) denotes the position of each of the three wells and $2s$ is the width of the Gaussian function in real configuration space. In this way the structure (interwell distances) and the spatial profile of the trapped particles orbitals enter in the augmented Hubbard model. In momentum space, the corresponding orbital $\psi_j(k)$ is given by the Fourier transform of $\psi_j(x)$, namely, $\psi_j(k) = (1/\sqrt{2\pi}) \int_{-\infty}^{\infty} \psi_j(x) \exp(ikx) dx$. Performing this Fourier transform, one finds

$$\psi_j(k) = \frac{2^{1/4} \sqrt{s}}{\pi^{1/4}} e^{-k^2 s^2} e^{id_j k}. \quad (20)$$

Naturally the spectral width of the orbital's profile in the momentum space is $1/s$.

In using orbitals localized on each well, our treatment of the augmented Hubbard trimer is similar to Coulson's treatment of the hydrogen molecule [60]. In broader terms, our use of localized orbitals (atomic orbitals) belongs to the general

methodology in chemistry known as linear combination of atomic orbitals–molecular orbitals (LCAO-MO) [61,62].

We stress that the cosinusoidal and sinusoidal dependencies of the momentum correlations derived here [and their coefficients C 's, B 's, and A 's; see Eqs. (29), (31), and (36) below] do not depend on the precise profile of the atomic orbital, as noted already in Ref. [60], where the general symbol $\mathfrak{A}(k)$ was used for the Fourier transform of $\psi_0(x)$ at $d_0 = 0$. For the hydrogen molecule, an obvious choice is a Slater-type orbital (see Eqs. (35) and (36) in Ref. [60]). The reason behind this behavior is the so-called shift property [63] of the Fourier transform, which applies to a displaced profile (centered at $d_j \neq 0$); it states that

$$\mathfrak{F}[\psi_j(x)] = \mathfrak{F}[\psi_0(x)] \exp(ikd_j) = \mathfrak{A}(k) \exp(ikd_j), \quad (21)$$

where \mathfrak{F} denotes the Fourier-transform operation [63]. The Fourier-transformed profile $\mathfrak{A}(k)$ at the initial site factors out in all expressions of the momentum correlations. The Gaussian profile (also used in aforementioned experimental publications [3–5,39]) in our paper was used for convenience; it is an obvious approximation for the lowest single-particle level in a deep potential [64] approaching a harmonic trap in the framework of experiments on neutral ultracold atoms [65].

For a discussion of the comparison, for the entire range of interatomic interactions, \mathcal{U} , between exact microscopic diagonalization of the Hamiltonian (configuration interaction, CI) calculations, results of the augmented Hubbard-model, and measurements from trapped ultracold-atoms experiments; see Ref. [66].

With the help of the single-boson orbitals in Eq. (20), each basis ket in Eq. (1) can be mapped onto a wave function of the three single-particle momenta k_1, k_2 , and k_3 . For each ket, this wave function naturally is a permanent built from the three bosonic orbitals. For a general eigenvector solution of the Hubbard Hamiltonian, the corresponding wave function $\Phi_i^b(k_1, k_2, k_3)$ (with $i = 1, \dots, 10$) in momentum space is a sum over such permanents, and the associated third-order correlation function is simply the modulus square, i.e.,

$${}^3\mathcal{G}_i^b(k_1, k_2, k_3) = |\Phi_i^b(k_1, k_2, k_3)|^2. \quad (22)$$

Because the expressions for the third-order correlations can become very long and cumbersome, for bookkeeping purposes, we found it advantageous to display and characterize instead the three-body wave functions $\Phi_i^b(k_1, k_2, k_3)$ themselves. Then the associated third-order correlations can be calculated using Eq. (22).

Below, in Eqs. (23) and (24), we list without commentary the momentum-space wave functions, $\Phi_1^{b,\pm\infty}(k_1, k_2, k_3)$ and $\Phi_2^{b,\pm\infty}(k_1, k_2, k_3)$, associated with the Hubbard eigenvectors, $\phi_1^{b,\pm\infty}$ and $\phi_2^{b,\pm\infty}$, respectively [see Eqs. (9) and (10)], at the limits of infinite repulsive or attractive strength (i.e., for $\mathcal{U} \rightarrow \pm\infty$). The commentary integrating these wave functions into the broader scheme of their evolution as a function of any interaction strength $-\infty < \mathcal{U} < +\infty$ is left for Sec. VI below. The three-body wave functions for the remaining eight excited states are listed in Appendix C. Note that the wave functions in Eqs. (23) and (24) below and in Appendix C are grouped

in pairs $(+\infty, -\infty)$, which are displayed using a common equation number.

Assuming that the wells are linearly placed at $d_1 = -d$, $d_2 = 0$, and $d_3 = d$, these momentum-space wave functions at $\mathcal{U} \rightarrow \pm\infty$ are as follows:

$$\Phi_1^{b,+\infty}(k_1, k_2, k_3) = \frac{2 \times 2^{1/4}}{\sqrt{3}\pi^{3/4}} s^{3/2} e^{-(k_1^2+k_2^2+k_3^2)s^2} \times [\cos(d(k_1 - k_2)) + \cos(d(k_1 - k_3)) + \cos(d(k_2 - k_3))],$$

$$\Phi_1^{b,-\infty}(k_1, k_2, k_3) = \left(\frac{2}{\pi}\right)^{3/4} s^{3/2} e^{-(k_1^2+k_2^2+k_3^2)s^2}, \quad (23)$$

$$\begin{aligned} \Phi_2^{b,+\infty}(k_1, k_2, k_3) &= \frac{i2^{3/4}}{5\sqrt{3}\pi^{3/4}} s^{3/2} e^{-(k_1^2+k_2^2+k_3^2)s^2} \\ &\times [\sqrt{5} \sin(d(-k_1 + k_2 + k_3)) \\ &+ \sqrt{5} \sin(d(k_1 + k_2 - k_3)) \\ &+ \sqrt{5} \sin(d(k_1 - k_2 + k_3)) \\ &+ 5 \sin(d(k_1 + k_2)) + 5 \sin(d(k_1 + k_3)) \\ &+ 5 \sin(d(k_2 + k_3)) + 2\sqrt{5} \sin(dk_1) \\ &+ 2\sqrt{5} \sin(dk_2) + 2\sqrt{5} \sin(dk_3)], \end{aligned}$$

$$\begin{aligned} \Phi_2^{b,-\infty}(k_1, k_2, k_3) &= \frac{2i2^{1/4}}{\pi^{3/4}} s^{3/2} e^{-(k_1^2+k_2^2+k_3^2)s^2} \\ &\times \sin(d(k_1 + k_2 + k_3)). \quad (24) \end{aligned}$$

Plots for the corresponding third-order momentum correlations ${}^3\mathcal{G}_i^{b,+\infty}(k_1, k_2, k_3)$, with $i = 1, \dots, 10$ [see Eq. (22)], are presented in Fig. 2. We note that we do not explicitly plot the third-order momentum correlations for the limit of infinite attraction ($\mathcal{U} \rightarrow -\infty$) because ${}^3\mathcal{G}_i^{b,-\infty}(k_1, k_2, k_3) = {}^3\mathcal{G}_j^{b,+\infty}(k_1, k_2, k_3)$ for the pairs $(i = 1, j = 10)$, $(i = 2, j =$

$9)$, $(i = 3, j = 8)$, $(i = 4, j = 3)$, $(i = 5, j = 2)$, $(i = 6, j = 5)$, $(i = 7, j = 4)$, $(i = 8, j = 7)$, $(i = 9, j = 6)$, and $(i = 10, j = 1)$ due to the equalities between eigenvectors listed in Eq. (11).

A. Explicit expression for the third-order correlation

$${}^3\mathcal{G}_1^{b,+\infty}(k_1, k_2, k_3)$$

Because of the special role played by the ground state $\phi_1^{b,+\infty} = |111\rangle$ at infinite repulsion, we explicitly list below the corresponding third-order correlation function, i.e.,

$$\begin{aligned} {}^3\mathcal{G}_1^{b,+\infty}(k_1, k_2, k_3) &= |\Phi_1^{b,+\infty}(k_1, k_2, k_3)|^2 \\ &= \frac{2\sqrt{2}}{3\pi^{3/2}} s^3 e^{-2s^2(k_1^2+k_2^2+k_3^2)} [3 + 2 \cos(d(k_1 + k_2 - 2k_3)) \\ &+ 2 \cos(d(k_2 + k_3 - 2k_1)) + 2 \cos(d(k_1 + k_3 - 2k_2)) \\ &+ \cos(2d(k_1 - k_2)) + 2 \cos(d(k_1 - k_2)) \\ &+ \cos(2d(k_1 - k_3)) + 2 \cos(d(k_1 - k_3)) \\ &+ \cos(2d(k_2 - k_3)) + 2 \cos(d(k_2 - k_3))]. \quad (25) \end{aligned}$$

It is worth noting that the expression (25) above for three bosons is similar to the third-order correlation for the triplet states (with total spin $S = 3/2$ and spin projections $S_z = 3/2$ or $S_z = 1/2$) for three fermions trapped in three wells, except that in the fermionic case the sign in front of the cosine terms with only 2-momenta in the cosine argument is negative; see Refs. [4,20].

V. THIRD-ORDER MOMENTUM CORRELATIONS FOR THREE BOSONS IN THREE WELLS: THE NONINTERACTING LIMIT $\mathcal{U} = 0$

Assuming that the wells are linearly placed at $d_1 = -d$, $d_2 = 0$, and $d_3 = d$, the noninteracting ground-state three-boson wave function in momentum space is given by

$$\begin{aligned} \frac{(2\pi)^{3/4}}{s^{3/2}} e^{(k_1^2+k_2^2+k_3^2)s^2} \Phi_1^{b,\mathcal{U}=0}(k_1, k_2, k_3) &= 1 + 2\sqrt{2} \cos(dk_1) \cos(dk_2) \cos(dk_3) + 2 \cos(dk_1) \cos(dk_2) + 2 \cos(dk_1) \cos(dk_3) \\ &+ \sqrt{2} \cos(dk_1) + 2 \cos(dk_2) \cos(dk_3) + \sqrt{2} \cos(dk_2) + \sqrt{2} \cos(dk_3). \quad (26) \end{aligned}$$

The above takes also the form of the general expression (29) below, i.e.,

$$\begin{aligned} \frac{(2\pi)^{3/4}}{s^{3/2}} e^{(k_1^2+k_2^2+k_3^2)s^2} \Phi_1^{b,\mathcal{U}=0}(k_1, k_2, k_3) &= 1 + \sqrt{2} [\cos(dk_1) + \cos(dk_2) + \cos(dk_3)] + \cos[d(k_1 - k_2)] + \cos[d(k_1 - k_3)] \\ &+ \cos[d(k_2 - k_3)] + \cos[d(k_1 + k_2)] + \cos[d(k_1 + k_3)] + \cos[d(k_2 + k_3)] \\ &+ \frac{1}{\sqrt{2}} \{ \cos[d(k_1 + k_2 - k_3)] + \cos[d(k_1 - k_2 + k_3)] + \cos[d(-k_1 + k_2 + k_3)] \\ &+ \cos[d(k_1 + k_2 + k_3)] \}. \quad (27) \end{aligned}$$

For the first-excited state, the three-boson noninteracting wave function in momentum space at $\mathcal{U} = 0$ was found to be

$$\begin{aligned} \frac{-i(2\pi)^{3/4} \sqrt{3}}{s^{3/2}} e^{(k_1^2+k_2^2+k_3^2)s^2} \Phi_2^{b,\mathcal{U}=0}(k_1, k_2, k_3) &= 2[\sin(dk_1) + \sin(dk_2) + \sin(dk_3)] + 2\sqrt{2} \{ \sin[d(k_1 + k_2)] + \sin[d(k_1 + k_3)] \\ &+ \sin[d(k_2 + k_3)] \} + \sin[d(k_1 - k_2 + k_3)] + \sin[d(-k_1 + k_2 + k_3)] \\ &+ \sin[d(k_1 + k_2 - k_3)] + 3 \sin[d(k_1 + k_2 + k_3)]. \quad (28) \end{aligned}$$

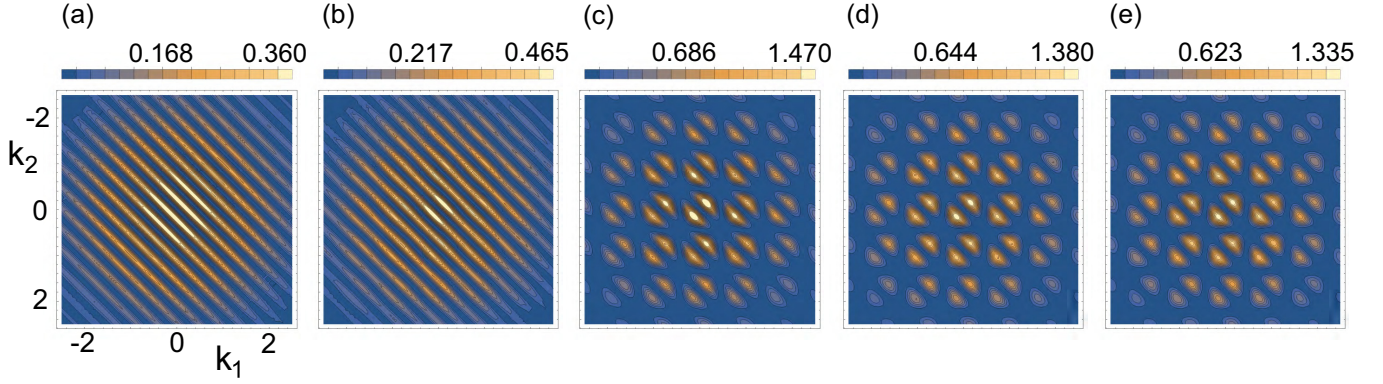


FIG. 4. Cuts ($k_3 = 0$) of third-order momentum correlation maps for the first-excited state of three bosons in three wells [see Eqs. (22) and (29) with $i = 2$]. (a) $\mathcal{U} = -200$. (b) $\mathcal{U} = -10$. (c) $\mathcal{U} = 0$. (d) $\mathcal{U} = 10$. (e) $\mathcal{U} = 200$. Parameters are interwell distance $d = 7 \mu\text{m}$ and spectral width of single-particle distribution in momentum space [see Eq. (20)] being the inverse of $s = 0.35 \mu\text{m}$. The correlation functions ${}^3\mathcal{G}^b(k_1, k_2, k_3 = 0)$ (map landscapes) are given in units of μm^3 according to the color bars on top of each panel, and the momenta k_1 and k_2 are in units of $1/\mu\text{m}$. The value of the plotted correlation functions was multiplied by a factor of 10 to achieve better contrast for the map features.

The noninteracting three-body wave functions for the remaining eight excited states are listed in Appendix D.

VI. THIRD-ORDER MOMENTUM CORRELATIONS FOR THREE BOSONS IN THREE WELLS AS A FUNCTION OF THE STRENGTH OF THE INTERACTION \mathcal{U}

The general cosinusoidal (or sinusoidal) expression of third-order correlations is too cumbersome and lengthy to be displayed in print in a paper. Instead, as mentioned earlier, we give here the general expression for the three-boson wave function $\Phi_i^b(k_1, k_2, k_3)$ (with $i = 1, \dots, 10$) calculated in the momentum space. Then the third-order momentum correlations are obtained simply as the modulus square of this wave function [see Eq. (22)].

Using MATHEMATICA, we found that the general cosinusoidal (or sinusoidal) expression of the three-body wave function has the form

$$\begin{aligned} \Phi_j^b(k_1, k_2, k_3) &= p^j s^{3/2} e^{-(k_1^2 + k_2^2 + k_3^2)s^2} \{C_0^j + C_1^j(\mathcal{F}(dk_1) + \mathcal{F}(dk_2) + \mathcal{F}(dk_3)) \\ &+ C_{1-1}^j(\mathcal{F}[d(k_1 - k_2)] + \mathcal{F}[d(k_1 - k_3)] + \mathcal{F}[d(k_2 - k_3)]) \\ &+ C_{1+1}^j(\mathcal{F}[d(k_1 + k_2)] + \mathcal{F}[d(k_1 + k_3)] + \mathcal{F}[d(k_2 + k_3)]) \\ &+ C_{1+1-1}^j(\mathcal{F}[d(k_1 + k_2 - k_3)] + \mathcal{F}[d(k_1 - k_2 + k_3)] \\ &+ \mathcal{F}[d(-k_1 + k_2 + k_3)]) + C_{1+1+1}^j \mathcal{F}[d(k_1 + k_2 + k_3)]\}, \end{aligned} \quad (29)$$

where $p^j = 1$ and \mathcal{F} stands for “cos” for the states $j = 1, 3r(4l), 4r(3l), 7r(8l), 8r(7l), 10$; $p^j = i$ (here $i^2 = -1$; it is not an index); and \mathcal{F} stands for “sin” for the remaining states $j = 2, 5r(6l), 6r(5l), 9$. The C_0 coefficient denotes an \mathcal{F} -independent term. The subscripts 1, 1 ± 1 , and $1 + 1 \pm 1$ in the other C coefficients reflect the number of terms in the argument of the \mathcal{F} functions and the sign in front of each of them (without consideration of any ordering of the k_1, k_2 , and k_3 momentum variables).

In general, there are 14 cosinusoidal (or sinusoidal) terms and six distinct \mathcal{U} -dependent coefficients C 's for a given state in expression (29). We note that $C_0 \equiv 0$ and $C_{1-1} \equiv 0$ for any \mathcal{U} for all the states of the second group above for which $\mathcal{F} \equiv \sin$. The C coefficients for the two lowest-in-energy eigenstates are plotted in Fig. 3 as a function of \mathcal{U} . The corresponding explicit numerical values can be found in a data file included in the Supplemental Material [67].

In the following, we utilize in the discussions the coefficients $C_{q_1 q_2 q_3}^{j, \mathcal{U}}$ for certain limiting values, 0, $-\infty$, and $+\infty$, of the on-site interatomic interaction \mathcal{U} ; in each case we explicitly include the limiting value as a superscript \mathcal{U} .

A. The ground state (state denoted as $i = 1$ for $-\infty < \mathcal{U} < +\infty$)

For $\mathcal{U} \rightarrow -\infty$, it is seen from Fig. 3(a) that only the coefficient $C_0^{1, -\infty} = (2/\pi)^{3/4} = 0.7127$ (denoting an \mathcal{F} -independent term) survives in expression (29); the ground state in momentum space is given by the second expression in Eq. (23). It is a simple Gaussian distribution associated with a Bose-Einstein condensate, reflecting the fact that all three bosons are localized in the middle well and occupy the same orbital; the corresponding Hubbard eigenvector is given by $\phi_1^{b, -\infty}$ [second expression in Eq. (9)] which contains only a single component from the primitive kets listed in Eq. (1), i.e., the basis ket no. 9 \rightarrow |030).

For $\mathcal{U} = 0$, all six coefficients, $C^{1, \mathcal{U}=0}$'s, are present, and their numerical values from Fig. 3(a) agree with the corresponding algebraic expressions for $\Phi_1^{b, \mathcal{U}=0}(k_1, k_2, k_3)$ in Eq. (27).

For $\mathcal{U} \rightarrow +\infty$, only the coefficient $C_{1-1}^{1, +\infty} = 2 \times 2^{1/4}/(\sqrt{3}\pi^{3/4}) = 0.5819$ survives in expression (29); see again Fig. 3(a). The ground state in momentum space comprises three cosinusoidal terms and is given by the first expression in Eq. (23). This form corresponds to the Hubbard eigenvector $\phi_1^{b, +\infty}$ [first expression in Eq. (9)], which contains only a single component from the primitive kets listed in Eq. (1), i.e., the basis ket no. 1 \rightarrow |111).

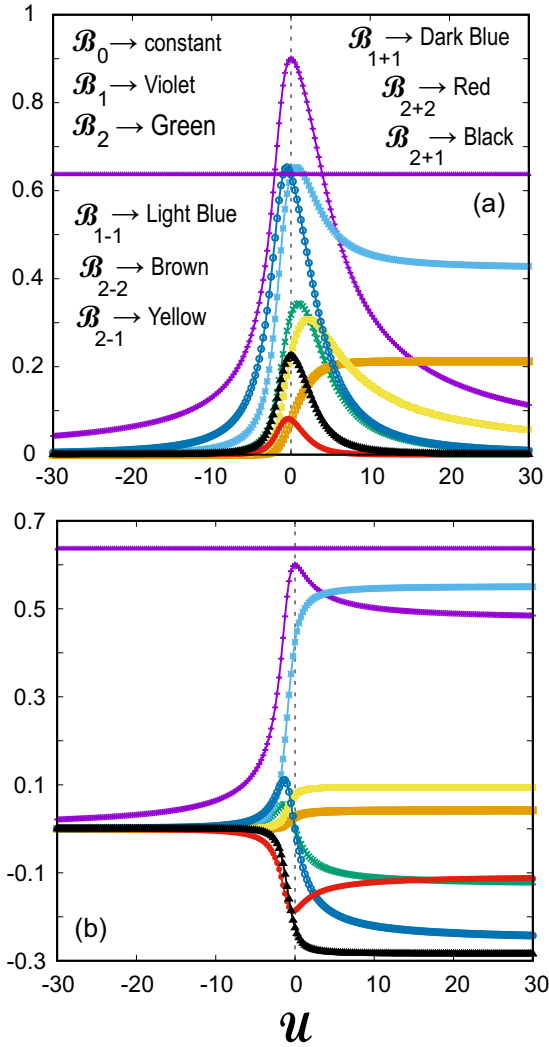


FIG. 5. The \mathcal{B} coefficients (dimensionless) [see Eq. (31)] for the two lowest-in-energy eigenstates of three bosons trapped in three linearly arranged wells as a function of the interaction strength \mathcal{U} (dimensionless). (a) Ground state ($i = 1$). (b) First-excited state ($i = 2$). See text for a detailed description. The choice of online colors is as follows: \mathcal{B}_0 , constant (violet); \mathcal{B}_1 , second violet; \mathcal{B}_2 , green; \mathcal{B}_{1-1} , light blue; \mathcal{B}_{2-2} , brown; \mathcal{B}_{2-1} , yellow; \mathcal{B}_{1+1} , dark blue; \mathcal{B}_{2+2} , red; and \mathcal{B}_{2+1} , black. For the print grayscale version, the positioning (referred to as $\#n$, with $n = 1, 2, 3, \dots$) of the curves from top to bottom at the point $\mathcal{U} = +2$ is as follows: (a) \mathcal{B}_0 (constant) \rightarrow #3; $\mathcal{B}_1 \rightarrow$ #1; $\mathcal{B}_2 \rightarrow$ #5; $\mathcal{B}_{1-1} \rightarrow$ #2; $\mathcal{B}_{2-2} \rightarrow$ #8; $\mathcal{B}_{2-1} \rightarrow$ #6; $\mathcal{B}_{1+1} \rightarrow$ #4; $\mathcal{B}_{2+2} \rightarrow$ #9; $\mathcal{B}_{2+1} \rightarrow$ #7; and (b) \mathcal{B}_0 (constant) \rightarrow #1; $\mathcal{B}_1 \rightarrow$ #2; $\mathcal{B}_2 \rightarrow$ #6; $\mathcal{B}_{1-1} \rightarrow$ #3; $\mathcal{B}_{2-2} \rightarrow$ #5; $\mathcal{B}_{2-1} \rightarrow$ #4; $\mathcal{B}_{1+1} \rightarrow$ #7; $\mathcal{B}_{2+2} \rightarrow$ #8; and $\mathcal{B}_{2+1} \rightarrow$ #9. For a description of the remaining eight excited states, see Appendix F.

As mentioned earlier, the primitive ket $|111\rangle$ represents a case where all three wells are singly occupied. Thus, it enables a direct mapping to quantum-optics investigations of the frequency-resolved interference of three temporally distinguishable photons prepared in three separate fibers (tritter) [38] [recall the analogies [15]: particle momentum (k) \leftrightarrow photon frequency (ω/c) and interwell distance (d) \leftrightarrow time-delay between single photons (τc)].

B. The first excited state (state denoted as $i = 2$ for $-\infty < \mathcal{U} < +\infty$)

For $\mathcal{U} \rightarrow -\infty$ only the coefficient $\mathcal{C}_{1+1+1}^{2,-\infty} = 2 \times 2^{1/4}/\pi^{3/4} = 1.0079$ survives in expression (29) [see Fig. 3(b)]; the corresponding state, $\phi_2^{b,-\infty}$ [second expression in Eq. (10)], is a NOON state of the form $(-|300\rangle + |003\rangle)/\sqrt{2}$, and the corresponding wave function in momentum space is given by the second expression in Eq. (24), which includes a single *sin* term only.

For $\mathcal{U} = 0$, four coefficients are present, namely $\mathcal{C}_1^{2,\mathcal{U}=0}$, $\mathcal{C}_{1+1}^{2,\mathcal{U}=0}$, $\mathcal{C}_{1+1-1}^{2,\mathcal{U}=0}$, and $\mathcal{C}_{1+1+1}^{2,\mathcal{U}=0}$. Their numerical values from Fig. 3(b) agree with the corresponding algebraic expressions for $\Phi_2^{b,\mathcal{U}=0}(k_1, k_2, k_3)$ in Eq. (28).

For $\mathcal{U} \rightarrow +\infty$, only three coefficients, $\mathcal{C}_1^{2,+\infty} = 2 \times 2^{3/4}/(\sqrt{15}\pi^{3/4}) = 0.3680$, $\mathcal{C}_{1+1}^{2,+\infty} = 2^{3/4}/(\sqrt{3}\pi^{3/4}) = 0.4115$, and $\mathcal{C}_{1+1-1}^{2,+\infty} = 2^{3/4}/(\sqrt{15}\pi^{3/4}) = 0.1840$, survive in expression (29) [see Fig. 3(b)]; the corresponding state, $\phi_2^{b,+\infty}$ [first expression in Eq. (10)] consists of all six primitive kets [see Eq. (1)] representing exclusively doubly occupied wells, and the corresponding wave function in momentum space has nine *sinusoidal* terms and is given by the first expression in Eq. (24).

In the main text of this paper, we restrict the \mathcal{U} evolution of the $\mathcal{C}(\mathcal{U})$'s coefficients in Eq. (29) to the two lowest-in-energy states. Indeed the ground state and the first excited state are the natural candidates for initial experiments. For example, for the case of two and three ultracold fermions (^6Li atoms), see Refs. [5] and [4], respectively; for recent experiments focused on the ground state of large bosonic Hubbard systems, see Refs. [6] and [8] (^{87}Rb atoms) and Refs. [9,10] ($^4\text{He}^*$ atoms). In the case of trapped ultracold atoms, other excited states are in principle accessible. Thus, in anticipation of future experimental activity, we complete in Appendix E the description of the details of the \mathcal{U} evolution of the $\mathcal{C}(\mathcal{U})$'s for the remaining eight excited states.

Figure 4 illustrates visually for the first-excited state ($i = 2$) the \mathcal{U} evolution of the third-order correlation maps described by expressions (22) and (29) when $i = 1$. The maps for five characteristic values of \mathcal{U} are plotted, namely, $\mathcal{U} = -200, -10, 0, 10, \text{ and } 200$. Corresponding illustrations for the ground state are left for Sec. IX.

VII. SECOND-ORDER MOMENTUM CORRELATIONS FOR THREE BOSONS IN THREE WELLS AS A FUNCTION OF THE STRENGTH OF THE INTERACTION \mathcal{U}

The second-order correlations are obtained through an integration of the third-order ones over the third momentum variable k_3 , i.e.,

$${}^2\mathcal{G}_i^b(k_1, k_2) = \int_{-\infty}^{\infty} {}^3\mathcal{G}_i^b(k_1, k_2, k_3) dk_3, \quad (30)$$

with $i = 1, \dots, 10$.

Using MATHEMATICA and neglecting the terms that vanish as $e^{-\gamma d^2/s^2}$ (for arbitrary $\gamma > 0$ and $d^2/s^2 \gg 1$), we found that the second-order correlations are given by the following

TABLE II. The nine distinct coefficients at $\mathcal{U} = 0$ present in Eq. (31) in the case of the ground state.

$\mathcal{B}_0^{1,\mathcal{U}=0}$	$\mathcal{B}_1^{1,\mathcal{U}=0}$	$\mathcal{B}_2^{1,\mathcal{U}=0}$	$\mathcal{B}_{-1}^{1,\mathcal{U}=0}$	$\mathcal{B}_{-2}^{1,\mathcal{U}=0}$	$\mathcal{B}_{-1}^{1,\mathcal{U}=0}$	$\mathcal{B}_{+1}^{1,\mathcal{U}=0}$	$\mathcal{B}_{+2}^{1,\mathcal{U}=0}$	$\mathcal{B}_{+1}^{1,\mathcal{U}=0}$
$2/\pi =$ 0.63662	$2\sqrt{2}/\pi =$ 0.90032	$1/\pi =$ 0.31831	$2/\pi =$ 0.63662	$1/(4\pi) =$ 0.07958	$1/(\sqrt{2}\pi) =$ 0.22508	$2/\pi =$ 0.63662	$1/(4\pi) =$ 0.07958	$1/(\sqrt{2}\pi) =$ 0.22508

general expression:

$$\begin{aligned}
{}^2\mathcal{G}_i^b(k_1, k_2) &= s^2 e^{-2(k_1^2+k_2^2)s^2} \\
&\times (\mathcal{B}_0^i + \mathcal{B}_1^i [\cos(dk_1) + \cos(dk_2)] \\
&+ \mathcal{B}_2^i [\cos(2dk_1) + \cos(2dk_2)] \\
&+ \mathcal{B}_{-1}^i \cos[d(k_1 - k_2)] + \mathcal{B}_{-2}^i \cos[2d(k_1 - k_2)] \\
&+ \mathcal{B}_{-1}^i \{\cos[d(k_1 - 2k_2)] + \cos[d(2k_1 - k_2)]\} \\
&+ \mathcal{B}_{+1}^i \cos[d(k_1 + k_2)] + \mathcal{B}_{+2}^i \cos[2d(k_1 + k_2)] \\
&+ \mathcal{B}_{+1}^i \{\cos[d(k_1 + 2k_2)] + \cos[d(2k_1 + k_2)]\}). \quad (31)
\end{aligned}$$

The \mathcal{B}_0 coefficient denotes a cos-independent term. The subscripts 1, 2, 1 ± 1 , 2 ± 1 , and 2 ± 2 in the other \mathcal{B} coefficients reflect the number of terms in the argument of the cos functions (one or two) and the factor of ± 1 or ± 2 in front of k_1 or k_2 (without consideration of any ordering of k_1 and k_2).

Including the constant term, there are 13 sinusoidal terms, but only nine distinct coefficients in Eq. (31). The first coefficient above is a constant, i.e., $\mathcal{B}_0^i = 2/\pi \approx 0.63662$ for all ten eigenstates. The remaining eight \mathcal{B} -coefficients in Eq. (31) are \mathcal{U} dependent. These \mathcal{U} -dependent \mathcal{B} coefficients for the two lowest-in-energy eigenstates are plotted in Fig. 5 as a function of \mathcal{U} . The corresponding explicit numerical values can be found in a data file included in the Supplemental Material [67]. Note that expression (31) has a total of 13 different cosine terms.

A. The ground state (state denoted as $i = 1$ for $-\infty < \mathcal{U} < +\infty$)

For $\mathcal{U} \rightarrow -\infty$ only the constant term \mathcal{B}_0^1 survives; see Fig. 5(a). The ground state is the triply occupied middle well [see the Hubbard eigenvector in the second expression of Eq. (9)]. In this case, the second-order correlation function is

$${}^2\mathcal{G}_1^{b,-\infty}(k_1, k_2) = \frac{2}{\pi} s^2 e^{-2(k_1^2+k_2^2)s^2}. \quad (32)$$

In the noninteracting case ($\mathcal{U} = 0$), for which the Hubbard eigenvector is given by Eq. (13), all 13 cosinusoidal terms and nine distinct coefficients (listed in Table II) are present in Eq. (31), in agreement with Fig. 5(a).

For $\mathcal{U} \rightarrow +\infty$, three terms survive, including the constant one; see Fig. 5(a). In this case, the ground state is that of all three wells being singly occupied. In this case, the second-order correlation function acquires a simple expression

$$\begin{aligned}
{}^2\mathcal{G}_1^{b,+\infty}(k_1, k_2) &= \frac{2}{3\pi} s^2 e^{-2(k_1^2+k_2^2)s^2} \\
&\times \{3 + 2 \cos[d(k_1 - k_2)] + \cos[2d(k_1 - k_2)]\}. \quad (33)
\end{aligned}$$

It is interesting to note that the second-order correlation function for three fermions with parallel spins trapped in three

wells in the limit $\mathcal{U} \rightarrow +\infty$ is given by the same expression as that in Eq. (33), but with the 2 and 1 coefficients in front of the $\cos[d(k_1 - k_2)]$ and $\cos[2d(k_1 - k_2)]$ terms being replaced by their negatives, -2 and -1 , respectively (see Eq. (9) and Table I (row for $i = 3$) in Ref. [20]). This naturally is a reflection of the different quantum statistics between bosons and fermions.

Figure 6 illustrates for the first-excited state the \mathcal{U} evolution of the second-order correlation maps described by expression (31) when $i = 2$. The maps for five specific values of \mathcal{U} are plotted, namely, $\mathcal{U} = -200, -10, 0, 10, \text{ and } 200$.

B. The first excited state (state denoted as $i = 2$ for $-\infty < \mathcal{U} < +\infty$)

For $\mathcal{U} \rightarrow -\infty$, only the constant term, $\mathcal{B}_0^2 = 2/\pi$, survives; the corresponding state is a NOON state of the form $(-|300\rangle + |003\rangle)/\sqrt{2}$. In this case, the second-order correlation function is again

$${}^2\mathcal{G}_2^{b,-\infty}(k_1, k_2) = \frac{2}{\pi} s^2 e^{-2(k_1^2+k_2^2)s^2}. \quad (34)$$

In the noninteracting case ($\mathcal{U} = 0$), for which the Hubbard eigenvector is given by Eq. (14), 10 cosinusoidal terms and seven distinct coefficients (listed in Table III) are present in Eq. (31), in agreement with Fig. 5(b).

For $\mathcal{U} \rightarrow +\infty$, all 13 sinusoidal terms survive in expression (31); the corresponding state is given by the first expression in Eq. (10). For this case, we give the nine distinct coefficients in Table IV.

These results are in agreement with the \mathcal{U} dependence portrayed in Fig. 5(b).

For a description of the remaining eight excited states, see Appendix F.

VIII. FIRST-ORDER MOMENTUM CORRELATIONS FOR THREE BOSONS IN THREE WELLS AS A FUNCTION OF THE STRENGTH OF THE INTERACTION \mathcal{U}

The first-order correlations are obtained through an integration of the second-order ones [see Eq. (31)] over the second momentum variable k_2 , i.e.,

$${}^1\mathcal{G}_i^b(k) = \int_{-\infty}^{\infty} {}^2\mathcal{G}_i^b(k, k_2) dk_2, \quad (35)$$

with $i = 1, \dots, 10$.

Exploiting the computational abilities of MATHEMATICA and neglecting terms that vanish as $e^{-\gamma d^2/s^2}$ (for arbitrary $\gamma > 0$ and $d^2/s^2 \gg 1$), one can find that the first-order correlations are given by the following general expression:

$${}^1\mathcal{G}_i^b(k) = s e^{-2k^2 s^2} \{ \mathcal{A}_0^i + \mathcal{A}_1^i \cos(dk) + \mathcal{A}_2^i \cos(2dk) \}. \quad (36)$$

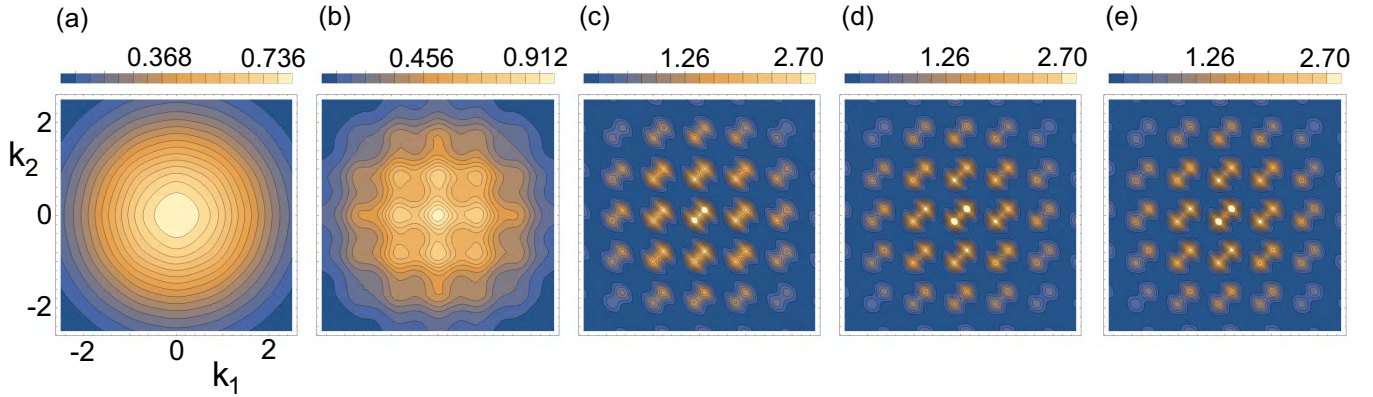


FIG. 6. Second-order momentum correlation maps for the first-excited state of three bosons in three wells [see Eq. (31) with $i = 2$]. (a) $\mathcal{U} = -200$. (b) $\mathcal{U} = -10$. (c) $\mathcal{U} = 0$. (d) $\mathcal{U} = 10$. (e) $\mathcal{U} = 200$. Parameters are interwell distance $d = 7 \mu\text{m}$ and spectral width of single-particle distribution in momentum space [see Eq. (20)] the inverse of $s = 0.35 \mu\text{m}$. The correlation functions ${}^2\mathcal{G}_i^b(k_1, k_2)$ (map landscapes) are given in units of μm^2 according to the color bars on top of each panel, and the momenta k_1 and k_2 are in units of $1/\mu\text{m}$. The value of the plotted correlation functions was multiplied by a factor of 10 to achieve better contrast for the map features.

$\mathcal{A}_0^i = \sqrt{2/\pi} \approx 0.797885$ above is \mathcal{U} independent for all ten eigenstates. The remaining two coefficients in Eq. (36), \mathcal{A}_1^i and \mathcal{A}_2^i , are \mathcal{U} dependent for nine out of the ten eigenstates. These \mathcal{U} -dependent \mathcal{A} coefficients for the two lowest-in-energy eigenstates are plotted as a function of \mathcal{U} in Fig. 7. The corresponding explicit numerical values can be found in a data file included in the Supplemental Material [67].

A. The ground state (state denoted as $i = 1$ for $-\infty < \mathcal{U} < +\infty$)

For the strong interatomic attraction limit $\mathcal{U} \rightarrow -\infty$, it is seen from Fig. 7(a) that only the constant coefficient \mathcal{A}_0^1 survives in expression (36); i.e., the first-order correlation (single-particle density) in momentum space is devoid of any oscillatory structure, being given simply by a Gaussian distribution function,

$${}^1\mathcal{G}_1^{b,-\infty}(k) = \sqrt{\frac{2}{\pi}} s e^{-2k^2 s^2}. \quad (37)$$

This structureless distribution corresponds to a photonic triple-slit experiment where Young's [68] "which way" question, related to the source of the particle detected with a time-of-flight measurement, can be answered with a 100% certainty as being one single well (zero quantum fluctuations in the single-particle occupation number per site). Indeed, the corresponding ground-state Hubbard eigenvector is given by $\phi_1^{b,-\infty}$ [second expression in Eq. (9)] which contains only one triply occupied component from the primitive kets listed in Eq. (1), i.e., the basis ket no. 9 $\rightarrow |030\rangle$.

For the noninteracting case ($\mathcal{U} = 0$), all three coefficients survive [see Fig. 7(a)]; specifically one has

$${}^1\mathcal{G}_1^{b,\mathcal{U}=0}(k) = \sqrt{\frac{2}{\pi}} s e^{-2k^2 s^2} \left[1 + \sqrt{2} \cos(dk) + \frac{1}{2} \cos(2dk) \right]. \quad (38)$$

Expression (38) exhibits a highly oscillatory interference pattern. It corresponds to the ground state given by the Hubbard eigenvector in Eq. (13), which is often described as a bosonic superfluid. Indeed, the quantum fluctuations in the single-particle occupation number per site are strongest and the single-particle bosonic orbitals are maximally delocalized over all three sites.

For the strong interatomic repulsion limit $\mathcal{U} \rightarrow +\infty$, it is seen from Fig. 7(a) that again only the \mathcal{U} -independent coefficient \mathcal{A}_0^1 survives in expression (36); i.e., the first-order correlation (single-particle density) in momentum space is devoid of any oscillatory structure, being given simply by a Gaussian distribution function like in Eq. (37), i.e.,

$${}^1\mathcal{G}_1^{b,+\infty}(k) = {}^1\mathcal{G}_1^{b,-\infty}(k). \quad (39)$$

Again, this structureless distribution corresponds to a photonic triple-slit experiment where Young's [68] "which way" question, related to the source of the particle detected with a time-of-flight measurement, can be answered with a 100% certainty as being one single well (zero quantum fluctuations in the single-particle occupation number per site). Indeed, the corresponding ground-state Hubbard eigenvector is given by $\phi_1^{b,+\infty}$ [first expression in Eq. (9)] which contains only the singly occupied component from the primitive kets listed in Eq. (1), i.e., the basis ket no. 1 $\rightarrow |111\rangle$. The implications

TABLE III. The seven distinct coefficients at $\mathcal{U} = 0$ present in Eq. (31) in the case of the first-excited state.

$\mathcal{B}_0^{2,\mathcal{U}=0}$	$\mathcal{B}_1^{2,\mathcal{U}=0}$	$\mathcal{B}_2^{2,\mathcal{U}=0}$	$\mathcal{B}_{1-1}^{2,\mathcal{U}=0}$	$\mathcal{B}_{2-2}^{2,\mathcal{U}=0}$	$\mathcal{B}_{2-1}^{2,\mathcal{U}=0}$	$\mathcal{B}_{1+1}^{2,\mathcal{U}=0}$	$\mathcal{B}_{2+2}^{2,\mathcal{U}=0}$	$\mathcal{B}_{2+1}^{2,\mathcal{U}=0}$
$2/\pi = 0.63662$	$4\sqrt{2}/\pi = 0.60021$	0	$4/(3\pi) = 0.42441$	$1/(12\pi) = 0.026526$	$1/(3\sqrt{2}\pi) = 0.075026$	0	$-7/(12\pi) = -0.185681$	$-1/(\sqrt{2}\pi) = -0.22508$

TABLE IV. The nine distinct coefficients at $\mathcal{U} \rightarrow +\infty$ present in Eq. (31) in the case of the first-excited state.

$\mathcal{B}_0^{2,+\infty}$	$\mathcal{B}_1^{2,+\infty}$	$\mathcal{B}_2^{2,+\infty}$	$\mathcal{B}_{1-1}^{2,+\infty}$	$\mathcal{B}_{2-2}^{2,+\infty}$	$\mathcal{B}_{2-1}^{2,+\infty}$	$\mathcal{B}_{1+1}^{2,+\infty}$	$\mathcal{B}_{2+2}^{2,+\infty}$	$\mathcal{B}_{2+1}^{2,+\infty}$
$2/\pi$	$2\sqrt{5}/(3\pi)$	$-2/(5\pi)$	$26/(15\pi)$	$2/(15\pi)$	$2/(3\sqrt{5})$	$-4/(5\pi)$	$-1/(3\pi)$	$-2/(\sqrt{5}\pi)$

of the above results encoded in Eqs. (37), (38), and (39) regarding phase transitions will be discussed below in Sec. IX.

B. The first excited state (state denoted as $i = 2$ for $-\infty < \mathcal{U} < +\infty$)

For $\mathcal{U} \rightarrow -\infty$, it is seen from Fig. 7(b) that only the constant coefficient \mathcal{A}_0 survives in expression (36); i.e., the first-order correlation (single-particle density) in momentum

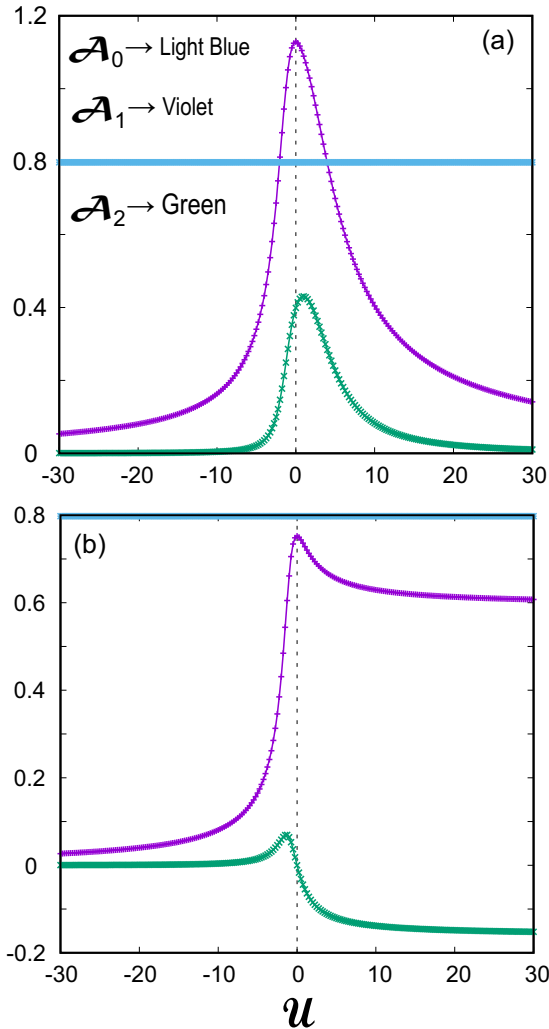


FIG. 7. The \mathcal{A} coefficients (dimensionless) [see Eq. (36)] for the two lowest-in-energy eigenstates of three bosons trapped in three linear wells as a function of the interaction strength \mathcal{U} (dimensionless). (a) Ground state ($i = 1$). (b) First-excited state ($i = 2$). See text for a detailed description. The choice of online colors is as follows: \mathcal{A}_0 , constant (light blue); \mathcal{A}_1 , violet; \mathcal{A}_2 , green. For the print grayscale version, excluding the top constant \mathcal{A}_0 horizontal line, the positioning of the two remaining curves in both frames is $\mathcal{A}_1 \rightarrow$ upper curve and $\mathcal{A}_2 \rightarrow$ lower curve. For a description of the remaining eight excited states, see Appendix G.

space is devoid of any oscillatory structure, being given simply by a Gaussian distribution function,

$${}^1\mathcal{G}_2^{b,-\infty}(k) = \sqrt{\frac{2}{\pi}} s e^{-2k^2 s^2}. \quad (40)$$

In this case, this structureless distribution does not correspond to zero quantum fluctuations in the single-particle occupation number per site (see detailed discussion in Sec. IX below). Indeed, the corresponding Hubbard eigenvector is given by $\phi_2^{b,-\infty}$ [second expression in Eq. (10)], which is a NOON state spread over two sites; i.e., it is a superposition of the two basis kets no. 8 \rightarrow $|300\rangle$ and no. 10 \rightarrow $|003\rangle$.

For the noninteracting case ($\mathcal{U} = 0$), two coefficients survive [see Fig. 7(b)]; specifically one has

$${}^1\mathcal{G}_2^{b,\mathcal{U}=0}(k) = \sqrt{\frac{2}{\pi}} s e^{-2k^2 s^2} \left\{ 1 + \frac{2\sqrt{2}}{3} \cos(dk) \right\}. \quad (41)$$

Expression (41) exhibits a highly oscillatory interference pattern. It corresponds to the state given by the Hubbard eigenvector in Eq. (14).

For $\mathcal{U} \rightarrow +\infty$, all three coefficients survive [see Fig. 7(b)], one of them being negative; specifically one has

$${}^1\mathcal{G}_2^{b,+\infty}(k) = \sqrt{\frac{2}{\pi}} s e^{-2k^2 s^2} \left\{ 1 + \frac{\sqrt{5}}{3} \cos(dk) - \frac{1}{5} \cos(2dk) \right\}. \quad (42)$$

Expression (42) exhibits a highly oscillatory interference pattern. It corresponds to the state given by the Hubbard eigenvector in the first expression of Eq. (10), which consists exclusively of double-single occupancy components [basis kets no. 2 to no. 7; see Eq. (1)].

Figure 8 illustrates for the first-excited state the \mathcal{U} evolution of the first-order correlations described by expression (36) when $i = 2$. The cases for five characteristic values of \mathcal{U} are plotted, namely, $\mathcal{U} = -200, -10, 0, 10,$ and 200 .

For a description of the remaining eight excited states, see Appendix G.

IX. SIGNATURES OF EMERGENT QUANTUM PHASE TRANSITIONS

The system of three bosons in three wells is a building block of bulk-size systems containing a large number of bosons (e.g., ^{87}Rb or $^4\text{He}^*$ atoms) in three (3D), two (2D), and one (1D) dimensional optical lattices. Such bulklike systems have been available already for some time and several physical aspects of them have been explored experimentally [6–10,69], accompanied by theoretical studies [32,33]. In particular, of direct interest to this paper are the observations, obtained through time-of-flight measurements, of the superfluid to Mott insulator phase transition [6–10] (in 3D lattices) and of the second-order particle interference [69] (in 1D lattices), in

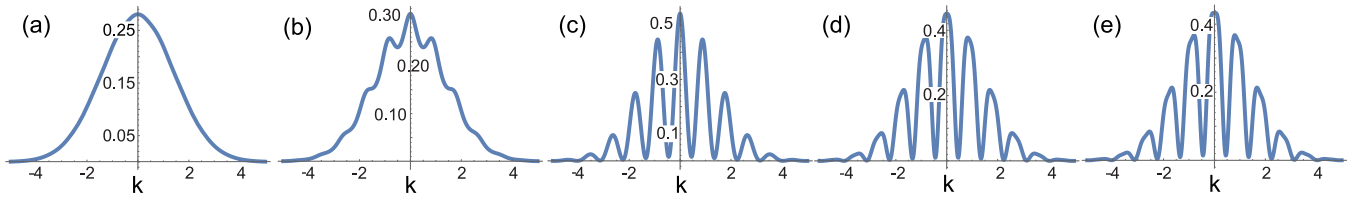


FIG. 8. First-order momentum correlation plots for the first-excited state of three bosons in three wells. From left to right: (a) $\mathcal{U} = -200$, (b) $\mathcal{U} = -10$, (c) $\mathcal{U} = 0$, (d) $\mathcal{U} = 10$, and (e) $\mathcal{U} = 200$ [see Eq. (36) with $i = 2$]. The correlation functions ${}^1\mathcal{G}_i^b(k)$ (vertical axes) are given in units of μm , and the momenta k are in units of $1/\mu\text{m}$. Parameters are interwell distance $d = 7 \mu\text{m}$ and width of single-particle distribution in momentum space [see Eq. (20)] being the inverse of $s = 0.35 \mu\text{m}$.

analogy with a quantal extension of Hanbury Brown–Twiss type of optical interference.

The detailed algebraic analysis of all-order correlations presented earlier for the system of three bosons in three wells provides the tools for exploring these major physical aspects (quantum phase transitions and quantum-optics analogies) in the context of a finite-size system. In this respect, it is a first step toward the deciphering of the evolution of these aspects as the system size increases from a few particles to the thermodynamic limit. In this section, we analyze the signatures for quantum phase transitions that appear already in the case of a finite system as small as three bosons.

We begin by collecting in a single figure (Fig. 9) and for the ground state of the three bosons–three wells (3b-3w) systems all three levels of correlations as a function of the interaction strength \mathcal{U} (with $\mathcal{U} = -200, -10, 0, 10$, and 300). For large \mathcal{U} ($\mathcal{U} = 300$, describing very strong repulsive interparticle interaction), the system’s ground-state Hubbard eigenvector is very close to the single ket no. 1 $\rightarrow |111\rangle$ [see $\phi_1^{b,+\infty}$ in Eq. (9)] which describes exclusively singly occupied sites. For three bosons in three wells, the state $|111\rangle$ is the analog of the Mott insulator phase, familiar from bulk systems. The associated three-body wave function is well approximated by the permanent $\Phi_1^{b,+\infty}(k_1, k_2, k_3)$ [see Eq. (23)] formed from the three localized orbitals $\psi_j(k)$ in Eq. (20).

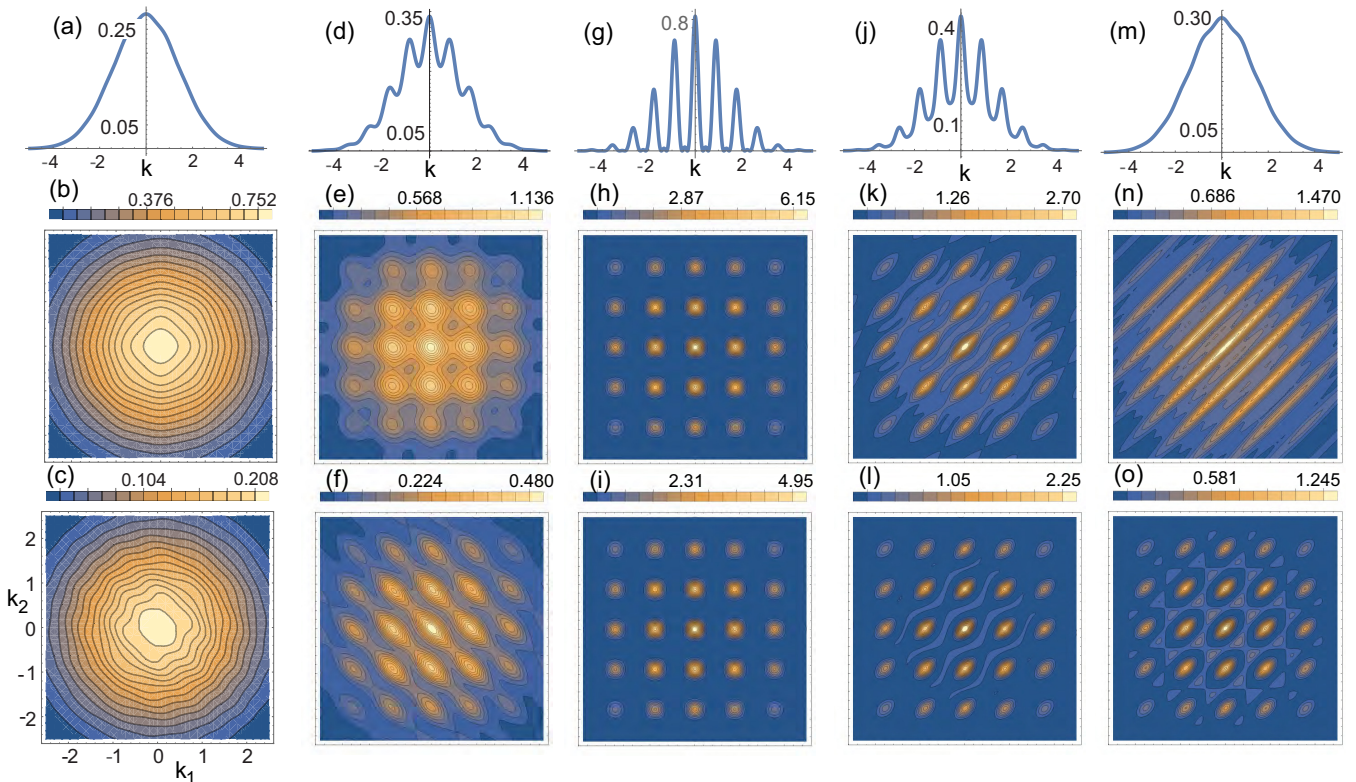


FIG. 9. Momentum correlation plots and maps for the ground state of three bosons in three wells. Top row [(a), (d), (g), (j), (m)]: first-order correlations ${}^1\mathcal{G}_i^b(k)$ (vertical axes) in units of μm . Middle row [(b), (e), (h), (k), (n)]: second-order correlations ${}^2\mathcal{G}_i^b(k_1, k_2)$ in units of μm^2 according to the color bars on top of each panel. Bottom row [(c), (f), (i), (l), (o)]: third-order (cuts at $k_3 = 0$) correlations ${}^3\mathcal{G}_i^b(k_1, k_2, k_3 = 0)$ in units of μm^3 according to the color bars on top of each panel. The momenta k , k_1 , and k_2 are in units of $1/\mu\text{m}$. From left to right column: $\mathcal{U} = -200, -10, 0, 10$, and 300 [see Eqs. (36) and (31) with $i = 1$, as well as Eqs. (22) and (29) with $i = 1$]. Parameters are interwell distance $d = 7 \mu\text{m}$ and spectral width of single-particle distribution in momentum space [see Eq. (20)] being the inverse of $s = 0.35 \mu\text{m}$. The value of the plotted correlation functions in the bottom two rows was multiplied by a factor of 10 to achieve better contrast for the map features.

A crucial observation is that the corresponding single-particle momentum density (first-order correlation) portrayed in Fig. 9(m) (in top row) is structureless and devoid of any oscillatory pattern, in contrast to fully developed oscillations present in the single-particle density of the noninteracting ground state [see Fig. 9(g)]. As was the case with the bulk systems, this structureless pattern in the first-order correlation can thus be used as a signature of the Mott insulator even in the case of a small system.

In analogy with the interpretation for bulk systems, the appearance of oscillations in the noninteracting case can be associated with the spreading of the single-particle orbitals over all the three sites (three wells). Namely, for $\mathcal{U} = 0$, the lowest energy single-particle wave function of the tight-binding Hamiltonian (in matrix representation)

$$H_{b,\text{TB}}^{\text{sp}} = -J \begin{pmatrix} 0 & 1 & 0 \\ 1 & 0 & 1 \\ 0 & 1 & 0 \end{pmatrix} \quad (43)$$

is a molecular orbital which is expressed as a coherent linear superposition of all three localized atomic orbitals $\psi_j(k)$ [with $j = 1, 2, 3$, see Eq. (20)], namely

$$\begin{aligned} \psi_{\text{MO}}(k) &= \frac{\psi_1(k)}{2} + \frac{\psi_2(k)}{\sqrt{2}} + \frac{\psi_3(k)}{2} \\ &= \frac{2^{1/4} \sqrt{s}}{\pi^{1/4}} e^{-k^2 s^2} \left(\frac{e^{-idk}}{2} + \frac{1}{\sqrt{2}} + \frac{e^{idk}}{2} \right). \end{aligned} \quad (44)$$

Then the three-body wave function is constructed by triply occupying this molecular orbital; i.e., it is given by the Bose-Einstein-condensate product

$$\Phi_1^{b,\mathcal{U}=0}(k_1, k_2, k_3) = \psi_{\text{MO}}(k_1) \psi_{\text{MO}}(k_2) \psi_{\text{MO}}(k_3). \quad (45)$$

Equation (45) above equals expression (26) derived by us earlier (see Sec. V) as the $\mathcal{U} = 0$ limit of the solution of the Bose-Hubbard Hamiltonian [Eq. (2)], obtained through the matrix representation [Eq. (3)] in the 10-ket basis [Eq. (1)] for the problem of three bosons trapped in three wells.

Because of the molecular orbital in Eq. (44), which expresses the delocalization of the single-particle wave functions over the whole system, the three-body wave function $\Phi_1^{b,\mathcal{U}=0}(k_1, k_2, k_3)$ can be characterized as describing a superfluid phase in analogy with the bulk case [6,70]. The natural difference of course is that in the bulk case the superfluid to Mott insulator transition happens abruptly at $\mathcal{U} = z \times 5.8$ [70], with z being the number of next neighbors of a lattice site, whereas for the small finite system this transition is not sharp but proceeds continuously as a function of \mathcal{U} . Some steps of this smooth evolution are illustrated in Figs. 9(g) ($\mathcal{U} = 0$), 9(j) ($\mathcal{U} = 10$), and 9(m) ($\mathcal{U} = 300$).

Furthermore, another aspect from the bulk studies that is relevant to our three-boson results is the determination, made deeply in the Mott insulator region, of a small oscillatory contribution to the single-particle density superimposed on the structureless background [7,8,32,33]. This contribution [71] was found to vary as $\propto -2 \sum_{v=x,y,z} \cos(k_v d) / \mathcal{U}$, as obtained via perturbative (or related) approaches around $\mathcal{U} \rightarrow +\infty$. Our exact algebraic expression for ${}^1\mathcal{G}_i^b(k)$ [Eq. (36)], which is valid for any \mathcal{U} , contains a second term $\cos(2dk)$ in addition to the $\cos(dk)$ term. Deeply in the Mott-insulator regime,

however, there is agreement at the qualitative level between our result and the bulk one, because the coefficient \mathcal{A}_2^1 vanishes much more quickly than the coefficient \mathcal{A}_1^1 as $\mathcal{U} \rightarrow +\infty$ as is revealed by an inspection of the curves in Fig. 7(a).

At the noninteracting limit ($\mathcal{U} = 0$), however, this second term cannot be neglected [see Fig. 7(a) and Eq. (38)]. In this limit, its effect is to narrow the width of the cosinusoidal peaks at $k = 2\pi j/d$, with $j = 0, 1, 2, \dots$. From this, one can conjecture [72] that for larger systems with N bosons, all cosine terms of the form $\cos(ndk)$ with $n = 1, 2, 3, \dots, N-1$ (corresponding to all possible interwell distances) will contribute. The summation of many of such terms will enhance further the shrinking of the width of the main peaks, while it will give a practically vanishing result in the in-between regions. Thus, the main peaks will acquire the shape of sharp spikes as was indeed observed [6] in the bulk systems.

In the present paper, we cover the full range of interaction strengths, from infinite attraction ($\mathcal{U} \rightarrow -\infty$) to infinite repulsion ($\mathcal{U} \rightarrow +\infty$). Following the sequence of frames from the third to the first frame in Fig. 9 (top row), it is seen that a structureless single-particle momentum density emerges also in the limit $\mathcal{U} \rightarrow -\infty$; for intermediate negative values of \mathcal{U} , the weight of the oscillatory pattern decreases gradually as the absolute value $|\mathcal{U}|$ increases. However, based on our full solution of the 3b-3w Hubbard system, it is apparent that this succession (i.e., from the third to the first frame of Fig. 9) does not reflect a transition from a superfluid to a Mott insulator phase. Indeed, the Hubbard ground-state eigenvector for $\mathcal{U} \rightarrow -\infty$ is given by $\phi_1^{b,-\infty}$ in the second expression of Eq. (9), which can properly be characterized as a Bose-Einstein condensate; namely, this ground state consists only of a single basis ket (no. 9 \rightarrow |030>) that represents a triply occupied atomic orbital $\psi_2(k)$ [see Eq. (20)] located in the middle well.

The caveat from the discussion above is that the first-order correlation does not uniquely characterize the associated many-body state. This is not an uncommon occurrence, as can be also seen from an inspection of Fig. 8, which illustrates a succession of ${}^1\mathcal{G}_2^b(k)$'s for the first excited state. Indeed, the single-particle momentum density in in Fig. 8(a) (case of $\mathcal{U} = -200$) is structureless; however, the corresponding Hubbard eigenvector is very well approximated by $\phi_2^{b,-\infty}$ in the second expression of Eq. (10). Naturally, this eigenvector represents a many-body state that is neither a Mott insulator nor a Bose-Einstein condensate. Rather it represents a $(-|300\rangle + |003\rangle)\sqrt{2}$ NOON state; the family of NOON states are a focal point in quantum-optics investigations [73,74].

For a complete characterization of the many-body state under consideration, additional information, beyond the first-order correlations, is needed. A natural candidate to this effect are the maps for the second-order (Sec. VII) and third-order (Sec. VI) correlations investigated earlier. For example, in the case of the structureless single-particle momentum density cases discussed above [i.e., Figs. 9(m) (top row), 9(a) (top row), and 8(a)], all three corresponding third-order correlation maps are drastically different [compare Figs. 9(c) (bottom row), Fig. 9(o) (bottom row), and Fig. 4(a)].

Note that the information provided by second-order correlation maps only is still not sufficient for the full characterization of the underlying many-body state. Indeed, the

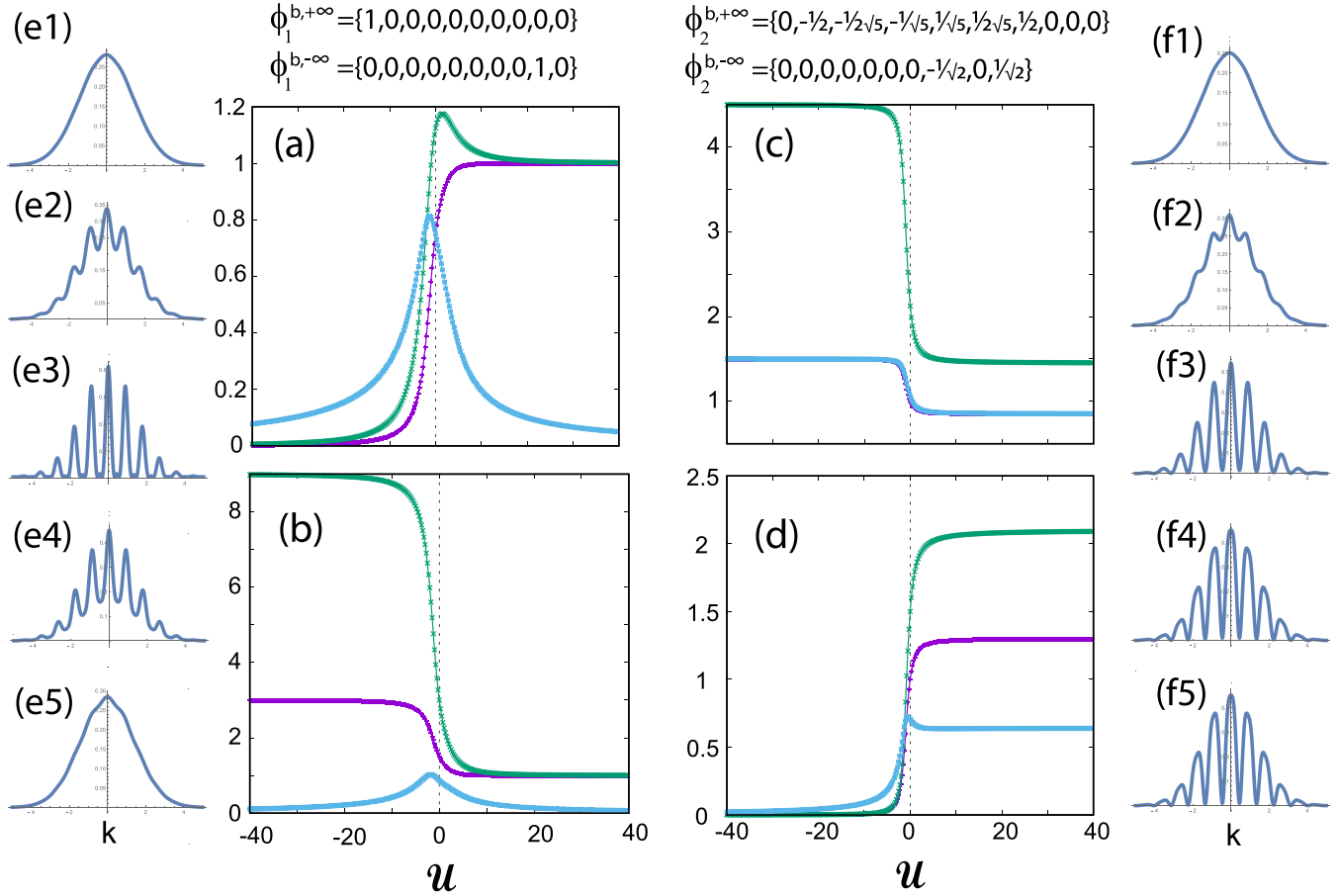


FIG. 10. [(a)–(d)] Site occupations (vertical axes, dimensionless) and their fluctuations (vertical axes, dimensionless) for the ground, $\phi_1^b(\mathcal{U})$ [(a), (b)], and first-excited, $\phi_2^b(\mathcal{U})$ [(c), (d)], states as a function of the strength \mathcal{U} of the interaction. Panels (a) and (c) refer to the left site (well), whereas panels (b) and (d) refer to the middle site (well). Violet color (middle curve at $\mathcal{U} = +40$): site occupations. Green color (upper curve at $\mathcal{U} = +40$): expectation value of the square of the site number operator. Light blue color (lower curve at $\mathcal{U} = +40$): standard deviation. Note that the middle and lower curves in frame (c) coincide for all practical purposes. The panels (e) and (f) show the first-order correlations for the ground (e1–e5) and first-excited (f1–f5) states, respectively, for five characteristic values: $\mathcal{U} = -200$ ($x = 1$) (close to $\rightarrow -\infty$), -10 ($x = 2$), 0 ($x = 3$), 10 ($x = 4$), and 300 ($x = 5$) (close to $\rightarrow +\infty$). The first-order correlations ${}^1\mathcal{G}^b(k)$ (vertical axes) are in units of μm and the momenta k are in units of $1/\mu\text{m}$. Parameters for the correlations are interwell distance $d = 7 \mu\text{m}$ and spectral width of single-particle distribution in momentum space [see Eq. (20)] being the inverse of $s = 0.35 \mu\text{m}$.

second-order correlation maps in Fig. 9(b) (second row) (case of the ground state at $\mathcal{U} = -200$) is very similar to that in Fig. 6(a) (case of the first-excited state at $\mathcal{U} = -200$).

We stress again at this point that Figs. 4, 6, 8, and 9 illustrate graphically the ability of our methodology to determine all three levels of momentum correlations and their evolution as a function of the interaction strength \mathcal{U} , from the attractive to the repulsive regime, and thus to provide the tools for a complete characterization of the underlying many-body states.

Before leaving this section, we found it worthwhile to explicitly investigate the conjecture that vanishing fluctuations in the site occupations are always associated with a structureless first-order momentum correlation. To this effect, we plot in Fig. 10 the site occupation, $\langle \phi_j^b(\mathcal{U}) | n_i | \phi_j^b(\mathcal{U}) \rangle$ [the site number operator $n_i = \hat{b}_i^\dagger \hat{b}_i$; see below Eq. (2)], the expectation value of the square of the site num-

ber operator, $\langle \phi_j^b(\mathcal{U}) | n_i^2 | \phi_j^b(\mathcal{U}) \rangle$, and the standard deviation, $\sqrt{\langle \phi_j^b(\mathcal{U}) | n_i^2 | \phi_j^b(\mathcal{U}) \rangle - \langle \phi_j^b(\mathcal{U}) | n_i | \phi_j^b(\mathcal{U}) \rangle^2}$ for the ground ($j = 1$) and first-excited ($j = 2$) states and for the left ($i = 1$) and middle ($i = 2$) sites (wells). As already noted in the introductory section of this paper, the connection between the fluctuations in site occupation and the appearance of structural patterns (or the lack thereof) in the first-order momentum correlations is a manifestation of the connection between the quantum phase-transition from superfluid (coherent) to localized (incoherent) states, and the quantum uncertainty relation connecting the fluctuations in phase and number (site occupancy).

From an inspection of Figs. 10(a)–10(d), one concludes that indeed in all four panels an oscillatory pattern in the single-particle momentum density [see Figs. 10(e2)–10(e4) and 10(f2)–10(f5)] is accompanied by a nonvanishing fluctuation in the site occupations. However, a structureless single-particle momentum density is not always associated with a

vanishing fluctuation; see the case of the NOON state $\phi_2^{b,-\infty}$ [Fig. 10(c)] for which the standard deviation of the left well is $3/2$, whereas the corresponding single-particle momentum density [Fig. 10(f1)] is structureless.

Finally, we mention that temperature effects on the quantum phase transitions in bosonic gases trapped in optical lattices have recently attracted some attention (see, e.g., Refs. [75,76]). Our beyond-mean-field theoretical approach can be generalized [72] to account for such effects, but this falls outside the scope of the present paper.

X. ANALOGIES WITH THREE-PHOTON INTERFERENCE IN QUANTUM OPTICS

In this section, we elaborate on the analogies between our results for the system of three massive bosons trapped in three wells with the three-photon interference in quantum optics, which is an area of frontline research activities [37,38,40,47–49,51,77]. Such three-photon interference investigations fall into two major categories: (1) The first category is those that employ a tritter [78] to produce a scattering event between three photons impinging on the input ports of a tritter and which measure coincidence probabilities for the photons exiting the three output ports [47–49,51,77]. At the abstract theoretical level, the scattering event is described by a unitary scattering matrix. The coincidence probabilities are denoted as P_{111} (one photon in each one of the output ports), P_{210} (two photons in the first port and a single photon in the second port), P_{300} (three photons in the first port), etc., and they are apparently a direct generalization of the P_{11} and P_{20} coincidence probabilities familiar from the celebrated HOM [41] two-photon interference experiment. Variations in the P_{ijk} , with $i, j, k = 0, 1, 2, 3$ and $i + j + k = 3$ probabilities are achieved through control of the time delays between photons and other parameters of the tritter. (2) The second category is those that resolve the intrinsic conjugate variables underlying the wave packets of the impinging photons on the tritter (i.e., frequency, ω , and time delay, τ) [37,38,40]; for earlier two-photon interference investigations in this category, see Refs. [34–36]. This category of experiments produces spectral correlation landscapes as a function of the three frequencies ω_1, ω_2 , and ω_3 .

In the case of the three bosons in three wells, the quantum-optics category (1) above finds an analog to *in situ* experiments and their theoretical treatments. Indeed, the analogs of the three-photon wave function in the output ports are the vector solutions [stationary or time-dependent (not considered in this paper)] of the Hubbard Hamiltonian matrix in Eq. (3); compare the general form of the Hubbard vector solutions [Eq. (7) in Sec. II] to Eq. (5) for the three-photon output state from a tritter in Ref. [47]. Control of these Hubbard vector solutions is achieved through variation of the interaction parameter \mathcal{U} and the choice of a ground or excited state. For example, choosing the ground-state vector, the probability for finding only one boson in each well is given by the modulus square of the \mathcal{U} -dependent coefficient in the Hubbard eigenvector [Eq. (7)] in front of the basis ket no. $1 \rightarrow |111\rangle$, i.e., $P_{111}(\mathcal{U}) = |\mathbf{c}_{111}(\mathcal{U})|^2$; naturally $P_{030}(\mathcal{U}) = |\mathbf{c}_{030}(\mathcal{U})|^2$.

In Fig. 11, we plot the $P_{111}(\mathcal{U})$ and $P_{030}(\mathcal{U})$ probabilities associated with the Hubbard ground-state eigenvector $\phi_1^b(\mathcal{U})$.

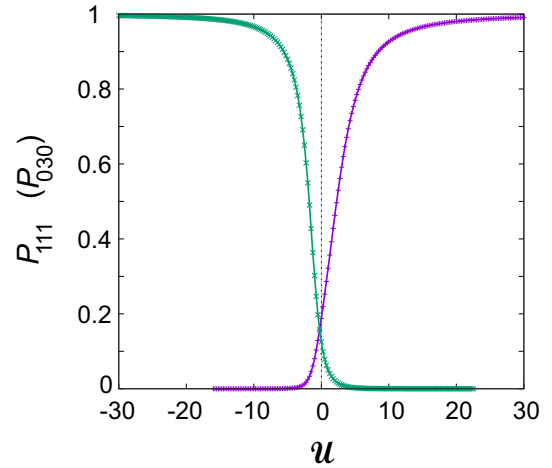


FIG. 11. The (dimensionless) Hong-Ou-Mandel-type probabilities P_{111} (violet, right curve) and P_{030} (green, left curve) associated with the Hubbard ground-state vector $\phi_1^b(\mathcal{U})$ as a function of the interaction strength \mathcal{U} (dimensionless).

This figure is reminiscent of Fig. 2 in Ref. [77] (see also Fig. 3 in Ref. [47]). It is interesting to note that the three-photon state $|300\rangle$ (experimentally realized in Ref. [77]) is described in quantum optics as a “three-photon bosonic coalescence,” whereas for atomic and molecular physics a description as a micro-Bose-Einstein condensate appears to come naturally in mind.

Note, further, that the P_{ijk} 's in Ref. [77] depend on two parameters, instead of a single one. For the case of three massive bosons in three wells, a second parameter becomes relevant by considering the time evolution of the Hubbard vector solutions [72]; see Refs. [15,26] for the consideration of the time evolution in the case of two massive bosons in two wells. Note further that, in quantum optics, two fully overlapping photons are described as perfectly *indistinguishable*, whereas two nonoverlapping photons are described as perfectly *distinguishable* [51,77]. In the context of the present study for three massive trapped bosons (which uses the assumption $d^2/s^2 \gg 1$), an example of the former is the ket no. $9 \rightarrow |030\rangle$, whereas an example of the latter is the ket no. $1 \rightarrow |111\rangle$. A double-single occupancy ket, like ket no. $2 \rightarrow |210\rangle$, can be referred to as a mode with two indistinguishable and one distinguishable bosons [51].

The analogy between the two-photon optical HOM formalism and the vector solutions of the Hubbard theoretical modeling for two bosons (or two fermions) in two wells was reported earlier in Refs. [14,15]

Furthermore, in the case of the three bosons in three wells, the quantum-optics category (2) above finds an analog to time-of-flight experiments and their theoretical treatments. This analogy derives from the following correspondence (revealed in Ref. [15]):

$$\begin{aligned} k &\longleftrightarrow \omega/c, \\ d &\longleftrightarrow \tau c, \\ kd &\longleftrightarrow \omega\tau. \end{aligned} \quad (46)$$

As was done [15] for the case of two massive trapped particles versus two interfering photons, this correspondence

can be used to establish a complete analogy between the cosinusoidal patterns of all three orders of momentum correlation functions presented in this paper for three massive and trapped bosons (and which can be determined experimentally through time-of-flight measurements [4]) with the landscapes [37,38] of the frequency-resolved three-photon interferograms (which are a function of the three photon frequencies, ω_1 , ω_2 , and ω_3). For example, the interferograms in Fig. 3 of Ref. [38] are analogous to the map in Fig. 9(i) (bottom row) of the $k_3 = 0$ cut of the third-order momentum correlation associated with three noninteracting trapped massive bosons. A difference to keep in mind is that in this paper the interwell distances were taken to be equal, whereas the time delays in Ref. [38] are unequal.

Furthermore, Eq. (S1) in the Supplemental Material of Ref. [38], which describes the three-photon output wave function at the detectors, $\psi(\omega_1, \omega_2, \omega_3)$, is a permanent of the three single-photon wave functions $\chi_j(\omega_i) = E_j(\omega_i) \exp(-i\omega_i t_j)$, with $i, j = 1, 2, 3$, where t_j denotes time instances [corresponding to the position of each well in our single-particle orbitals displayed in Eq. (20)]. As a result, for $E_1(\omega_i) = E_2(\omega_i) = E_3(\omega_i) = E(\omega_i)$ and $t_1 = -\tau$, $t_2 = 0$, and $t_3 = \tau$, it reduces exactly to the form of the three-body wave function $\Phi_1^{b,+ \infty}(k_1, k_2, k_3)$ [see top expression in Eq. (23)] in this paper, which is associated with the case of the three singly occupied wells, i.e., the Hubbard solution at infinite repulsion, $|111\rangle$ (perfectly distinguishable bosons).

A central focus in the recent quantum-optics literature has been the demonstration of genuine three-photon interference [48,49], that is, interference effects that cannot be inferred by a knowledge of the one- and two-photon interference patterns. In the language of many-body literature for massive particles, this is equivalent to isolating the *connected* terms, \mathcal{G}_{con} , in the total third-order correlations by subtracting the *disconnected* ones, \mathcal{G}_{dis} . Reflecting its name, the disconnected contribution to the total third-order correlation consists of products of the first- and second-order correlations.

For the case of three perfectly distinguishable bosons in three wells (described by the ket $|111\rangle$), one can observe that the first-order momentum correlation given in Eqs. (39) and (37) does not contain any cosine (or sine) terms, whereas the second-order momentum correlation given in Eq. (33) contains cosine terms with two momenta in the cosine arguments. As a result, the connected part of the third-order momentum correlations [see Eq. (25)] is necessarily reflected in the cosine terms having an argument that depends on all three single-particle momenta k_1 , k_2 , and k_3 . Another way to view the above remarks is that the genuine three-body interference involves a total phase φ which is the sum of three partial phases φ_1 , φ_2 , and φ_3 , associated with the individual bosons, i.e., $\varphi = \varphi_1 + \varphi_2 + \varphi_3$. Such a triple phase (referred to also as a triad phase) has been prominent in the quantum-optics literature [48,49] regarding genuine three-photon interference.

Specifically, the disconnected part of the third-order correlation for three bosons is given by the expression

$$\begin{aligned} {}^3\mathcal{G}_{\text{dis}}^b(k_1, k_2, k_3) &= -2^1 \mathcal{G}^b(k_1) {}^1\mathcal{G}^b(k_2) {}^1\mathcal{G}^b(k_3) \\ &+ {}^1\mathcal{G}^b(k_1) {}^2\mathcal{G}^b(k_2, k_3) + {}^1\mathcal{G}^b(k_2) {}^2\mathcal{G}^b(k_1, k_3) \\ &+ {}^1\mathcal{G}^b(k_3) {}^2\mathcal{G}^b(k_1, k_2). \end{aligned} \quad (47)$$

We can apply the above expression immediately to the case of the Hubbard ground-state eigenvector $|111\rangle$ (limit of infinite repulsion, three perfectly distinguishable bosons), because we have derived explicit algebraic expressions for the corresponding third-order [Eq. (25)], second-order [Eq. (33)], and first-order momentum correlations [Eqs. (39) and (37)]. Indeed, one finds for the connected correlation part

$$\begin{aligned} {}^3\mathcal{G}_{1,\text{con}}^{b,+ \infty}(k_1, k_2, k_3) &= {}^3\mathcal{G}_1^{b,+ \infty}(k_1, k_2, k_3) - {}^3\mathcal{G}_{1,\text{dis}}^{b,+ \infty}(k_1, k_2, k_3) \\ &= \frac{4\sqrt{2}}{3\pi^{3/2}} s^3 e^{-2s^2(k_1^2+k_2^2+k_3^2)} \{ \cos(d(k_1+k_2-2k_3)) \\ &+ \cos(d(k_2+k_3-2k_1)) + \cos(d(k_1+k_3-2k_2)) \}. \end{aligned} \quad (48)$$

It is worth noting that the result in Eq. (48) above for the connected correlation part for three perfectly distinguishable bosons in three wells coincides with the corresponding result [4,20] for three perfectly distinguishable *fully spin-polarized fermions* in three wells.

XI. SUMMARY

In this paper, we develop and expand a formalism and a theoretical framework, which, with the use of an algebraic-language computations tool (MATHEMATICA [57]), allows us to derive explicit analytic expressions for all three orders (third, second, and first) of momentum-space correlations for three interacting ultracold bosonic atoms confined in three optical wells in a linear geometry. This 3b-3w system was modeled as a three-site Bose-Hubbard Hamiltonian whose ten eigenvectors were mapped onto first-quantization three-body wave functions in momentum space by (1) associating the bosons with the Fourier transforms of displaced Gaussian functions centered on each well, and (2) constructing the permanents associated with the basis kets of the Hubbard Hilbert space by using the Fourier transforms of the displaced Gaussians describing the trapped bosons. The third-order momentum-space correlations are the modulus square of such three-body wave functions, and the second- and first-order correlations are derived through successive integrations over the unresolved momentum variables. This methodology applies to all bosonic states with strong [79] or without entanglement, and does not rely on the standard Wick's factorization scheme, employed in earlier studies (see, e.g., Refs. [80–82]) of higher order momentum correlations for expanding or colliding Bose-Einstein condensates of ultracold atoms.

The availability of such explicit analytic correlation functions will greatly assist in the analysis of anticipated future TOF measurements with few ($N > 2$) ultracold atoms trapped in optical lattices, following the demonstrated feasibility of determining higher-than-first-order momentum correlation functions via single-particle detection in the case of $N = 2$ fermionic ${}^6\text{Li}$ atoms [5], $N = 3$ fully spin-polarized fermionic ${}^6\text{Li}$ atoms [4], and a large number of bosonic ${}^4\text{He}^*$ atoms [10].

The availability of the complete set of all-order momentum correlations enabled us to reveal and explore in detail two major physical aspects of the 3b-3w ultracold-atom system: (1) That a small system of only three bosons exhibits

indeed an embryonic behavior akin to an emergent superfluid to Mott transition, and (2) that both the *in situ* and TOF spectroscopies of the 3b-3w system exhibit analogies with the quantum-optics three-photon interference, including the aspects of genuine three-photon interference which cannot be understood from the knowledge of the lower second- and first-order correlations alone [48,49].

The superfluid to Mott-insulator transition in extended optical lattices [6–8] was explored based on the variations in the shape of the first-order momentum correlations. For the 3b-3w system, we reported clear variations of the first-order momentum correlations, from being oscillatory with a period that depends on the interwell distance, characteristic of a coherent state of a superfluid phase with multiple site-occupancies by each of the trapped ultracold bosonic atoms (high site-occupancy uncertainty), to a structureless shape characteristic of localized states (see below) with low site-occupancy uncertainty and consequent high phase uncertainty (incoherent phase). Furthermore, we also concluded that the first-order momentum correlations are not sufficient to characterize uniquely the underlying nature of a state of the 3b-3w system. To this effect, knowledge of all three orders of correlations is needed. Indeed, a structureless first-order correlation relates to three different 3b-3w states, i.e., the $|030\rangle$ ground state at $\mathcal{U} \rightarrow -\infty$ (Bose-Einstein condensate), the $|111\rangle$ ground state at $\mathcal{U} \rightarrow +\infty$ (Mott insulator), and the $(-|300\rangle + |003\rangle)/\sqrt{2}$ first-excited state at $\mathcal{U} \rightarrow -\infty$ (NOON state).

Concerning the quantum optics analogies, we established that *in situ* measurements of the site occupation probabilities as a function of \mathcal{U} , $P_{ijk}(\mathcal{U})$ (with $i, j = 1, \dots, 3$) provide analogs of the celebrated HOM coincidence probabilities for three photons at the output ports of a tritter as discussed in Refs. [47,77]. We further established that the momentum-space all-order correlations for the 3b-3w system parallel the frequency-resolved interferograms of distinguishable photons as explored in Refs. [37,38,40]. The analogies with the genuine three-photon interference were established in the framework of the many-body theoretical concepts of disconnected versus connected correlation terms.

To achieve simplicity in this paper, we assumed throughout that the interwell separation is much larger than the width of the single-particle Gaussian function in the real configuration space, i.e., $d^2/s^2 \gg 1$ (see Sec. IV). This is equivalent to considering localized bosons with vanishing overlaps (distinguishable bosons in different wells) or unity overlaps (indistinguishable bosons in the same well); indeed, the overlap of two single-particle wave functions according to Eq. (20) is given by $S = e^{-d^2/(8s^2)}$. Considering cases with small, but finite S , which represent partial indistinguishability [51], complicates substantially the analytic results [72].

Finally, we note here that our all-order momentum-space correlations for the 3b-3w system can contribute an alternative way to study and explore with massive particles aspects of the boson sampling problem [50], and in particular its extension to the multiboson correlation sampling [52,53]. We note that boson sampling problems have become a major focus (see, e.g., Refs. [51–55]) in quantum-optics investigations because they are considered to be an intermediate step on the road toward the implementation of the quantum computer.

ACKNOWLEDGMENTS

This work has been supported by a grant from the Air Force Office of Scientific Research (AFOSR, USA) under Award No. FA9550-15-1-0519. Calculations were carried out at the GATECH Center for Computational Materials Science.

APPENDIX A: HUBBARD EIGENVECTORS: THE INFINITE REPULSIVE OR ATTRACTIVE INTERACTION ($\mathcal{U} \rightarrow \pm\infty$) LIMIT FOR THE REMAINING EIGHT EXCITED STATES

This Appendix complements Sec. II A by listing without commentary the Hubbard eigenvectors of the remaining eight excited states not discussed in the main text.

$$\phi_3^{b,+\infty} = \left\{ 0, \frac{1}{2}, \frac{1}{2\sqrt{5}}, \frac{1}{\sqrt{5}}, \frac{1}{\sqrt{5}}, \frac{1}{2\sqrt{5}}, \frac{1}{2}, 0, 0, 0 \right\},$$

$$\phi_3^{b,-\infty} = \left\{ 0, 0, 0, 0, 0, 0, 0, \frac{1}{\sqrt{2}}, 0, \frac{1}{\sqrt{2}} \right\}, \quad (\text{A1})$$

$$\phi_4^{b,+\infty} = \left\{ 0, 0, \sqrt{\frac{2}{5}}, -\frac{1}{\sqrt{10}}, -\frac{1}{\sqrt{10}}, \sqrt{\frac{2}{5}}, 0, 0, 0, 0 \right\},$$

$$\phi_4^{b,-\infty} = \left\{ 0, -\frac{1}{2}, -\frac{1}{2\sqrt{5}}, -\frac{1}{\sqrt{5}}, -\frac{1}{\sqrt{5}}, -\frac{1}{2\sqrt{5}}, -\frac{1}{2}, 0, 0, 0 \right\}, \quad (\text{A2})$$

$$\phi_5^{b,+\infty} = \left\{ 0, 0, -\sqrt{\frac{2}{5}}, \frac{1}{\sqrt{10}}, -\frac{1}{\sqrt{10}}, \sqrt{\frac{2}{5}}, 0, 0, 0, 0 \right\},$$

$$\phi_5^{b,-\infty} = \left\{ 0, \frac{1}{2}, \frac{1}{2\sqrt{5}}, \frac{1}{\sqrt{5}}, -\frac{1}{\sqrt{5}}, -\frac{1}{2\sqrt{5}}, -\frac{1}{2}, 0, 0, 0 \right\}, \quad (\text{A3})$$

$$\phi_6^{b,+\infty} = \left\{ 0, -\frac{1}{2}, \frac{1}{2\sqrt{5}}, \frac{1}{\sqrt{5}}, -\frac{1}{\sqrt{5}}, -\frac{1}{2\sqrt{5}}, \frac{1}{2}, 0, 0, 0 \right\},$$

$$\phi_6^{b,-\infty} = \left\{ 0, 0, -\sqrt{\frac{2}{5}}, \frac{1}{\sqrt{10}}, -\frac{1}{\sqrt{10}}, \sqrt{\frac{2}{5}}, 0, 0, 0, 0 \right\}, \quad (\text{A4})$$

$$\phi_7^{b,+\infty} = \left\{ 0, \frac{1}{2}, -\frac{1}{2\sqrt{5}}, -\frac{1}{\sqrt{5}}, -\frac{1}{\sqrt{5}}, -\frac{1}{2\sqrt{5}}, \frac{1}{2}, 0, 0, 0 \right\},$$

$$\phi_7^{b,-\infty} = \left\{ 0, 0, \sqrt{\frac{2}{5}}, -\frac{1}{\sqrt{10}}, -\frac{1}{\sqrt{10}}, \sqrt{\frac{2}{5}}, 0, 0, 0, 0 \right\}, \quad (\text{A5})$$

$$\phi_8^{b,+\infty} = \left\{ 0, 0, 0, 0, 0, 0, 0, \frac{1}{\sqrt{2}}, 0, \frac{1}{\sqrt{2}} \right\},$$

$$\phi_8^{b,-\infty} = \left\{ 0, -\frac{1}{2}, \frac{1}{2\sqrt{5}}, \frac{1}{\sqrt{5}}, \frac{1}{\sqrt{5}}, \frac{1}{2\sqrt{5}}, -\frac{1}{2}, 0, 0, 0 \right\}, \quad (\text{A6})$$

$$\phi_9^{b,+\infty} = \left\{ 0, 0, 0, 0, 0, 0, 0, -\frac{1}{\sqrt{2}}, 0, \frac{1}{\sqrt{2}} \right\},$$

$$\phi_9^{b,-\infty} = \left\{ 0, \frac{1}{2}, -\frac{1}{2\sqrt{5}}, -\frac{1}{\sqrt{5}}, \frac{1}{\sqrt{5}}, \frac{1}{2\sqrt{5}}, -\frac{1}{2}, 0, 0, 0 \right\}, \quad (\text{A7})$$

$$\begin{aligned}\phi_{10}^{b,+\infty} &= \{0, 0, 0, 0, 0, 0, 0, 0, 1, 0\}, \\ \phi_{10}^{b,-\infty} &= \{-1, 0, 0, 0, 0, 0, 0, 0, 0, 0\}.\end{aligned}\quad (\text{A8})$$

APPENDIX B: HUBBARD EIGENVECTORS: THE NONINTERACTING ($\mathcal{U} = 0$) LIMIT FOR THE REMAINING EIGHT EXCITED STATES

Because of the three pairwise degeneracies [see Eq. (12)], care must be used when determining the six eigenvectors 3, 4, 5, 6, 7, and 8 at $\mathcal{U} = 0$. The proper Hubbard eigenvectors listed below were determined by taking the limit $\mathcal{U} \rightarrow 0+$. For the eigenvectors nos. 3, 4, 7, and 8, the associated algebraic formulas are lengthy, and as a result we give below the numerical expressions of these eigenvectors. Eigenvector no. 5 is \mathcal{U} independent:

$$\begin{aligned}\phi_{3r(4l)}^{b,\mathcal{U}=0} &= \{-0.553362, 0.189903, -0.419079, 0.142399, \\ &0.142399, -0.419079, 0.189903, 0.232583, \\ &0.348804, 0.232583\},\end{aligned}\quad (\text{B1})$$

$$\begin{aligned}\phi_{4r(3l)}^{b,\mathcal{U}=0} &= \{-0.079316, 0.346679, 0.165823, -0.205481, \\ &-0.205481, 0.165823, 0.346679, 0.424594, \\ &-0.503325, 0.424594\},\end{aligned}\quad (\text{B2})$$

$$\phi_{5r(6l)}^{b,\mathcal{U}=0} = \phi_5^{b,+\infty} = \phi_6^{b,-\infty}, \quad (\text{B3})$$

$$\phi_{6r(5l)}^{b,\mathcal{U}=0} = \left\{0, 0, \frac{\sqrt{3}}{4}, \frac{\sqrt{3}}{2}, -\frac{\sqrt{3}}{2}, -\frac{\sqrt{3}}{4}, 0, -\frac{\sqrt{5}}{4}, 0, \frac{\sqrt{5}}{4}\right\}, \quad (\text{B4})$$

$$\begin{aligned}\phi_{7r(8l)}^{b,\mathcal{U}=0} &= \{0.553362, -0.189903, -0.419079, 0.142399, \\ &0.142399, -0.419079, -0.189903, 0.232583, \\ &-0.348804, 0.232583\},\end{aligned}\quad (\text{B5})$$

$$\begin{aligned}\phi_{8r(7l)}^{b,\mathcal{U}=0} &= \{0.079316, -0.346679, 0.165823, -0.205481, \\ &-0.205481, 0.165823, -0.346679, 0.424594, \\ &0.503325, 0.424594\}.\end{aligned}\quad (\text{B6})$$

Finally, the remaining two eigenvectors nos. 9 and 10 are given by

$$\begin{aligned}\phi_9^{b,\mathcal{U}=0} &= \left\{0, \frac{1}{2}, -\frac{1}{4\sqrt{2}}, -\frac{1}{2\sqrt{2}}, \frac{1}{2\sqrt{2}}, \frac{1}{4\sqrt{2}}, -\frac{1}{2}, \right. \\ &\left. -\frac{\sqrt{\frac{3}{2}}}{4}, 0, \frac{\sqrt{\frac{3}{2}}}{4}\right\}\end{aligned}\quad (\text{B7})$$

and

$$\begin{aligned}\phi_{10}^{b,\mathcal{U}=0} &= \left\{-\frac{\sqrt{3}}{4}, -\frac{\sqrt{\frac{3}{2}}}{4}, \frac{\sqrt{3}}{8}, \frac{\sqrt{3}}{4}, \frac{\sqrt{3}}{4}, \frac{\sqrt{3}}{8}, -\frac{\sqrt{\frac{3}{2}}}{4}, \frac{1}{8}, \right. \\ &\left. -\frac{1}{2\sqrt{2}}, \frac{1}{8}\right\}.\end{aligned}\quad (\text{B8})$$

APPENDIX C: THIRD-ORDER MOMENTUM CORRELATIONS FOR THREE BOSONS IN THREE WELLS: THE INFINITE-INTERACTION LIMIT ($\mathcal{U} \rightarrow \pm\infty$) FOR THE REMAINING EIGHT STATES

This Appendix complements Sec. IV by listing without commentary the momentum-space wave functions, $\Phi_i^{b,\pm\infty}(k_1, k_2, k_3)$ (with $i = 3, \dots, 10$), associated with the corresponding Hubbard eigenvectors, $\phi_i^{b,\pm\infty}$ [see Eqs. (A1)–(A8)], at the limits of infinite repulsive or attractive strength (i.e., for $\mathcal{U} \rightarrow \pm\infty$). The commentary integrating these wave functions into the broader scheme of their evolution as a function of any interaction strength $-\infty < \mathcal{U} < +\infty$ is left for Appendix E:

$$\begin{aligned}\Phi_3^{b,+\infty}(k_1, k_2, k_3) &= \frac{2^{3/4}}{5\sqrt{3}\pi^{3/4}} s^{3/2} e^{-(k_1^2+k_2^2+k_3^2)s^2} [\sqrt{5} \cos(d(-k_1 + k_2 + k_3)) + \sqrt{5} \cos(d(k_1 + k_2 - k_3)) \\ &+ \sqrt{5} \cos(d(k_1 - k_2 + k_3)) + 5 \cos(d(k_1 + k_2)) + 5 \cos(d(k_1 + k_3)) + 5 \cos(d(k_2 + k_3)) \\ &+ 2\sqrt{5} \cos(dk_1) + 2\sqrt{5} \cos(dk_2) + 2\sqrt{5} \cos(dk_3)], \\ \Phi_3^{b,-\infty}(k_1, k_2, k_3) &= \frac{2 \times 2^{1/4}}{\pi^{3/4}} s^{3/2} e^{-(k_1^2+k_2^2+k_3^2)s^2} \cos(d(k_1 + k_2 + k_3)),\end{aligned}\quad (\text{C1})$$

$$\begin{aligned}\Phi_4^{b,+\infty}(k_1, k_2, k_3) &= -\frac{2 \times 2^{1/4}}{\sqrt{15}\pi^{3/4}} s^{3/2} e^{-(k_1^2+k_2^2+k_3^2)s^2} [\cos(dk_1) + \cos(dk_2) + \cos(dk_3) - 2 \cos(d(-k_1 + k_2 + k_3)) \\ &- 2 \cos(d(k_1 - k_2 + k_3)) - 2 \cos(d(k_1 + k_2 - k_3))], \\ \Phi_4^{b,-\infty}(k_1, k_2, k_3) &= -\frac{2^{3/4}}{5\sqrt{3}\pi^{3/4}} s^{3/2} e^{-(k_1^2+k_2^2+k_3^2)s^2} [\sqrt{5} \cos(d(-k_1 + k_2 + k_3)) + \sqrt{5} \cos(d(k_1 + k_2 - k_3)) \\ &+ \sqrt{5} \cos(d(k_1 - k_2 + k_3)) + 5 \cos(d(k_1 + k_2)) + 5 \cos(d(k_1 + k_3)) + 5 \cos(d(k_2 + k_3)) \\ &+ 2\sqrt{5} \cos(dk_1) + 2\sqrt{5} \cos(dk_2) + 2\sqrt{5} \cos(dk_3)].\end{aligned}\quad (\text{C2})$$

$$\begin{aligned}\Phi_5^{b,+\infty}(k_1, k_2, k_3) &= -\frac{i2 \times 2^{1/4}}{\sqrt{15}\pi^{3/4}} s^{3/2} e^{-(k_1^2+k_2^2+k_3^2)s^2} [\sin(dk_1) + \sin(dk_2) + \sin(dk_3) - 2 \sin(d(-k_1 + k_2 + k_3)) \\ &- 2 \sin(d(k_1 - k_2 + k_3)) - 2 \sin(d(k_1 + k_2 - k_3))],\end{aligned}$$

$$\begin{aligned}\Phi_5^{b,-\infty}(k_1, k_2, k_3) = & -\frac{i2^{3/4}}{5\sqrt{3}\pi^{3/4}}s^{3/2}e^{-(k_1^2+k_2^2+k_3^2)s^2}[\sqrt{5}\sin(d(-k_1+k_2+k_3)) + \sqrt{5}\sin(d(k_1+k_2-k_3)) \\ & + \sqrt{5}\sin(d(k_1-k_2+k_3)) + 5\sin(d(k_1+k_2)) + 5\sin(d(k_1+k_3)) + 5\sin(d(k_2+k_3)) + 2\sqrt{5}\sin(dk_1) \\ & + 2\sqrt{5}\sin(dk_2) + 2\sqrt{5}\sin(dk_3)],\end{aligned}\quad (C3)$$

$$\begin{aligned}\Phi_6^{b,+\infty}(k_1, k_2, k_3) = & -\frac{i2^{3/4}}{5\sqrt{3}\pi^{3/4}}s^{3/2}e^{-(k_1^2+k_2^2+k_3^2)s^2}[\sqrt{5}\sin(d(-k_1+k_2+k_3)) + \sqrt{5}\sin(d(k_1+k_2-k_3)) \\ & + \sqrt{5}\sin(d(k_1-k_2+k_3)) - 5\sin(d(k_1+k_2)) - 5\sin(d(k_1+k_3)) - 5\sin(d(k_2+k_3)) + 2\sqrt{5}\sin(dk_1) \\ & + 2\sqrt{5}\sin(dk_2) + 2\sqrt{5}\sin(dk_3)],\end{aligned}$$

$$\begin{aligned}\Phi_6^{b,-\infty}(k_1, k_2, k_3) = & -\frac{i2 \times 2^{1/4}}{\sqrt{15}\pi^{3/4}}s^{3/2}e^{-(k_1^2+k_2^2+k_3^2)s^2}[\sin(dk_1) + \sin(dk_2) + \sin(dk_3) - 2\sin(d(-k_1+k_2+k_3)) \\ & - 2\sin(d(k_1-k_2+k_3)) - 2\sin(d(k_1+k_2-k_3))],\end{aligned}\quad (C4)$$

$$\begin{aligned}\Phi_7^{b,+\infty}(k_1, k_2, k_3) = & -\frac{2^{3/4}}{5\sqrt{3}\pi^{3/4}}s^{3/2}e^{-(k_1^2+k_2^2+k_3^2)s^2}[\sqrt{5}\cos(d(-k_1+k_2+k_3)) + \sqrt{5}\cos(d(k_1+k_2-k_3)) \\ & + \sqrt{5}\cos(d(k_1-k_2+k_3)) - 5\cos(d(k_1+k_2)) - 5\cos(d(k_1+k_3)) - 5\cos(d(k_2+k_3)) + 2\sqrt{5}\cos(dk_1) \\ & + 2\sqrt{5}\cos(dk_2) + 2\sqrt{5}\cos(dk_3)],\end{aligned}$$

$$\begin{aligned}\Phi_7^{b,-\infty}(k_1, k_2, k_3) = & -\frac{2 \times 2^{1/4}}{\sqrt{15}\pi^{3/4}}s^{3/2}e^{-(k_1^2+k_2^2+k_3^2)s^2}[\cos(dk_1) + \cos(dk_2) + \cos(dk_3) - 2\cos(d(-k_1+k_2+k_3)) \\ & - 2\cos(d(k_1-k_2+k_3)) - 2\cos(d(k_1+k_2-k_3))],\end{aligned}\quad (C5)$$

$$\Phi_8^{b,+\infty}(k_1, k_2, k_3) = \frac{2 \times 2^{1/4}}{\pi^{3/4}}s^{3/2}e^{-(k_1^2+k_2^2+k_3^2)s^2}\cos(d(k_1+k_2+k_3)),$$

$$\begin{aligned}\Phi_8^{b,-\infty}(k_1, k_2, k_3) = & \frac{2^{3/4}}{5\sqrt{3}\pi^{3/4}}s^{3/2}e^{-(k_1^2+k_2^2+k_3^2)s^2}[\sqrt{5}\cos(d(-k_1+k_2+k_3)) + \sqrt{5}\cos(d(k_1+k_2-k_3)) \\ & + \sqrt{5}\cos(d(k_1-k_2+k_3)) - 5\cos(d(k_1+k_2)) - 5\cos(d(k_1+k_3)) - 5\cos(d(k_2+k_3)) + 2\sqrt{5}\cos(dk_1) \\ & + 2\sqrt{5}\cos(dk_2) + 2\sqrt{5}\cos(dk_3)],\end{aligned}\quad (C6)$$

$$\Phi_9^{b,+\infty}(k_1, k_2, k_3) = \frac{2i2^{1/4}}{\pi^{3/4}}s^{3/2}e^{-(k_1^2+k_2^2+k_3^2)s^2}\sin(d(k_1+k_2+k_3)),$$

$$\begin{aligned}\Phi_9^{b,-\infty}(k_1, k_2, k_3) = & \frac{i2^{3/4}}{5\sqrt{3}\pi^{3/4}}s^{3/2}e^{-(k_1^2+k_2^2+k_3^2)s^2}[\sqrt{5}\sin(d(-k_1+k_2+k_3)) + \sqrt{5}\sin(d(k_1+k_2-k_3)) \\ & + \sqrt{5}\sin(d(k_1-k_2+k_3)) - 5\sin(d(k_1+k_2)) - 5\sin(d(k_1+k_3)) - 5\sin(d(k_2+k_3)) + 2\sqrt{5}\sin(dk_1) \\ & + 2\sqrt{5}\sin(dk_2) + 2\sqrt{5}\sin(dk_3)],\end{aligned}\quad (C7)$$

$$\Phi_{10}^{b,+\infty}(k_1, k_2, k_3) = -\left(\frac{2}{\pi}\right)^{3/4}s^{3/2}e^{-(k_1^2+k_2^2+k_3^2)s^2},$$

$$\Phi_{10}^{b,-\infty}(k_1, k_2, k_3) = -\frac{2 \times 2^{1/4}}{\sqrt{3}\pi^{3/4}}s^{3/2}e^{-(k_1^2+k_2^2+k_3^2)s^2}[\cos(d(k_1-k_2)) + \cos(d(k_1-k_3)) + \cos(d(k_2-k_3))].\quad (C8)$$

APPENDIX D: THIRD-ORDER MOMENTUM CORRELATIONS FOR THREE BOSONS IN THREE WELLS: THE NONINTERACTING LIMIT $\mathcal{U} = 0$ FOR THE REMAINING EIGHT STATES

This Appendix complements Sec. V by listing without commentary the momentum-space three-body wave functions for the remaining eight excited states, that is,

$$\begin{aligned}s^{-3/2}e^{(k_1^2+k_2^2+k_3^2)s^2}\Phi_{3r(4l)}^{b,\mathcal{U}=0}(k_1, k_2, k_3) \\ = 0.248595 + 0.117189[\cos(dk_1) + \cos(dk_2) + \cos(dk_3)] - 0.322013\{\cos[d(k_1-k_2)] + \cos[d(k_1-k_3)] \\ + \cos[d(k_2-k_3)]\} + 0.156283\{\cos[d(k_1+k_2)] + \cos[d(k_1+k_3)] + \cos[d(k_2+k_3)]\} - 0.344886\{\cos[d(k_1-k_2+k_3)] \\ + \cos[d(k_1-k_2-k_3)] + \cos[d(k_1+k_2-k_3)]\} + 0.331527\cos[d(k_1+k_2+k_3)],\end{aligned}\quad (D1)$$

$$\begin{aligned}
& s^{-3/2} e^{(k_1^2+k_2^2+k_3^2)s^2} \Phi_{4r(3l)}^{b,\mathcal{U}=0}(k_1, k_2, k_3) \\
&= -0.358722 - 0.169103[\cos(dk_1) + \cos(dk_2) + \cos(dk_3)] - 0.0461557\{\cos[d(k_1 - k_2)] + \cos[d(k_1 - k_3)] \\
&\quad + \cos[d(k_2 - k_3)]\} + 0.285304\{\cos[d(k_1 + k_2)] + \cos[d(k_1 + k_3)] + \cos[d(k_2 + k_3)]\} + 0.136466\{\cos[d(k_1 - k_2 + k_3)] \\
&\quad + \cos[d(k_1 - k_2 - k_3)] + \cos[d(k_1 + k_2 - k_3)]\} + 0.605221 \cos[d(k_1 + k_2 + k_3)], \tag{D2}
\end{aligned}$$

$$\Phi_{5r(6l)}^{b,\mathcal{U}=0}(k_1, k_2, k_3) = \Phi_5^{b,+\infty}(k_1, k_2, k_3) = \Phi_6^{b,-\infty}(k_1, k_2, k_3), \tag{D3}$$

$$\begin{aligned}
& \frac{-i2^{1/4}\sqrt{5}\pi^{3/4}}{s^{3/2}} e^{(k_1^2+k_2^2+k_3^2)s^2} \Phi_{6r(5l)}^{b,\mathcal{U}=0}(k_1, k_2, k_3) \\
&= 2[\sin(dk_1) + \sin(dk_2) + \sin(dk_3)] + \sin[d(k_1 - k_2 + k_3)] + \sin[d(-k_1 + k_2 + k_3)] \\
&\quad + \sin[d(k_1 + k_2 - k_3)] - 5 \sin[d(k_1 + k_2 + k_3)], \tag{D4}
\end{aligned}$$

$$\begin{aligned}
& s^{-3/2} e^{(k_1^2+k_2^2+k_3^2)s^2} \Phi_{7r(8l)}^{b,\mathcal{U}=0}(k_1, k_2, k_3) \\
&= -0.248595 + 0.117189[\cos(dk_1) + \cos(dk_2) + \cos(dk_3)] + 0.322013\{\cos[d(k_1 - k_2)] + \cos[d(k_1 - k_3)] \\
&\quad + \cos[d(k_2 - k_3)]\} - 0.156283\{\cos[d(k_1 + k_2)] + \cos[d(k_1 + k_3)] + \cos[d(k_2 + k_3)]\} - 0.344886\{\cos[d(k_1 - k_2 + k_3)] \\
&\quad + \cos[d(k_1 - k_2 - k_3)] + \cos[d(k_1 + k_2 - k_3)]\} + 0.331527 \cos[d(k_1 + k_2 + k_3)], \tag{D5}
\end{aligned}$$

$$\begin{aligned}
& s^{-3/2} e^{(k_1^2+k_2^2+k_3^2)s^2} \Phi_{8r(7l)}^{b,\mathcal{U}=0}(k_1, k_2, k_3) \\
&= 0.358722 - 0.169103[\cos(dk_1) + \cos(dk_2) + \cos(dk_3)] + 0.0461557\{\cos[d(k_1 - k_2)] + \cos[d(k_1 - k_3)] \\
&\quad + \cos[d(k_2 - k_3)]\} - 0.285304\{\cos[d(k_1 + k_2)] + \cos[d(k_1 + k_3)] + \cos[d(k_2 + k_3)]\} + 0.136466\{\cos[d(k_1 - k_2 + k_3)] \\
&\quad + \cos[d(k_1 - k_2 - k_3)] + \cos[d(k_1 + k_2 - k_3)]\} + 0.605221 \cos[d(k_1 + k_2 + k_3)], \tag{D6}
\end{aligned}$$

$$\begin{aligned}
& \frac{i(2\pi)^{3/4}\sqrt{3}}{s^{3/2}} e^{(k_1^2+k_2^2+k_3^2)s^2} \Phi_9^{b,\mathcal{U}=0}(k_1, k_2, k_3) \\
&= 2[\sin(dk_1) + \sin(dk_2) + \sin(dk_3)] - 2\sqrt{2}\{\sin[d(k_1 + k_2)] + \sin[d(k_1 + k_3)] + \sin[d(k_2 + k_3)]\} + \sin[d(k_1 - k_2 + k_3)] \\
&\quad + \sin[d(-k_1 + k_2 + k_3)] + \sin[d(k_1 + k_2 - k_3)] + 3 \sin[d(k_1 + k_2 + k_3)], \tag{D7}
\end{aligned}$$

$$\begin{aligned}
& \frac{(2\pi)^{3/4}}{s^{3/2}} e^{(k_1^2+k_2^2+k_3^2)s^2} \Phi_{10}^{b,\mathcal{U}=0}(k_1, k_2, k_3) \\
&= -1 + \sqrt{2}[\cos(dk_1) + \cos(dk_2) + \cos(dk_3)] - \cos[d(k_1 - k_2)] - \cos[d(k_1 - k_3)] \\
&\quad - \cos[d(k_2 - k_3)] - \cos[d(k_1 + k_2)] - \cos[d(k_1 + k_3)] - \cos[d(k_2 + k_3)] + \frac{1}{\sqrt{2}}\{\cos[d(k_1 + k_2 - k_3)] \\
&\quad + \cos[d(k_1 - k_2 + k_3)] + \cos[d(-k_1 + k_2 + k_3)] + \cos[d(k_1 + k_2 + k_3)]\}. \tag{D8}
\end{aligned}$$

APPENDIX E: THIRD-ORDER MOMENTUM CORRELATIONS AS A FUNCTION OF \mathcal{U} FOR THE REMAINING EIGHT EXCITED STATES

Figure 12 complements Fig. 3 in that it displays the six coefficients $C^i(\mathcal{U})$'s for the remaining eight excited states (explicit numerical values can be found in the Supplemental Material [67]). The dependence of these coefficients on the interaction strength \mathcal{U} is better deciphered by using as reference points the special cases at $\mathcal{U} \rightarrow \pm\infty$ and $\mathcal{U} = 0$. Note that in all cases the C^i values at the end points $\mathcal{U} = \pm 30$ in the figure are close to the corresponding limiting values at $\mathcal{U} \rightarrow \pm\infty$.

In particular, for the excited state denoted as $i = 3r(4l)$ ($i = 3$ for $0 < \mathcal{U} < +\infty$ and $i = 4$ for $-\infty < \mathcal{U} < 0$) and for $\mathcal{U} \rightarrow -\infty$, only three coefficients, $C_1^{4,-\infty} = -2 \times 2^{3/4}/(\sqrt{15}\pi^{3/4}) = -0.3680$, $C_{1+1}^{4,-\infty} = -2^{3/4}/(\sqrt{3}\pi^{3/4}) = -0.4115$, and $C_{1+1-1}^{4,-\infty} = -2^{3/4}/(\sqrt{15}\pi^{3/4}) = -0.1840$, survive in expression (29) [see Fig. 12(a)]; the corresponding Hubbard eigenvector, $\phi_4^{b,-\infty}$ [second expression in Eq. (A2)] consists of all six primitive kets [see Eq. (1)] representing

exclusively doubly occupied wells, and the corresponding wave function in momentum space has nine cosinusoidal terms and is given by the second expression in Eq. (C2).

For $\mathcal{U} = 0$, all six coefficients, $C^{3r(4l),\mathcal{U}=0}$'s, are present, and their numerical values from Fig. 12(a) agree with the numerical values for $\Phi_{3r(4l)}^{b,\mathcal{U}=0}(k_1, k_2, k_3)$ in Eq. (D1).

For $\mathcal{U} \rightarrow +\infty$, again only three coefficients, $C_1^{3,+ \infty} = 2 \times 2^{3/4}/(\sqrt{15}\pi^{3/4}) = 0.3680$, $C_{1+1}^{3,+ \infty} = 2^{3/4}/(\sqrt{3}\pi^{3/4}) = 0.4115$, and $C_{1+1-1}^{3,+ \infty} = 2^{3/4}/(\sqrt{15}\pi^{3/4}) = 0.1840$, survive in expression (29) [see Fig. 12(a)]; the corresponding Hubbard eigenvector, $\phi_3^{b,+ \infty}$ [first expression in Eq. (A1)] consists of all six primitive kets [see Eq. (1)] representing exclusively doubly occupied wells, and the corresponding wave function in momentum space has nine cosinusoidal terms and is given by the second expression in Eq. (C1).

The excited state denoted as $i = 4r(3l)$ ($i = 4$ for $0 < \mathcal{U} < +\infty$ and $i = 3$ for $-\infty < \mathcal{U} < 0$) and for $\mathcal{U} \rightarrow -\infty$, only one coefficient, $C_{1+1+1}^{3,-\infty} = 2 \times 2^{1/4}/\pi^{3/4} = 1.0079$, survives in expression (29) [see Fig. 12(b)]; the corresponding

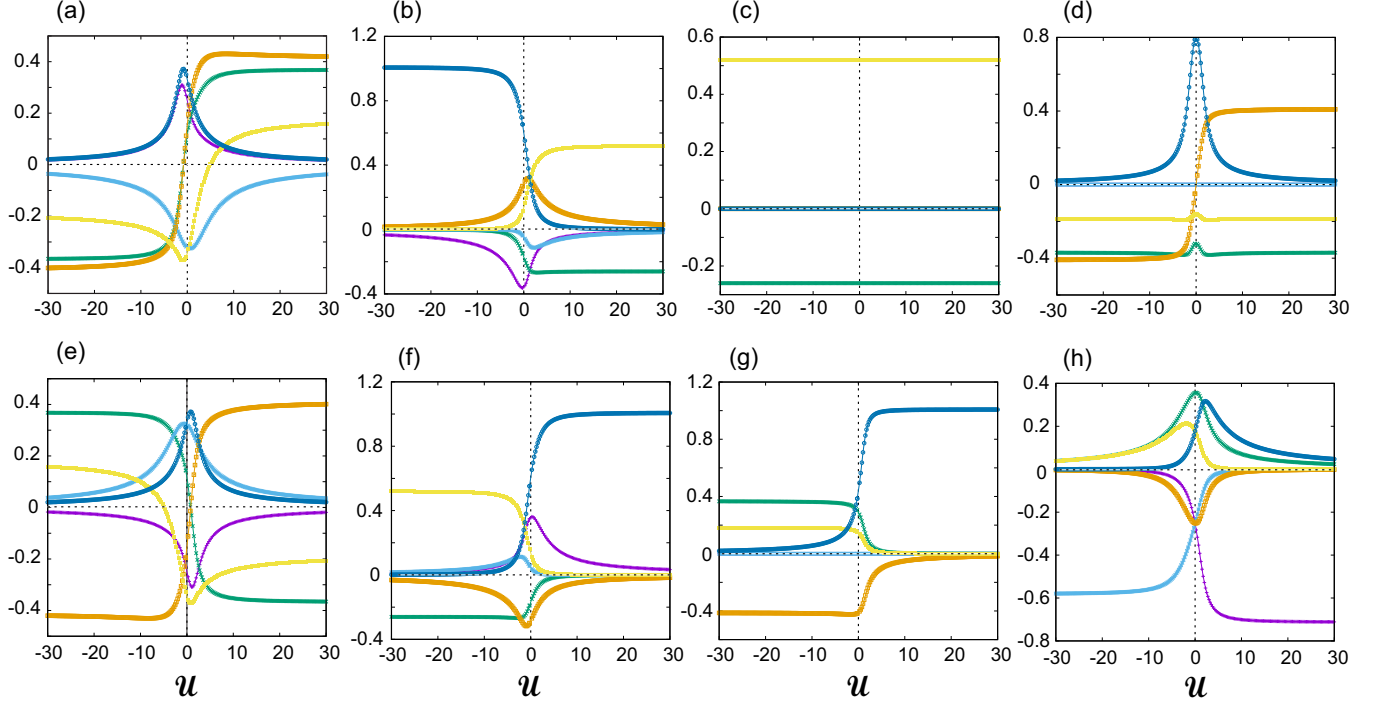


FIG. 12. The six different \mathcal{C} coefficients (dimensionless) [see Eq. (29)] for the eight remaining excited states of three bosons trapped in three linearly arranged wells as a function of \mathcal{U} (horizontal axis, dimensionless). This figure complements Fig. 3 in the main text. (a) $i = 3r(4l)$. (b) $i = 4r(3l)$. (c) $i = 5r(6l)$. (d) $i = 6r(5l)$. (e) $i = 7r(8l)$. (f) $i = 8r(7l)$. (g) $i = 9$. (h) $i = 10$. The choice of online colors is the same as in Fig. 3, that is, \mathcal{C}_0 , violet; \mathcal{C}_1 , green; \mathcal{C}_{1-1} , light blue; \mathcal{C}_{1+1} , brown; \mathcal{C}_{1+1-1} , yellow; \mathcal{C}_{1+1+1} , dark blue. For the print grayscale version, the positioning (referred to as $\#n$, with $n = 1, 2, 3, \dots$) of the curves from top to bottom at the point $\mathcal{U} = -30$ is as follows: (a) $\mathcal{C}_0 \rightarrow \#2$ (overlaps with $\#1$); $\mathcal{C}_1 \rightarrow \#5$; $\mathcal{C}_{1-1} \rightarrow \#3$; $\mathcal{C}_{1+1} \rightarrow \#6$; $\mathcal{C}_{1+1-1} \rightarrow \#4$; $\mathcal{C}_{1+1+1} \rightarrow \#1$ (overlaps with $\#2$). (b) $\mathcal{C}_0 \rightarrow \#6$; $\mathcal{C}_1 \rightarrow \#5$ (overlaps with $\#3$ and $\#4$); $\mathcal{C}_{1-1} \rightarrow \#4$; $\mathcal{C}_{1+1} \rightarrow \#2$; $\mathcal{C}_{1+1-1} \rightarrow \#3$; $\mathcal{C}_{1+1+1} \rightarrow \#1$. (c) $\mathcal{C}_0 = \mathcal{C}_{1-1} = \mathcal{C}_{1+1} = \mathcal{C}_{1+1+1} = 0$; $\mathcal{C}_1 \rightarrow$ lower curve; $\mathcal{C}_{1+1-1} \rightarrow$ upper curve. (d) $\mathcal{C}_0 \rightarrow \#3$ (overlaps with $\#2$); $\mathcal{C}_1 \rightarrow \#5$; $\mathcal{C}_{1-1} \rightarrow \#2$; $\mathcal{C}_{1+1} \rightarrow \#6$; $\mathcal{C}_{1+1-1} \rightarrow \#4$; $\mathcal{C}_{1+1+1} \rightarrow \#1$. (e) $\mathcal{C}_0 \rightarrow \#5$; $\mathcal{C}_1 \rightarrow \#1$; $\mathcal{C}_{1-1} \rightarrow \#3$; $\mathcal{C}_{1+1} \rightarrow \#6$; $\mathcal{C}_{1+1-1} \rightarrow \#2$; $\mathcal{C}_{1+1+1} \rightarrow \#4$. (f) $\mathcal{C}_0 \rightarrow \#3$ (overlaps with $\#2$); $\mathcal{C}_1 \rightarrow \#6$; $\mathcal{C}_{1-1} \rightarrow \#2$; $\mathcal{C}_{1+1} \rightarrow \#5$; $\mathcal{C}_{1+1-1} \rightarrow \#1$; $\mathcal{C}_{1+1+1} \rightarrow \#4$; (g) $\mathcal{C}_0 \rightarrow \#5$ (overlaps with $\#4$); $\mathcal{C}_1 \rightarrow \#1$; $\mathcal{C}_{1-1} \rightarrow \#4$; $\mathcal{C}_{1+1} \rightarrow \#6$; $\mathcal{C}_{1+1-1} \rightarrow \#2$; $\mathcal{C}_{1+1+1} \rightarrow \#3$. (h) $\mathcal{C}_0 \rightarrow \#4$ (overlaps with $\#3$ and $\#5$); $\mathcal{C}_1 \rightarrow \#1$ (overlaps with $\#2$); $\mathcal{C}_{1-1} \rightarrow \#6$; $\mathcal{C}_{1+1} \rightarrow \#5$; $\mathcal{C}_{1+1-1} \rightarrow \#2$; $\mathcal{C}_{1+1+1} \rightarrow \#3$.

Hubbard eigenvector, $\phi_3^{b,-\infty}$ [second expression in Eq. (A1)] is a NOON state of the form $(|300\rangle + |003\rangle)/\sqrt{2}$, and the corresponding wave function in momentum space is given by the second expression in Eq. (C1), which includes a cos term only.

For $\mathcal{U} = 0$, all six coefficients, $\mathcal{C}_i^{4r(3l), \mathcal{U}=0}$'s, are present, and their numerical values from Fig. 12(b) agree with the numerical values for $\Phi_{4r(3l)}^{b, \mathcal{U}=0}(k_1, k_2, k_3)$ in Eq. (D2).

For $\mathcal{U} \rightarrow +\infty$, only two coefficients, $\mathcal{C}_1^{4,+ \infty} = -2 \times 2^{1/4}/(\sqrt{15}\pi^{3/4}) = -0.2602$ and $\mathcal{C}_{1+1-1}^{4,+ \infty} = 4 \times 2^{1/4}/(\sqrt{15}\pi^{3/4}) = 0.5205$, survive in expression (29) [see Fig. 12(b)]; the corresponding Hubbard eigenvector, $\phi_4^{b,+ \infty}$ [first expression in Eq. (A2)] consists of four primitive kets [see Eq. (1)] representing exclusively doubly occupied wells, and the corresponding wave function in momentum space has six cosinusoidal terms and is given by the first expression in Eq. (C2).

For the excited state denoted as $i = 5r(6l)$ ($i = 5$ for $0 < \mathcal{U} < +\infty$ and $i = 6$ for $-\infty < \mathcal{U} < 0$), the Hubbard eigenvector solution is \mathcal{U} independent; see the first expression in Eq. (A3), second expression in Eq. (A4), or Eq. (B3). In this case, two distinct coefficients survive

in expression (29), that is, $\mathcal{C}_1^{6,-\infty} = \mathcal{C}_1^{5,+ \infty} = \mathcal{C}_1^{5r(6l), \mathcal{U}=0} = -2 \times 2^{1/4}/(\sqrt{15}\pi^{3/4}) = -0.2602$, and $\mathcal{C}_{1+1-1}^{6,-\infty} = \mathcal{C}_{1+1-1}^{5,+ \infty} = \mathcal{C}_{1+1-1}^{5r(6l), \mathcal{U}=0} = 4 \times 2^{1/4}/(\sqrt{15}\pi^{3/4}) = 0.5205$, in agreement with Fig. 12(c). The corresponding Hubbard eigenvectors, $\phi_5^{b,+ \infty} = \phi_6^{b,-\infty} = \phi_{5r(6l)}^{b, \mathcal{U}=0}$, consist of four primitive kets [see Eq. (1)] representing exclusively doubly occupied wells, and the corresponding wave function in momentum space has six cosinusoidal terms and is given by the second expression in Eq. (C4) or the first expression in Eq. (C3).

For the excited state denoted as $i = 6r(5l)$ ($i = 6$ for $0 < \mathcal{U} < +\infty$ and $i = 5$ for $-\infty < \mathcal{U} < 0$) and for $\mathcal{U} \rightarrow -\infty$, only three coefficients, $\mathcal{C}_1^{5,-\infty} = -2 \times 2^{3/4}/(\sqrt{15}\pi^{3/4}) = -0.3680$, $\mathcal{C}_{1+1}^{5,-\infty} = -2^{3/4}/(\sqrt{3}\pi^{3/4}) = -0.4115$, and $\mathcal{C}_{1+1-1}^{5,-\infty} = -2^{3/4}/(\sqrt{15}\pi^{3/4}) = -0.1840$, survive in expression (29) [see Fig. 12(d)]; the corresponding Hubbard eigenvector, $\phi_5^{b,-\infty}$ [second expression in Eq. (A3)] consists of all six primitive kets [see Eq. (1)] representing exclusively doubly occupied wells, and the corresponding wave function in momentum space has nine sinusoidal terms and is given by the second expression in Eq. (C3).

For $\mathcal{U} = 0$, three coefficients are present, namely $\mathcal{C}_1^{6r(5l), \mathcal{U}=0}$, $\mathcal{C}_{1+1-1}^{6r(5l), \mathcal{U}=0}$, and $\mathcal{C}_{1+1+1}^{6r(5l), \mathcal{U}=0}$. Their numerical

values from Fig. 12(d) agree with the corresponding algebraic expressions for $\Phi_{6r(5l)}^{b,U=0}(k_1, k_2, k_3)$ in Eq. (D4).

For $\mathcal{U} \rightarrow +\infty$, again only three coefficients, $C_1^{6,+ \infty} = -2 \times 2^{3/4}/(\sqrt{15}\pi^{3/4}) = -0.3680$, $C_{1+1}^{6,+ \infty} = 2^{3/4}/(\sqrt{3}\pi^{3/4}) = 0.4115$, and $C_{1+1-1}^{6,+ \infty} = -2^{3/4}/(\sqrt{15}\pi^{3/4}) = -0.1840$, survive in expression (29) [see Fig. 12(d)]; the corresponding Hubbard eigenvector, $\phi_6^{b,+ \infty}$ [first expression in Eq. (A4)] consists of all six primitive kets [see Eq. (1)] representing exclusively doubly occupied wells, and the corresponding wave function in momentum space has nine *sinusoidal* terms and is given by the first expression in Eq. (C4).

For the excited state denoted as $i = 7r(8l)$ ($i = 7$ for $0 < \mathcal{U} < +\infty$ and $i = 8$ for $-\infty < \mathcal{U} < 0$) and for $\mathcal{U} \rightarrow -\infty$, only three coefficients, $C_1^{8,- \infty} = 2 \times 2^{3/4}/(\sqrt{15}\pi^{3/4}) = 0.3680$, $C_{1+1}^{8,- \infty} = -2^{3/4}/(\sqrt{3}\pi^{3/4}) = -0.4115$, and $C_{1+1-1}^{8,- \infty} = 2^{3/4}/(\sqrt{15}\pi^{3/4}) = 0.1840$, survive in expression (29) [see Fig. 12(e)]; the corresponding Hubbard eigenvector, $\phi_8^{b,- \infty}$ [second expression in Eq. (A6)] consists of all six primitive kets [see Eq. (1)] representing exclusively doubly occupied wells, and the corresponding wave function in momentum space has nine cosinusoidal terms and is given by the second expression in Eq. (C6).

For $\mathcal{U} = 0$, all six coefficients, $C_{7r(8l), \mathcal{U}=0}^{7,+ \infty}$'s, are present, and their numerical values from Fig. 12(e) agree with the numerical values for $\Phi_{7r(8l)}^{b,U=0}(k_1, k_2, k_3)$ in Eq. (D5).

For $\mathcal{U} \rightarrow +\infty$, again only three coefficients, $C_1^{7,+ \infty} = -2 \times 2^{3/4}/(\sqrt{15}\pi^{3/4}) = -0.3680$, $C_{1+1}^{7,+ \infty} = 2^{3/4}/(\sqrt{3}\pi^{3/4}) = 0.4115$, and $C_{1+1-1}^{7,+ \infty} = -2^{3/4}/(\sqrt{15}\pi^{3/4}) = -0.1840$, survive in expression (29) [see Fig. 12(e)]; the corresponding Hubbard eigenvector, $\phi_7^{b,+ \infty}$ [first expression in Eq. (A5)] consists of all six primitive kets [see Eq. (1)] representing exclusively doubly occupied wells, and the corresponding wave function in momentum space has nine cosinusoidal terms and is given by the first expression in Eq. (C5).

For the excited state denoted as $i = 8r(7l)$ ($i = 8$ for $0 < \mathcal{U} < +\infty$ and $i = 7$ for $-\infty < \mathcal{U} < 0$) and for $\mathcal{U} \rightarrow -\infty$, only two coefficients, $C_1^{7,- \infty} = -2 \times 2^{1/4}/(\sqrt{15}\pi^{3/4}) = -0.2602$, and $C_{1+1-1}^{7,- \infty} = 4 \times 2^{1/4}/(\sqrt{15}\pi^{3/4}) = 0.5205$, survive in expression (29) [see Fig. 12(f)]; the corresponding Hubbard eigenvector, $\phi_7^{b,- \infty}$ [second expression in Eq. (A5)] consists of four primitive kets [see Eq. (1)] representing exclusively doubly occupied wells, and the corresponding wave function in momentum space has six cosinusoidal terms and is given by the second expression in Eq. (C5).

For $\mathcal{U} = 0$, all six coefficients, $C_{8r(7l), \mathcal{U}=0}^{8,+ \infty}$'s, are present, and their numerical values from Fig. 12(f) agree with the numerical values for $\Phi_{8r(7l)}^{b,U=0}(k_1, k_2, k_3)$ in Eq. (D6).

For $\mathcal{U} \rightarrow +\infty$, only one coefficient, $C_{1+1+1}^{8,+ \infty} = 2 \times 2^{1/4}/\pi^{3/4} = 1.0079$, survives in expression (29) [see Fig. 12(f)]; the corresponding Hubbard eigenvector, $\phi_8^{b,+ \infty}$ [first expression in Eq. (A6)] is a NOON state of the form $(|300\rangle + |003\rangle)/\sqrt{2}$, and the corresponding wave function in momentum space is given by the first expression in Eq. (C6), which includes a cos term only.

For the excited state denoted as $i = 9$ for $-\infty < \mathcal{U} < +\infty$ and for $\mathcal{U} \rightarrow -\infty$, only three coefficients, $C_1^{5,- \infty} =$

$2 \times 2^{3/4}/(\sqrt{15}\pi^{3/4}) = 0.3680$, $C_{1+1}^{5,- \infty} = -2^{3/4}/(\sqrt{3}\pi^{3/4}) = -0.4115$, and $C_{1+1-1}^{5,- \infty} = 2^{3/4}/(\sqrt{15}\pi^{3/4}) = 0.1840$, survive in expression (29) [see Fig. 12(g)]; the corresponding Hubbard eigenvector, $\phi_9^{b,- \infty}$ [second expression in Eq. (A7)] consists of all six primitive kets [see Eq. (1)] representing exclusively doubly occupied wells, and the corresponding wave function in momentum space has nine *sinusoidal* terms and is given by the second expression in Eq. (C7).

For $\mathcal{U} = 0$, four coefficients are present, namely $C_{1+1+1}^{9,\mathcal{U}=0}$, $C_{1+1-1}^{9,\mathcal{U}=0}$, $C_{1+1-1-1}^{9,\mathcal{U}=0}$, and $C_{1+1+1}^{9,\mathcal{U}=0}$. Their numerical values from Fig. 12(g) agree with the corresponding algebraic expressions for $\Phi_9^{b,U=0}(k_1, k_2, k_3)$ in Eq. (D7).

For $\mathcal{U} \rightarrow +\infty$, only one coefficient, $C_{1+1+1}^{9,+ \infty} = 2 \times 2^{1/4}/\pi^{3/4} = 1.0079$, survives in expression (29) [see Fig. 12(g)]; the corresponding Hubbard eigenvector, $\phi_9^{b,+ \infty}$ [first expression in Eq. (A7)] is a NOON state of the form $(-|300\rangle + |003\rangle)/\sqrt{2}$, and the corresponding wave function in momentum space is given by the first expression in Eq. (C7), which includes a *sin* term only.

For the highest excited state denoted as $i = 10$ for $-\infty < \mathcal{U} < +\infty$ and for $\mathcal{U} \rightarrow -\infty$, only the coefficient $C_{1-1}^{10,- \infty} = -2 \times 2^{1/4}/(\sqrt{3}\pi^{3/4}) = -0.5819$ survives in expression (29); see Fig. 12(h). The corresponding momentum-space wave function comprises three cosinusoidal terms and is given by the second expression in Eq. (C8). The corresponding Hubbard eigenvector $\phi_{10}^{b,- \infty}$ [second expression in Eq. (A8)] contains only a single component from the primitive kets listed in Eq. (1), i.e., the basis ket no. 1 \rightarrow $|111\rangle$, reflecting the fact that all three wells are singly occupied.

For $\mathcal{U} = 0$, all six coefficients, $C_{10,\mathcal{U}=0}^{10,+ \infty}$'s, are present, and their numerical values from Fig. 12(h) agree with the numerical values for $\Phi_{10}^{b,U=0}(k_1, k_2, k_3)$ in Eq. (D8).

For $\mathcal{U} \rightarrow +\infty$, it is seen from Fig. 12(h) that only the constant coefficient $C_0^{10,- \infty} = -(2/\pi)^{3/4} = -0.7127$ survives in expression (29); the corresponding wave function in momentum space is given by the first expression in Eq. (C8). It is a simple Gaussian distribution associated with a Bose-Einstein condensate, reflecting the fact that all three bosons are localized in the middle well and occupy the same orbital; the corresponding Hubbard eigenvector is given by $\phi_{10}^{b,+ \infty}$ [first expression in Eq. (A8)], which contains only a single component from the primitive kets listed in Eq. (1), i.e., the basis ket no. 9 \rightarrow $|030\rangle$.

APPENDIX F: SECOND-ORDER MOMENTUM CORRELATIONS AS A FUNCTION OF \mathcal{U} FOR THE REMAINING EIGHT EXCITED STATES

Figure 13 complements Fig. 5 in that it displays the nine distinct coefficients $\mathcal{B}^i(\mathcal{U})$'s for the remaining eight excited states (explicit numerical values can be found in the Supplemental Material [67]). The dependence of these coefficients on the interaction strength \mathcal{U} is better deciphered by using as reference points the special cases at $\mathcal{U} \rightarrow \pm\infty$ and $\mathcal{U} = 0$. Note that in all cases the \mathcal{B}^i values at the end points $\mathcal{U} = \pm 30$ in the figure are close to the corresponding limiting values at $\mathcal{U} \rightarrow \pm\infty$.

In particular, for the excited state denoted as $i = 3r(4l)$ ($i = 3$ for $0 < \mathcal{U} < +\infty$ and $i = 4$ for $-\infty < \mathcal{U} < 0$) and

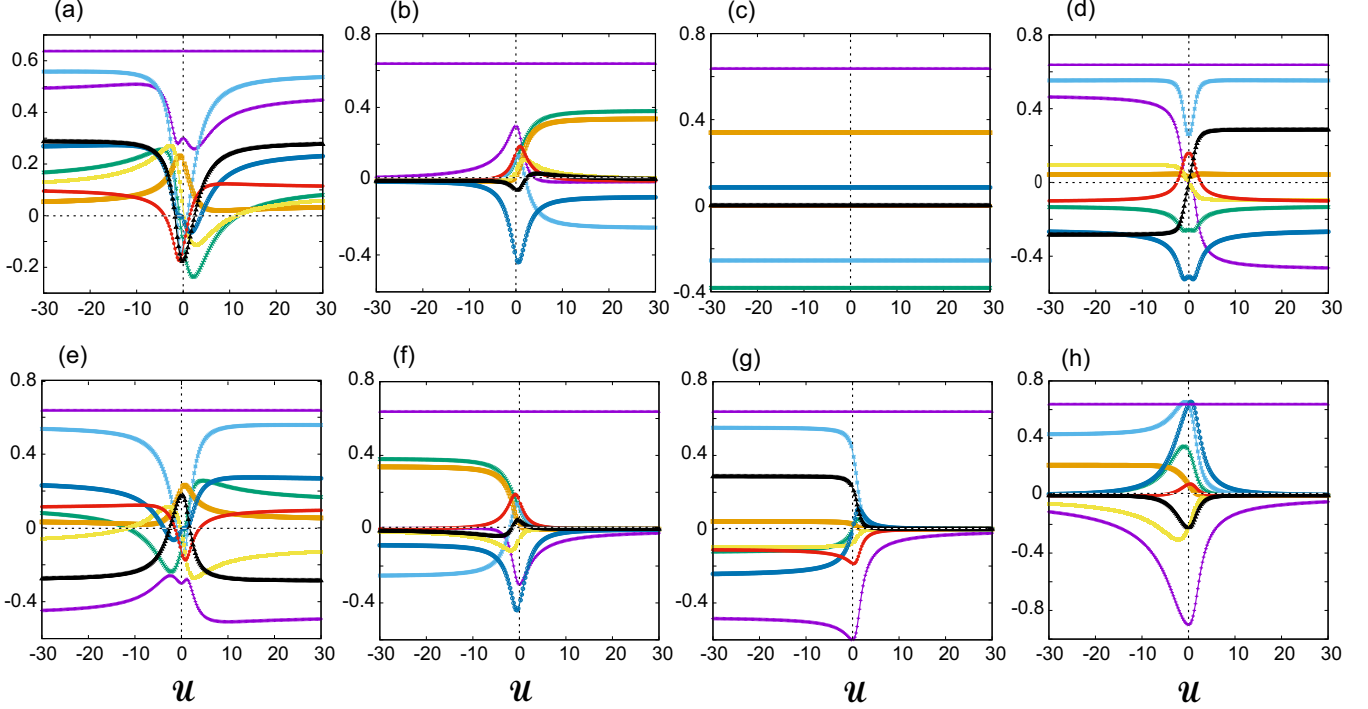


FIG. 13. The nine \mathcal{B} coefficients (dimensionless) [see Eq. (31)] for the remaining eight excited eigenstates of three bosons trapped in three linearly arranged wells as a function of \mathcal{U} (horizontal axis, dimensionless). This figure complements Fig. 5 in the main text. (a) $i = 3r(4l)$. (b) $i = 4r(3l)$. (c) $i = 5r(6l)$. (d) $i = 6r(5l)$. (e) $i = 7r(8l)$. (f) $i = 8r(7l)$, (g) $i = 9$, (h) $i = 10$. See text for a detailed description. The choice of colors is the same as in Fig. 5, that is, \mathcal{B}_0 , constant (violet); \mathcal{B}_1 , second violet; \mathcal{B}_2 , green; \mathcal{B}_{1-1} , light blue; \mathcal{B}_{2-2} , brown; \mathcal{B}_{2-1} , yellow; \mathcal{B}_{1+1} , dark blue; \mathcal{B}_{2+2} , red; \mathcal{B}_{2+1} , black. For the print grayscale version, the positioning (referred to as $\#n$, with $n = 1, 2, 3, \dots$) of the curves from top to bottom at the point $\mathcal{U} = -30$ is as follows: (a) $\mathcal{B}_0 \rightarrow \#1$; $\mathcal{B}_1 \rightarrow \#3$; $\mathcal{B}_2 \rightarrow \#6$; $\mathcal{B}_{1-1} \rightarrow \#2$; $\mathcal{B}_{2-2} \rightarrow \#9$; $\mathcal{B}_{2-1} \rightarrow \#7$; $\mathcal{B}_{1+1} \rightarrow \#5$; $\mathcal{B}_{2+2} \rightarrow \#8$; $\mathcal{B}_{2+1} \rightarrow \#4$. (b) $\mathcal{B}_0 \rightarrow \#1$; $\mathcal{B}_1 \rightarrow \#2$; $\mathcal{B}_2 \rightarrow \#5$ (overlaps with $\#3, \#4, \#6, \#7, \#8, \#9$); $\mathcal{B}_{1-1} \rightarrow \#4$; $\mathcal{B}_{2-2} \rightarrow \#7$; $\mathcal{B}_{2-1} \rightarrow \#6$; $\mathcal{B}_{1+1} \rightarrow \#9$; $\mathcal{B}_{2+2} \rightarrow \#3$; $\mathcal{B}_{2+1} \rightarrow \#8$. (c) $\mathcal{B}_0 \rightarrow \#1$; $\mathcal{B}_1 \rightarrow \#4$ (overlaps with $\#5, \#6, \#7$); $\mathcal{B}_2 \rightarrow \#9$; $\mathcal{B}_{1-1} \rightarrow \#8$; $\mathcal{B}_{2-2} \rightarrow \#2$; $\mathcal{B}_{2-1} \rightarrow \#5$; $\mathcal{B}_{1+1} \rightarrow \#3$; $\mathcal{B}_{2+2} \rightarrow \#6$; $\mathcal{B}_{2+1} \rightarrow \#7$. (d) $\mathcal{B}_0 \rightarrow \#1$; $\mathcal{B}_1 \rightarrow \#3$; $\mathcal{B}_2 \rightarrow \#7$; $\mathcal{B}_{1-1} \rightarrow \#2$; $\mathcal{B}_{2-2} \rightarrow \#5$; $\mathcal{B}_{2-1} \rightarrow \#4$; $\mathcal{B}_{1+1} \rightarrow \#8$; $\mathcal{B}_{2+2} \rightarrow \#6$; $\mathcal{B}_{2+1} \rightarrow \#9$. (e) $\mathcal{B}_0 \rightarrow \#1$; $\mathcal{B}_1 \rightarrow \#9$; $\mathcal{B}_2 \rightarrow \#5$; $\mathcal{B}_{1-1} \rightarrow \#2$; $\mathcal{B}_{2-2} \rightarrow \#6$; $\mathcal{B}_{2-1} \rightarrow \#7$; $\mathcal{B}_{1+1} \rightarrow \#3$; $\mathcal{B}_{2+2} \rightarrow \#4$; $\mathcal{B}_{2+1} \rightarrow \#8$. (f) $\mathcal{B}_0 \rightarrow \#1$; $\mathcal{B}_1 \rightarrow \#5$ (overlaps with $\#4, \#6, \#7$); $\mathcal{B}_2 \rightarrow \#2$; $\mathcal{B}_{1-1} \rightarrow \#9$; $\mathcal{B}_{2-2} \rightarrow \#3$; $\mathcal{B}_{2-1} \rightarrow \#7$; $\mathcal{B}_{1+1} \rightarrow \#8$; $\mathcal{B}_{2+2} \rightarrow \#4$; $\mathcal{B}_{2+1} \rightarrow \#6$. (g) $\mathcal{B}_0 \rightarrow \#1$; $\mathcal{B}_1 \rightarrow \#9$; $\mathcal{B}_2 \rightarrow \#7$ (overlaps with $\#5, \#6$); $\mathcal{B}_{1-1} \rightarrow \#2$; $\mathcal{B}_{2-2} \rightarrow \#4$; $\mathcal{B}_{2-1} \rightarrow \#5$; $\mathcal{B}_{1+1} \rightarrow \#8$; $\mathcal{B}_{2+2} \rightarrow \#6$; $\mathcal{B}_{2+1} \rightarrow \#3$. (h) $\mathcal{B}_0 \rightarrow \#1$; $\mathcal{B}_1 \rightarrow \#9$; $\mathcal{B}_2 \rightarrow \#5$ (overlaps with $\#4$); $\mathcal{B}_{1-1} \rightarrow \#2$; $\mathcal{B}_{2-2} \rightarrow \#3$; $\mathcal{B}_{2-1} \rightarrow \#8$; $\mathcal{B}_{1+1} \rightarrow \#4$; $\mathcal{B}_{2+2} \rightarrow \#6$ (overlaps with $\#7$); $\mathcal{B}_{2+1} \rightarrow \#7$.

for $\mathcal{U} \rightarrow -\infty$, all nine distinct coefficients survive [see Fig. 13(a)]; this state consists of only doubly and singly occupied sites [see second expression of Eq. (A2)]. In this case, the nine distinct coefficients are $\mathcal{B}_0^{4,-\infty} = 2/\pi$, $\mathcal{B}_1^{4,-\infty} = 2\sqrt{5}/(3\pi)$, $\mathcal{B}_2^{4,-\infty} = 2/(5\pi)$, $\mathcal{B}_{1-1}^{4,-\infty} = 26/(15\pi)$, $\mathcal{B}_{2-2}^{4,-\infty} = 2/(15\pi)$, $\mathcal{B}_{2-1}^{4,-\infty} = 2/(3\sqrt{5}\pi)$, $\mathcal{B}_{1+1}^{4,-\infty} = 4/(5\pi)$, $\mathcal{B}_{2+2}^{4,-\infty} = 1/(3\pi)$, and $\mathcal{B}_{2+1}^{4,-\infty} = 2/(\sqrt{5}\pi)$.

In the noninteracting case ($\mathcal{U} = 0$), for which the Hubbard eigenvector is given by Eq. (B1), all 13 cosinusoidal terms and nine distinct coefficients are present in Eq. (31), in agreement with Fig. 13(a), that is, $\mathcal{B}_0^{3r(4l),\mathcal{U}=0} = 2/\pi = 0.63662$, $\mathcal{B}_1^{3r(4l),\mathcal{U}=0} = 0.300105$, $\mathcal{B}_2^{3r(4l),\mathcal{U}=0} = -0.111766$, $\mathcal{B}_{1-1}^{3r(4l),\mathcal{U}=0} = -0.124185$, $\mathcal{B}_{2-2}^{3r(4l),\mathcal{U}=0} = 0.214057$, $\mathcal{B}_{2-1}^{3r(4l),\mathcal{U}=0} = 0.0243414$, $\mathcal{B}_{1+1}^{3r(4l),\mathcal{U}=0} = -0.0135114$, $\mathcal{B}_{2+2}^{3r(4l),\mathcal{U}=0} = -0.127997$, and $\mathcal{B}_{2+1}^{3r(4l),\mathcal{U}=0} = -0.178398$.

For $\mathcal{U} \rightarrow +\infty$, all 13 cosinusoidal terms survive in expression (31); the corresponding state is given by the first expression in Eq. (A1). In this case, the nine distinct coefficients are $\mathcal{B}_0^{3,+ \infty} = 2/\pi$, $\mathcal{B}_1^{3,+ \infty} = 2\sqrt{5}/(3\pi)$, $\mathcal{B}_2^{3,+ \infty} = 2/(5\pi)$,

$$\mathcal{B}_{1-1}^{3,+ \infty} = 26/(15\pi), \mathcal{B}_{2-2}^{3,+ \infty} = 2/(15\pi), \mathcal{B}_{2-1}^{3,+ \infty} = 2/(3\sqrt{5}\pi), \mathcal{B}_{1+1}^{3,+ \infty} = 4/(5\pi), \mathcal{B}_{2+2}^{3,+ \infty} = 1/(3\pi), \text{ and } \mathcal{B}_{2+1}^{3,+ \infty} = 2/(\sqrt{5}\pi).$$

We note that ${}^2\mathcal{G}_4^{b,-\infty}(k_1, k_2) = {}^2\mathcal{G}_3^{b,+ \infty}(k_1, k_2)$.

For the excited state denoted as $i = 4r(3l)$ ($i = 4$ for $0 < \mathcal{U} < +\infty$ and $i = 3$ for $-\infty < \mathcal{U} < 0$) and for $\mathcal{U} \rightarrow -\infty$, only the constant term survives in expression (31); the corresponding state is given by the second expression in Eq. (A1) and is a NOON state of the form $(|300\rangle + |003\rangle)/\sqrt{2}$. In this case, the second-order correlation function is given by

$${}^2\mathcal{G}_3^{b,-\infty}(k_1, k_2) = \frac{2}{\pi} s^2 e^{-2(k_1^2 + k_2^2)s^2}. \quad (\text{F1})$$

In the noninteracting case ($\mathcal{U} = 0$), for which the Hubbard eigenvector is given by Eq. (B2), all 13 cosinusoidal terms and nine distinct coefficients are present in Eq. (31), in agreement with Fig. 13(b), that is, $\mathcal{B}_0^{4r(3l),\mathcal{U}=0} = 2/\pi = 0.63662$, $\mathcal{B}_1^{4r(3l),\mathcal{U}=0} = 0.300105$, $\mathcal{B}_2^{4r(3l),\mathcal{U}=0} = 0.111766$, $\mathcal{B}_{1-1}^{4r(3l),\mathcal{U}=0} = 0.124185$, $\mathcal{B}_{2-2}^{4r(3l),\mathcal{U}=0} = 0.0246755$, $\mathcal{B}_{2-1}^{4r(3l),\mathcal{U}=0} = 0.0506849$, $\mathcal{B}_{1+1}^{4r(3l),\mathcal{U}=0} = -0.410902$, $\mathcal{B}_{2+2}^{4r(3l),\mathcal{U}=0} = 0.154523$, and $\mathcal{B}_{2+1}^{4r(3l),\mathcal{U}=0} = -0.0466808$.

For $\mathcal{U} \rightarrow +\infty$, six cosinusoidal terms survive in expression (31); see Fig. 13(b). The corresponding state is given by the first expression in Eq. (A2). In this case, the five nonzero distinct coefficients are $\mathcal{B}_0^{4,+\infty} = 2/\pi$, $\mathcal{B}_1^{4,+\infty} = 0$, $\mathcal{B}_2^{4,+\infty} = 6/(5\pi)$, $\mathcal{B}_{1-1}^{4,+\infty} = -4/(5\pi)$, $\mathcal{B}_{2-2}^{4,+\infty} = 16/(15\pi)$, $\mathcal{B}_{2-1}^{4,+\infty} = 0$, $\mathcal{B}_{1+1}^{4,+\infty} = -4/(15\pi)$, $\mathcal{B}_{2+2}^{4,+\infty} = 0$, and $\mathcal{B}_{2+1}^{4,+\infty} = 0$.

The excited state denoted as $i = 5r(6l)$ ($i = 5$ for $0 < \mathcal{U} < +\infty$ and $i = 6$ for $-\infty < \mathcal{U} < 0$) is \mathcal{U} independent; see the first expression in Eq. (A3) or second expression in Eq. (A4). In this case, five distinct coefficients (corresponding to six cosinusoidal terms) survive in expression (31), that is, $\mathcal{B}_0^{5,+\infty} = \mathcal{B}_0^{6,-\infty} = \mathcal{B}_0^{5r(6l),\mathcal{U}=0} = 2/\pi$, $\mathcal{B}_1^{5,+\infty} = \mathcal{B}_1^{6,-\infty} = \mathcal{B}_1^{5r(6l),\mathcal{U}=0} = 0$, $\mathcal{B}_2^{5,+\infty} = \mathcal{B}_2^{6,-\infty} = \mathcal{B}_2^{5r(6l),\mathcal{U}=0} = -6/(5\pi)$, $\mathcal{B}_{1-1}^{5,+\infty} = \mathcal{B}_{1-1}^{6,-\infty} = \mathcal{B}_{1-1}^{5r(6l),\mathcal{U}=0} = -4/(5\pi)$, $\mathcal{B}_{2-2}^{5,+\infty} = \mathcal{B}_{2-2}^{6,-\infty} = \mathcal{B}_{2-2}^{5r(6l),\mathcal{U}=0} = 16/(15\pi)$, $\mathcal{B}_{2-1}^{5,+\infty} = \mathcal{B}_{2-1}^{6,-\infty} = \mathcal{B}_{2-1}^{5r(6l),\mathcal{U}=0} = 0$, $\mathcal{B}_{1+1}^{5,+\infty} = \mathcal{B}_{1+1}^{6,-\infty} = \mathcal{B}_{1+1}^{5r(6l),\mathcal{U}=0} = 4/(15\pi)$, $\mathcal{B}_{2+2}^{5,+\infty} = \mathcal{B}_{2+2}^{6,-\infty} = \mathcal{B}_{2+2}^{5r(6l),\mathcal{U}=0} = 0$, and $\mathcal{B}_{2+1}^{5,+\infty} = \mathcal{B}_{2+1}^{6,-\infty} = \mathcal{B}_{2+1}^{5r(6l),\mathcal{U}=0} = 0$; see Fig. 13(c).

For the excited state denoted as $i = 6r(5l)$ ($i = 6$ for $0 < \mathcal{U} < +\infty$ and $i = 5$ for $-\infty < \mathcal{U} < 0$) and for $\mathcal{U} \rightarrow -\infty$, all nine distinct coefficients [see Fig. 13(d)] and 13 cosinusoidal terms survive in expression (31); the corresponding state is given by the second expression in Eq. (A3). In this case, the nine distinct coefficients are $\mathcal{B}_0^{5,-\infty} = 2/\pi$, $\mathcal{B}_1^{5,-\infty} = 2\sqrt{5}/(3\pi)$, $\mathcal{B}_2^{5,-\infty} = -2/(5\pi)$, $\mathcal{B}_{1-1}^{5,-\infty} = 26/(15\pi)$, $\mathcal{B}_{2-2}^{5,-\infty} = 2/(15\pi)$, $\mathcal{B}_{2-1}^{5,-\infty} = 2/(3\sqrt{5}\pi)$, $\mathcal{B}_{1+1}^{5,-\infty} = -4/(5\pi)$, $\mathcal{B}_{2+2}^{5,-\infty} = -1/(3\pi)$, and $\mathcal{B}_{2+1}^{5,-\infty} = -2/(\sqrt{5}\pi)$.

In the noninteracting case ($\mathcal{U} = 0$), for which the Hubbard eigenvector is given by Eq. (B4), six distinct coefficients (corresponding to seven cosinusoidal terms) are present in expression (31), in agreement with Fig. 13(d). That is, $\mathcal{B}_0^{6r(5l),\mathcal{U}=0} = 2/\pi = 0.63662$, $\mathcal{B}_1^{6r(5l),\mathcal{U}=0} = 0$, $\mathcal{B}_2^{6r(5l),\mathcal{U}=0} = -4/(5\pi)$, $\mathcal{B}_{1-1}^{6r(5l),\mathcal{U}=0} = 4/(5\pi)$, $\mathcal{B}_{2-2}^{6r(5l),\mathcal{U}=0} = 1/(10\pi)$, $\mathcal{B}_{2-1}^{6r(5l),\mathcal{U}=0} = 0$, $\mathcal{B}_{1+1}^{6r(5l),\mathcal{U}=0} = -8/(5\pi)$, $\mathcal{B}_{2+2}^{6r(5l),\mathcal{U}=0} = 1/(2\pi)$, and $\mathcal{B}_{2+1}^{6r(5l),\mathcal{U}=0} = 0$.

For $\mathcal{U} \rightarrow +\infty$, all 13 cosinusoidal terms survive in expression (31); the corresponding state is given by the first expression in Eq. (A4). In this case, in agreement with the frame (d) of Fig. 13, the nine distinct coefficients are $\mathcal{B}_0^{6,+ \infty} = 2/\pi$, $\mathcal{B}_1^{6,+ \infty} = -2\sqrt{5}/(3\pi)$, $\mathcal{B}_2^{6,+ \infty} = -2/(5\pi)$, $\mathcal{B}_{1-1}^{6,+ \infty} = 26/(15\pi)$, $\mathcal{B}_{2-2}^{6,+ \infty} = 2/(15\pi)$, $\mathcal{B}_{2-1}^{6,+ \infty} = -2/(3\sqrt{5}\pi)$, $\mathcal{B}_{1+1}^{6,+ \infty} = -4/(5\pi)$, $\mathcal{B}_{2+2}^{6,+ \infty} = -1/(3\pi)$, and $\mathcal{B}_{2+1}^{6,+ \infty} = 2/(\sqrt{5}\pi)$.

For the excited state denoted as $i = 7r(8l)$ ($i = 7$ for $0 < \mathcal{U} < +\infty$ and $i = 8$ for $-\infty < \mathcal{U} < 0$) and for $\mathcal{U} \rightarrow -\infty$, all nine distinct coefficients [see Fig. 13(e)] and 13 cosinusoidal terms survive in expression (31); the corresponding state is given by the second expression in Eq. (A6). In this case, the nine distinct coefficients are $\mathcal{B}_0^{8,-\infty} = 2/\pi$, $\mathcal{B}_1^{8,-\infty} = -2\sqrt{5}/(3\pi)$, $\mathcal{B}_2^{8,-\infty} = 2/(5\pi)$, $\mathcal{B}_{1-1}^{8,-\infty} = 26/(15\pi)$, $\mathcal{B}_{2-2}^{8,-\infty} = 2/(15\pi)$, $\mathcal{B}_{2-1}^{8,-\infty} = -2/(3\sqrt{5}\pi)$, $\mathcal{B}_{1+1}^{8,-\infty} = 4/(5\pi)$, $\mathcal{B}_{2+2}^{8,-\infty} = 1/(3\pi)$, and $\mathcal{B}_{2+1}^{8,-\infty} = -2/(\sqrt{5}\pi)$.

In the noninteracting case ($\mathcal{U} = 0$), for which the Hubbard eigenvector is given by Eq. (B5), all 13 cosinusoidal terms and nine distinct coefficients are present in Eq. (31), in agreement with Fig. 13(e), that is, $\mathcal{B}_0^{7r(8l),\mathcal{U}=0} = 2/\pi = 0.63662$, $\mathcal{B}_1^{7r(8l),\mathcal{U}=0} = -0.300105$, $\mathcal{B}_2^{7r(8l),\mathcal{U}=0} = -0.111766$, $\mathcal{B}_{1-1}^{7r(8l),\mathcal{U}=0} = -0.124185$, $\mathcal{B}_{2-2}^{7r(8l),\mathcal{U}=0} = 0.214057$, $\mathcal{B}_{2-1}^{7r(8l),\mathcal{U}=0} = -0.0243414$, $\mathcal{B}_{1+1}^{7r(8l),\mathcal{U}=0} = -0.0135114$, $\mathcal{B}_{2+2}^{7r(8l),\mathcal{U}=0} = -0.127997$, and $\mathcal{B}_{2+1}^{7r(8l),\mathcal{U}=0} = 0.178398$.

For $\mathcal{U} \rightarrow +\infty$, all nine distinct coefficients [see Fig. 13(e)] and 13 cosinusoidal terms survive in expression (31); the corresponding state is given by the first expression in Eq. (A5). In this case, the nine distinct coefficients are $\mathcal{B}_0^{7,+ \infty} = 2/\pi$, $\mathcal{B}_1^{7,+ \infty} = -2\sqrt{5}/(3\pi)$, $\mathcal{B}_2^{7,+ \infty} = 2/(5\pi)$, $\mathcal{B}_{1-1}^{7,+ \infty} = 26/(15\pi)$, $\mathcal{B}_{2-2}^{7,+ \infty} = 2/(15\pi)$, $\mathcal{B}_{2-1}^{7,+ \infty} = -2/(3\sqrt{5}\pi)$, $\mathcal{B}_{1+1}^{7,+ \infty} = 4/(5\pi)$, $\mathcal{B}_{2+2}^{7,+ \infty} = 1/(3\pi)$, and $\mathcal{B}_{2+1}^{7,+ \infty} = -2/(\sqrt{5}\pi)$.

We note that ${}^2\mathcal{G}_8^{b,-\infty}(k_1, k_2) = {}^2\mathcal{G}_7^{b,+ \infty}(k_1, k_2)$.

For the excited state denoted as $i = 8r(7l)$ ($i = 8$ for $0 < \mathcal{U} < +\infty$ and $i = 7$ for $-\infty < \mathcal{U} < 0$) and for $\mathcal{U} \rightarrow -\infty$, five distinct coefficients [see Fig. 13(f)] and six cosinusoidal terms survive in expression (31); the corresponding state is given by the second expression in Eq. (A5). In this case, the five distinct coefficients are $\mathcal{B}_0^{7,-\infty} = 2/\pi$, $\mathcal{B}_1^{7,-\infty} = 0$, $\mathcal{B}_2^{7,-\infty} = 6/(5\pi)$, $\mathcal{B}_{1-1}^{7,-\infty} = -4/(5\pi)$, $\mathcal{B}_{2-2}^{7,-\infty} = 16/(15\pi)$, $\mathcal{B}_{2-1}^{7,-\infty} = 0$, $\mathcal{B}_{1+1}^{7,-\infty} = -4/(15\pi)$, $\mathcal{B}_{2+2}^{7,-\infty} = 0$, and $\mathcal{B}_{2+1}^{7,-\infty} = 0$.

In the noninteracting case ($\mathcal{U} = 0$), for which the Hubbard eigenvector is given by Eq. (B6), all 13 cosinusoidal terms and nine distinct coefficients are present in Eq. (31), in agreement with Fig. 13(f), that is, $\mathcal{B}_0^{8r(7l),\mathcal{U}=0} = 2/\pi = 0.63662$, $\mathcal{B}_1^{8r(7l),\mathcal{U}=0} = -0.300105$, $\mathcal{B}_2^{8r(7l),\mathcal{U}=0} = 0.111766$, $\mathcal{B}_{1-1}^{8r(7l),\mathcal{U}=0} = 0.124185$, $\mathcal{B}_{2-2}^{8r(7l),\mathcal{U}=0} = 0.0246755$, $\mathcal{B}_{2-1}^{8r(7l),\mathcal{U}=0} = -0.0506849$, $\mathcal{B}_{1+1}^{8r(7l),\mathcal{U}=0} = -0.410902$, $\mathcal{B}_{2+2}^{8r(7l),\mathcal{U}=0} = 0.154523$, and $\mathcal{B}_{2+1}^{8r(7l),\mathcal{U}=0} = 0.0466808$.

For $\mathcal{U} \rightarrow +\infty$, only the constant coefficient survives [see Fig. 13(f)]. The corresponding state is given by the first expression in Eq. (A6) and it is a NOON state of the form $(|300\rangle + |003\rangle)/\sqrt{2}$. In this case, the second-order correlation is

$${}^2\mathcal{G}_8^{b,+ \infty}(k_1, k_2) = \frac{2}{\pi} s^2 e^{-2(k_1^2 + k_2^2)s^2}. \quad (\text{F2})$$

For the excited state denoted as $i = 9$ for $-\infty < \mathcal{U} < +\infty$ and for $\mathcal{U} \rightarrow -\infty$, all nine distinct coefficients [see Fig. 13(g)] and 13 cosinusoidal terms survive in expression (31); the corresponding state is given by the second expression in Eq. (A7). In this case, the nine distinct coefficients are $\mathcal{B}_0^{9,-\infty} = 2/\pi$, $\mathcal{B}_1^{9,-\infty} = -2\sqrt{5}/(3\pi)$, $\mathcal{B}_2^{9,-\infty} = -2/(5\pi)$, $\mathcal{B}_{1-1}^{9,-\infty} = 26/(15\pi)$, $\mathcal{B}_{2-2}^{9,-\infty} = 2/(15\pi)$, $\mathcal{B}_{2-1}^{9,-\infty} = -2/(3\sqrt{5}\pi)$, $\mathcal{B}_{1+1}^{9,-\infty} = -4/(5\pi)$, $\mathcal{B}_{2+2}^{9,-\infty} = -1/(3\pi)$, and $\mathcal{B}_{2+1}^{9,-\infty} = 2/(\sqrt{5}\pi)$.

In the noninteracting case ($\mathcal{U} = 0$), for which the Hubbard eigenvector is given by Eq. (B7), 10 cosinusoidal terms and seven distinct coefficients are present in Eq. (31), in agreement with Fig. 13(g), that is, $\mathcal{B}_0^{9,\mathcal{U}=0} = 2/\pi = 0.63662$, $\mathcal{B}_1^{9,\mathcal{U}=0} = -4\sqrt{2}/(3\pi)$, $\mathcal{B}_2^{9,\mathcal{U}=0} = 0$, $\mathcal{B}_{1-1}^{9,\mathcal{U}=0} = 4/(3\pi)$,

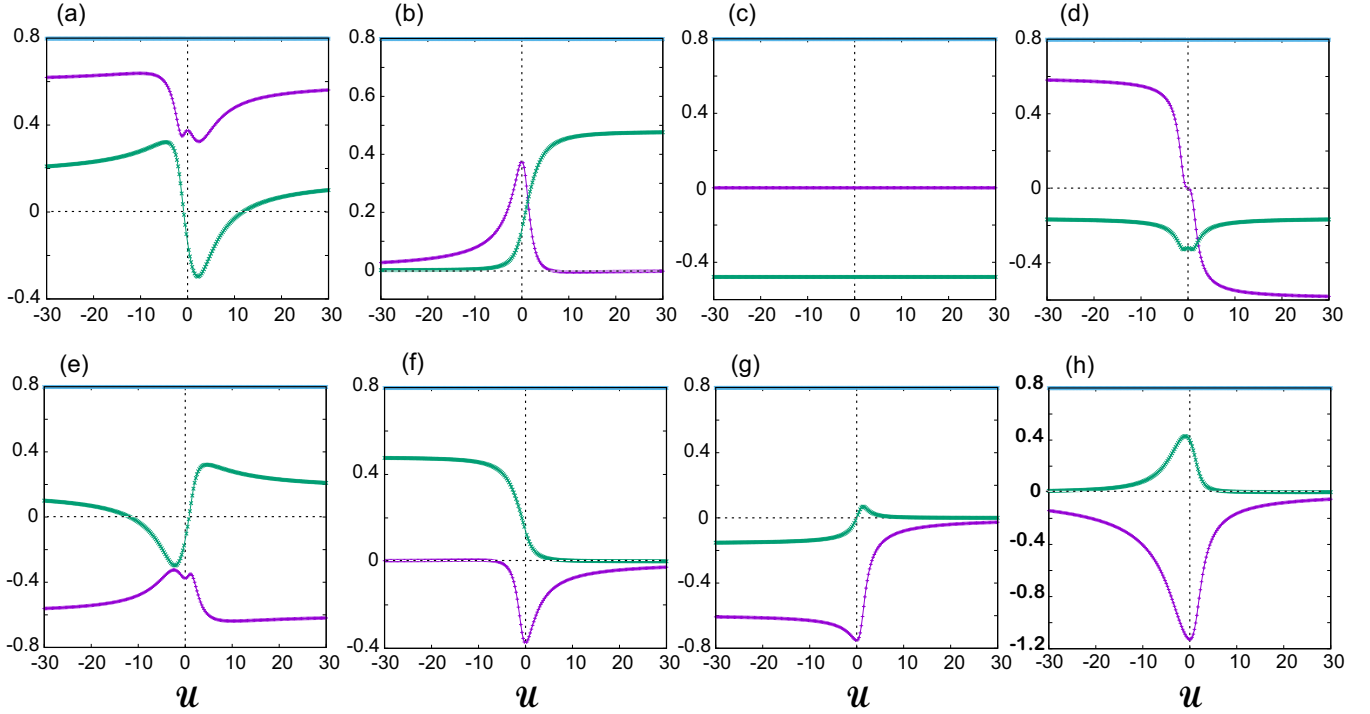


FIG. 14. The \mathcal{A} coefficients (dimensionless) [see Eq. (36)] for the remaining eight excited eigenstates of three bosons trapped in three linearly arranged wells as a function of \mathcal{U} (horizontal axis, dimensionless). This figure complements Fig. 7 in the main text. (a) $i = 3r(4l)$. (b) $i = 4r(3l)$. (c) $i = 5r(6l)$. (d) $i = 6r(5l)$. (e) $i = 7r(8l)$. (f) $i = 8r(7l)$. (g) $i = 9$. (h) $i = 10$. See text for a detailed description. The choice of online colors is the same as in Fig. 7, that is, \mathcal{A}_0 , constant (light blue); \mathcal{A}_1 , violet; \mathcal{A}_2 , green. For the print grayscale version, excluding the top constant \mathcal{A}_0 horizontal line, the positioning of the two remaining curves at $\mathcal{U} = -30$ is as follows: [(a)–(d)] $\mathcal{A}_1 \rightarrow$ upper curve; $\mathcal{A}_2 \rightarrow$ lower curve. [(e)–(h)] $\mathcal{A}_1 \rightarrow$ lower curve; $\mathcal{A}_2 \rightarrow$ upper curve.

$$\mathcal{B}_{2-2}^{9,\mathcal{U}=0} = 1/(12\pi), \quad \mathcal{B}_{2-1}^{9,\mathcal{U}=0} = -1/(3\sqrt{2}\pi), \quad \mathcal{B}_{1+1}^{9,\mathcal{U}=0} = 0, \\ \mathcal{B}_{2+2}^{9,\mathcal{U}=0} = -7/(12\pi), \quad \text{and } \mathcal{B}_{2+1}^{9,\mathcal{U}=0} = 1/(\sqrt{2}\pi).$$

For $\mathcal{U} \rightarrow +\infty$, only the constant coefficient survives [see Fig. 13(g)]. The corresponding state is given by the first expression in Eq. (A7) and it is a NOON state of the form $(-|300\rangle + |003\rangle)/\sqrt{2}$. In this case, the second-order correlation function is

$${}^2\mathcal{G}_9^{b,+\infty}(k_1, k_2) = \frac{2}{\pi} s^2 e^{-2(k_1^2 + k_2^2)s^2}. \quad (\text{F3})$$

For the excited state denoted as $i = 10$ for $-\infty < \mathcal{U} < +\infty$ and for $\mathcal{U} \rightarrow -\infty$, three terms survive, including the constant one [see Fig. 13(h)]. The corresponding state is that of all three wells being singly occupied. In this case, the second-order correlation function is given by

$${}^2\mathcal{G}_{10}^{b,-\infty}(k_1, k_2) = \frac{2}{3\pi} s^2 e^{-2(k_1^2 + k_2^2)s^2} \{3 + 2 \cos[d(k_1 - k_2)] \\ + \cos[2d(k_1 - k_2)]\}. \quad (\text{F4})$$

In the noninteracting case ($\mathcal{U} = 0$), for which the Hubbard eigenvector is given by Eq. (B8), all 13 cosinusoidal terms and nine distinct coefficients are present in Eq. (31), in agreement with Fig. 13(h), that is, $\mathcal{B}_0^{10,\mathcal{U}=0} = 2/\pi = 0.63662$, $\mathcal{B}_1^{10,\mathcal{U}=0} = -2\sqrt{2}/\pi$, $\mathcal{B}_2^{10,\mathcal{U}=0} = 1/\pi$, $\mathcal{B}_{1-1}^{10,\mathcal{U}=0} = 2/\pi$, $\mathcal{B}_{2-2}^{10,\mathcal{U}=0} = 1/(4\pi)$, $\mathcal{B}_{2-1}^{10,\mathcal{U}=0} = -1/(\sqrt{2}\pi)$, $\mathcal{B}_{1+1}^{10,\mathcal{U}=0} = 2/\pi$, $\mathcal{B}_{2+2}^{10,\mathcal{U}=0} = 1/(4\pi)$, and $\mathcal{B}_{2+1}^{10,\mathcal{U}=0} = -1/(\sqrt{2}\pi)$.

For $\mathcal{U} \rightarrow +\infty$ only the constant term, $\mathcal{B}_0^{10} = 2/\pi$, survives [see Fig. 13(h)]. The corresponding state is the triply occupied middle well. In this case, the second-order correlation function is

$${}^2\mathcal{G}_{10}^{b,+\infty}(k_1, k_2) = \frac{2}{\pi} s^2 e^{-2(k_1^2 + k_2^2)s^2}. \quad (\text{F5})$$

APPENDIX G: FIRST-ORDER MOMENTUM CORRELATIONS AS A FUNCTION OF \mathcal{U} FOR THE REMAINING EIGHT EXCITED STATES

Figure 14 complements Fig. 7 in that it displays the three distinct coefficients $\mathcal{A}^i(\mathcal{U})$'s for the remaining eight excited states (explicit numerical values can be found in the Supplemental Material [67]). The dependence of these coefficients on the interaction strength \mathcal{U} is better deciphered by using as reference points the special cases at $\mathcal{U} \rightarrow \pm\infty$ and $\mathcal{U} = 0$. Note that in all cases the \mathcal{B}^i values at the end points $\mathcal{U} = \pm 30$ in the figure are close to the corresponding limiting values at $\mathcal{U} \rightarrow \pm\infty$.

In particular, for the excited state denoted as $i = 3r(4l)$ ($i = 3$ for $0 < \mathcal{U} < +\infty$ and $i = 4$ for $-\infty < \mathcal{U} < 0$) and for $\mathcal{U} \rightarrow -\infty$, all three cosinusoidal terms survive in expression (36) [see Fig. 14](a); specifically one has $\mathcal{A}_0^{4,-\infty} = 0.797885 = \sqrt{2}/\pi$, $\mathcal{A}_1^{4,-\infty} = \sqrt{10}/(3\sqrt{\pi})$, and $\mathcal{A}_2^{4,-\infty} = \sqrt{2}/(5\sqrt{\pi})$.

For the noninteracting case ($\mathcal{U} = 0$), all three coefficients survive in expression (36) [see Fig. 14(a)];

specifically one has $\mathcal{A}_0^{3r(4l),\mathcal{U}=0} = 0.797885 = \sqrt{2/\pi}$, $\mathcal{A}_1^{3r(4l),\mathcal{U}=0} = 0.376126$, and $\mathcal{A}_2^{3r(4l),\mathcal{U}=0} = -0.140078$.

For $\mathcal{U} \rightarrow +\infty$, all three cosinusoidal terms survive in expression (36) [see Fig. 14(a)]; specifically one has $\mathcal{A}_0^{3,+ \infty} = 0.797885 = \sqrt{2/\pi}$, $\mathcal{A}_1^{3,+ \infty} = \sqrt{10}/(3\sqrt{\pi})$, and $\mathcal{A}_2^{3,+ \infty} = \sqrt{2}/(5\sqrt{\pi})$.

For the excited state denoted as $i = 4r(3l)$ ($i = 4$ for $0 < \mathcal{U} < +\infty$ and $i = 3$ for $-\infty < \mathcal{U} < 0$) and for $\mathcal{U} \rightarrow -\infty$, only one cosinusoidal term survives in expression (36) [see Fig. 14(b)]; specifically one has $\mathcal{A}_0^{3,- \infty} = 0.797885 = \sqrt{2/\pi}$, $\mathcal{A}_1^{3,- \infty} = 0$, and $\mathcal{A}_2^{3,- \infty} = 0$.

For the noninteracting case ($\mathcal{U} = 0$), all three coefficients survive in expression (36) [see Fig. 14(b)]; specifically one has $\mathcal{A}_0^{4r(3l),\mathcal{U}=0} = 0.797885 = \sqrt{2/\pi}$, $\mathcal{A}_1^{4r(3l),\mathcal{U}=0} = 0.376126$, and $\mathcal{A}_2^{4r(3l),\mathcal{U}=0} = 0.140078$.

For $\mathcal{U} \rightarrow +\infty$, two cosinusoidal terms survive in expression (36) [see Fig. 14(b)]; specifically one has $\mathcal{A}_0^{4,+ \infty} = 0.797885 = \sqrt{2/\pi}$, $\mathcal{A}_1^{4,+ \infty} = 0$, and $\mathcal{A}_2^{4,+ \infty} = 3\sqrt{2}/(5\sqrt{\pi})$.

The excited state denoted as $i = 5r(6l)$ ($i = 5$ for $0 < \mathcal{U} < +\infty$ and $i = 6$ for $-\infty < \mathcal{U} < 0$) is \mathcal{U} independent; see the first expression in Eq. (A3) or second expression in Eq. (A4). In this case, two distinct coefficients (corresponding to two cosinusoidal terms) survive in expression (36), that is, $\mathcal{A}_0^{5,+ \infty} = \mathcal{A}_0^{6,- \infty} = \sqrt{2/\pi} = \mathcal{A}_0^{5r(6l),\mathcal{U}=0} = 0.797885$, $\mathcal{A}_1^{5,+ \infty} = \mathcal{A}_1^{6,- \infty} = \mathcal{A}_1^{5r(6l),\mathcal{U}=0} = 0$, and $\mathcal{A}_2^{5,+ \infty} = \mathcal{A}_2^{6,- \infty} = \mathcal{A}_2^{5r(6l),\mathcal{U}=0} = -3\sqrt{2}/(5\sqrt{\pi})$; see Fig. 14(c).

For the excited state denoted as $i = 6r(5l)$ ($i = 6$ for $0 < \mathcal{U} < +\infty$ and $i = 5$ for $-\infty < \mathcal{U} < 0$) and for $\mathcal{U} \rightarrow -\infty$, all three cosinusoidal terms survive in expression (36) [see in Fig. 14(d)]; specifically one has $\mathcal{A}_0^{5,- \infty} = 0.797885 = \sqrt{2/\pi}$, $\mathcal{A}_1^{5,- \infty} = \sqrt{10}/(3\sqrt{\pi})$, and $\mathcal{A}_2^{5,- \infty} = -\sqrt{2}/(5\sqrt{\pi})$.

For the noninteracting case ($\mathcal{U} = 0$), two coefficients are present in expression (36) [see Fig. 14(d)]; specifically one has: $\mathcal{A}_0^{6r(5l),\mathcal{U}=0} = 0.797885 = \sqrt{2/\pi}$, $\mathcal{A}_1^{6r(5l),\mathcal{U}=0} = 0$, and $\mathcal{A}_2^{6r(5l),\mathcal{U}=0} = -2\sqrt{2}/(5\sqrt{\pi})$.

For $\mathcal{U} \rightarrow +\infty$, all three cosinusoidal terms survive in expression (36) [see Fig. 14(d)]; specifically one has $\mathcal{A}_0^{6,+ \infty} = 0.797885 = \sqrt{2/\pi}$, $\mathcal{A}_1^{6,+ \infty} = -\sqrt{10}/(3\sqrt{\pi})$, and $\mathcal{A}_2^{6,+ \infty} = -\sqrt{2}/(5\sqrt{\pi})$.

For the excited state denoted as $i = 7r(8l)$ ($i = 7$ for $0 < \mathcal{U} < +\infty$ and $i = 8$ for $-\infty < \mathcal{U} < 0$) and for $\mathcal{U} \rightarrow -\infty$, all three cosinusoidal terms survive in expression (36) [see Fig. 14(e)]; specifically one has $\mathcal{A}_0^{8,- \infty} = 0.797885 = \sqrt{2/\pi}$, $\mathcal{A}_1^{8,- \infty} = -\sqrt{10}/(3\sqrt{\pi})$, and $\mathcal{A}_2^{8,- \infty} = \sqrt{2}/(5\sqrt{\pi})$.

For the noninteracting case ($\mathcal{U} = 0$), all three coefficients are present in expression (36) [see Fig. 14(e)]; specifically one has $\mathcal{A}_0^{7r(8l),\mathcal{U}=0} = 0.797885 = \sqrt{2/\pi}$, $\mathcal{A}_1^{7r(8l),\mathcal{U}=0} = -0.376126$, and $\mathcal{A}_2^{7r(8l),\mathcal{U}=0} = -0.140078$.

For $\mathcal{U} \rightarrow +\infty$, all three cosinusoidal terms survive in expression (36) [see Fig. 14(e)]; specifically one has $\mathcal{A}_0^{7,+ \infty} = 0.797885 = \sqrt{2/\pi}$, $\mathcal{A}_1^{7,+ \infty} = -\sqrt{10}/(3\sqrt{\pi})$, and $\mathcal{A}_2^{7,+ \infty} = \sqrt{2}/(5\sqrt{\pi})$.

For the excited state denoted as $i = 8r(7l)$ ($i = 8$ for $0 < \mathcal{U} < +\infty$ and $i = 7$ for $-\infty < \mathcal{U} < 0$) and for $\mathcal{U} \rightarrow -\infty$, two cosinusoidal terms are present in expression (36) [see Fig. 14(f)]; specifically one has $\mathcal{A}_0^{7,- \infty} = 0.797885 = \sqrt{2/\pi}$, $\mathcal{A}_1^{7,- \infty} = 0$, and $\mathcal{A}_2^{7,- \infty} = 3\sqrt{2}/(5\sqrt{\pi})$.

For the noninteracting case ($\mathcal{U} = 0$), all three coefficients are present in expression (36) [see Fig. 14(f)]; specifically one has $\mathcal{A}_0^{8r(7l),\mathcal{U}=0} = 0.797885 = \sqrt{2/\pi}$, $\mathcal{A}_1^{8r(7l),\mathcal{U}=0} = -0.376126$, and $\mathcal{A}_2^{8r(7l),\mathcal{U}=0} = 0.140078$.

For $\mathcal{U} \rightarrow +\infty$, only the \mathcal{U} -independent term survives in expression (36) [see Fig. 14(f)]; specifically one has $\mathcal{A}_0^{8,+ \infty} = 0.797885 = \sqrt{2/\pi}$, $\mathcal{A}_1^{8,+ \infty} = 0$, and $\mathcal{A}_2^{8,+ \infty} = 0$.

For the excited state denoted as $i = 9$ for $-\infty < \mathcal{U} < +\infty$ and for $\mathcal{U} \rightarrow -\infty$, all three cosinusoidal terms are present in expression (36) [see Fig. 14(g)]; specifically one has $\mathcal{A}_0^{9,- \infty} = 0.797885 = \sqrt{2/\pi}$, $\mathcal{A}_1^{9,- \infty} = -\sqrt{10}/(3\sqrt{\pi})$, and $\mathcal{A}_2^{9,- \infty} = -\sqrt{2}/(5\sqrt{\pi})$.

For the noninteracting case ($\mathcal{U} = 0$), two coefficients are present in expression (36) [see Fig. 14(g)]; specifically one has $\mathcal{A}_0^{9,\mathcal{U}=0} = 0.797885 = \sqrt{2/\pi}$, $\mathcal{A}_1^{9,\mathcal{U}=0} = -4/(3\sqrt{\pi})$, and $\mathcal{A}_2^{9,\mathcal{U}=0} = 0$.

For $\mathcal{U} \rightarrow +\infty$, only the \mathcal{U} -independent term survives in expression (36) [see Fig. 14(g)]; specifically one has $\mathcal{A}_0^{9,+ \infty} = 0.797885 = \sqrt{2/\pi}$, $\mathcal{A}_1^{9,+ \infty} = 0$, and $\mathcal{A}_2^{9,+ \infty} = 0$.

For the excited state denoted as $i = 10$ for $-\infty < \mathcal{U} < +\infty$ and for $\mathcal{U} \rightarrow -\infty$, only the \mathcal{U} -independent term is present in expression (36) [see Fig. 14(h)]; specifically one has $\mathcal{A}_0^{10,- \infty} = 0.797885 = \sqrt{2/\pi}$, $\mathcal{A}_1^{10,- \infty} = 0$, and $\mathcal{A}_2^{10,- \infty} = 0$.

For the noninteracting case ($\mathcal{U} = 0$), all three coefficients are present in expression (36) [see Fig. 14(h)]; specifically one has $\mathcal{A}_0^{10,\mathcal{U}=0} = 0.797885 = \sqrt{2/\pi}$, $\mathcal{A}_1^{10,\mathcal{U}=0} = -2/\sqrt{\pi}$, and $\mathcal{A}_2^{10,\mathcal{U}=0} = 1/\sqrt{2\pi}$.

For $\mathcal{U} \rightarrow +\infty$, only the \mathcal{U} -independent term survives in expression (36) [see Fig. 14(h)]; specifically one has $\mathcal{A}_0^{10,+ \infty} = 0.797885 = \sqrt{2/\pi}$, $\mathcal{A}_1^{10,+ \infty} = 0$, and $\mathcal{A}_2^{10,+ \infty} = 0$.

[1] J. I. Cirac and P. Zoller, Goals and opportunities in quantum simulation, *Nat. Phys.* **8**, 264 (2012).
 [2] M. A. García-March, B. Juliá-Díaz, G. E. Astrakharchik, T. Busch, J. Boronat and A. Polls, Quantum correlations and spatial localization in one-dimensional ultracold bosonic mixtures, *New J. Phys.* **16**, 103004 (2014).
 [3] J. H. Becher, E. Sindici, R. Klemt, S. Jochim, A. J. Daley, and P. M. Preiss, Measurement of identical particle entanglement and the influence of antisymmetrisation, [arXiv:2002.11207](https://arxiv.org/abs/2002.11207).

[4] P. M. Preiss, J. H. Becher, R. Klemt, V. Klinkhamer, A. Bergschneider, and S. Jochim, High-Contrast Interference of Ultracold Fermions, *Phys. Rev. Lett.* **122**, 143602 (2019).
 [5] A. Bergschneider, V. M. Klinkhamer, J. H. Becher, R. Klemt, L. Palm, G. Zürn, S. Jochim, and P. M. Preiss, Experimental characterization of two-particle entanglement through position and momentum correlations, *Nat. Phys.* **15**, 640 (2019).
 [6] M. Greiner, O. Mandel, T. Esslinger, T. W. Hänsch, and I. Bloch, Quantum phase transition from a superfluid to a Mott

- insulator in a gas of ultracold atoms, *Nature (London)* **415**, 39 (2002).
- [7] F. Gerbier, A. Widera, S. Fölling, O. Mandel, T. Gericke, and I. Bloch, Phase Coherence of an Atomic Mott Insulator, *Phys. Rev. Lett.* **95**, 050404 (2005).
- [8] F. Gerbier, A. Widera, S. Fölling, O. Mandel, T. Gericke, and I. Bloch, Interference pattern and visibility of a Mott insulator, *Phys. Rev. A* **72**, 053606 (2005).
- [9] H. Cayla, C. Carcy, Q. Bouton, R. Chang, G. Carleo, M. Mancini, and D. Clément, Single-atom-resolved probing of lattice gases in momentum space, *Phys. Rev. A* **97**, 061609(R) (2018).
- [10] C. Carcy, H. Cayla, A. Tenart, A. Aspect, M. Mancini, and D. Clément, Momentum-Space Atom Correlations in a Mott Insulator, *Phys. Rev. X* **9**, 041028 (2019).
- [11] S. S. Hodgman, R. I. Khakimov, R. J. Lewis-Swan, A. G. Truscott, and K. V. Kheruntsyan, Solving the Quantum Many-Body Problem via Correlations Measured with a Momentum Microscope, *Phys. Rev. Lett.* **118**, 240402 (2017).
- [12] H. Ott, Single atom detection in ultracold quantum gases: A review of current progress, *Rep. Prog. Phys.* **79**, 054401 (2016).
- [13] B. B. Brandt, C. Yannouleas, and U. Landman, Two-point momentum correlations of few ultracold quasi-one-dimensional trapped fermions: Diffraction patterns, *Phys. Rev. A* **96**, 053632 (2017).
- [14] B. B. Brandt, C. Yannouleas, and U. Landman, Interatomic interaction effects on second-order momentum correlations and Hong-Ou-Mandel interference of double-well-trapped ultracold fermionic atoms, *Phys. Rev. A* **97**, 053601 (2018).
- [15] C. Yannouleas, B. B. Brandt, and U. Landman, Interference, spectral momentum correlations, entanglement, and Bell inequality for a trapped interacting ultracold atomic dimer: Analogies with biphoton interferometry, *Phys. Rev. A* **99**, 013616 (2019).
- [16] C. Yannouleas and U. Landman, Anyon optics with time-of-flight two-particle interference of double-well-trapped interacting ultracold atoms, *Phys. Rev. A* **100**, 013605 (2019).
- [17] S. Murmann, A. Bergschneider, V. M. Klinkhamer, G. Zürn, T. Lompe, and S. Jochim, Two Fermions in a Double Well: Exploring a Fundamental Building Block of the Hubbard Model, *Phys. Rev. Lett.* **114**, 080402 (2015).
- [18] D. Bouwmeester, J.-W. Pan, M. Daniell, H. Weinfurter, and A. Zeilinger, Observation of Three-Photon Greenberger-Horne-Zeilinger Entanglement, *Phys. Rev. Lett.* **82**, 1345 (1999).
- [19] W. Dür, G. Vidal, and J. I. Cirac, Three qubits can be entangled in two inequivalent ways, *Phys. Rev. A* **62**, 062314 (2000).
- [20] C. Yannouleas and U. Landman, Third-order momentum correlation interferometry maps for entangled quantal states of three singly trapped massive ultracold fermions, *Phys. Rev. A* **100**, 023618 (2019).
- [21] A. Gallemí, M. Guilleumas, J. Martorell, R. Mayol, A. Polls, and B. Juliá-Díaz, Fragmented condensation in Bose-Hubbard trimers with tunable tunnelling, *New J. Phys.* **17**, 073014 (2015).
- [22] D. Raventós, T. Graß, M. Lewenstein, and B. Juliá-Díaz, Cold bosons in optical lattices: A tutorial for exact diagonalization, *J. Phys. B: At. Mol. Opt. Phys.* **50**, 113001 (2017).
- [23] H. Shiba and P. A. Pincus, Thermodynamic properties of the one-dimensional half-filled-band Hubbard model, *Phys. Rev. B* **5**, 1966 (1972).
- [24] J. Callaway, D. P. Chen, and R. Tang, Ground-state and thermodynamic properties of the Hubbard model applied to small clusters, *Phys. Rev. B* **35**, 3705 (1987).
- [25] E. Dagotto, Correlated electrons in high-temperature superconductors, *Rev. Mod. Phys.* **66**, 763 (1994).
- [26] A. M. Kaufman, B. J. Lester, C. M. Reynolds, M. L. Wall, M. Foss-Feig, K. R. A. Hazzard, A. M. Rey, and C. A. Regal, Two-particle quantum interference in tunnel-coupled optical tweezers, *Science* **345**, 306 (2014).
- [27] A. M. Kaufman, M. C. Tichy, F. Mintert, A. M. Rey, and C. A. Regal, The Hong-Ou-Mandel effect with atoms, *Adv. At. Mol. Opt. Phys.* **67**, 377 (2018).
- [28] D. Peçak and T. Sowinski, Few strongly interacting ultracold fermions in one-dimensional traps of different shapes, *Phys. Rev. A* **94**, 042118 (2016); T. Plaßmann, S. I. Mistakidis, and P. Schmelcher, Quench dynamics of finite bosonic ensembles in optical lattices with spatially modulated interactions, *J. Phys. B: At. Mol. Opt. Phys.* **51**, 225001 (2018).
- [29] A. G. Volosniev, D. V. Fedorov, A. S. Jensen, N. T. Zinner, and M. Valiente, Multicomponent strongly interacting few-fermion systems in one dimension, *Few-Body Syst.* **55**, 839 (2014).
- [30] The algebraic scripts for the formulas presented in this paper can be obtained from the authors upon request.
- [31] In a finite system, there are no sharp phase transitions associated with symmetry breaking. Our solutions of the Hubbard trimer are exact (they do not break any symmetries of the Hamiltonian). Accordingly, we use here the terminology “signatures of emergent phase transitions.” This terminology is used in the literature of finite systems [see, e.g., T. Papenbrock and H. A. Weidenmüller, Effective field theory of emergent symmetry breaking in deformed atomic nuclei, *J. Phys. G: Nucl. Part. Phys.* **42**, 105103 (2015)] to indicate that symmetry breaking and the sharp phase transitions emerge gradually from the behavior of finite systems in the limit of $N \rightarrow \infty$. We choose here this terminology over an alternative one, namely “phase-crossover” that is used in some cases to discuss the broad phase-related changes in finite systems.
- [32] K. Sengupta and N. Dupuis, Mott-insulator-to-superfluid transition in the Bose-Hubbard model: A strong-coupling approach, *Phys. Rev. A* **71**, 033629 (2005).
- [33] J. K. Freericks, H. R. Krishnamurthy, Y. Kato, N. Kawashima, and N. Trivedi, Strong-coupling expansion for the momentum distribution of the Bose-Hubbard model with benchmarking against exact numerical results, *Phys. Rev. A* **79**, 053631 (2009).
- [34] T. Legero, T. Wilk, M. Hennrich, G. Rempe, and A. Kuhn, Quantum Beat of Two Single Photons, *Phys. Rev. Lett.* **93**, 070503 (2004).
- [35] T. Gerrits, F. Marsili, V. B. Verma, L. K. Shalm, M. Shaw, R. P. Mirin, and S. W. Nam, Spectral correlation measurements at the Hong-Ou-Mandel interference dip, *Phys. Rev. A* **91**, 013830 (2015).
- [36] R.-B. Jin, T. Gerrits, M. Fujiwara, R. Wakabayashi, T. Yamashita, S. Miki, H. Terai, R. Shimizu, M. Takeoka, and M. Sasaki, Spectrally resolved Hong-Ou-Mandel interference between independent photon sources, *Opt. Express* **23**, 28836 (2015).
- [37] X.-J. Wang, B. Jing, P.-F. Sun, C.-W. Yang, Y. Yu, V. Tamma, X.-H. Bao, and J.-W. Pan, Experimental Time-Resolved

- Interference with Multiple Photons of Different Colors, *Phys. Rev. Lett.* **121**, 080501 (2018).
- [38] V. V. Orre, E. A. Goldschmidt, V. Tamma, M. Hafezi, and S. Mittal, Interference of Multiple Temporally Distinguishable Photons Using Frequency-Resolved Detection, *Phys. Rev. Lett.* **123**, 123603 (2019).
- [39] M. Bonneau, W. J. Munro, K. Nemoto, and J. Schmiedmayer, Characterizing twin-particle entanglement in double-well potentials, *Phys. Rev. A* **98**, 033608 (2018).
- [40] S. Laibacher and V. Tamma, Symmetries and entanglement features of inner-mode-resolved correlations of interfering non-identical photons, *Phys. Rev. A* **98**, 053829 (2018).
- [41] C. K. Hong, Z. Y. Ou, and L. Mandel, Measurement of Subpicosecond Time Intervals Between Two Photons by Interference, *Phys. Rev. Lett.* **59**, 2044 (1987).
- [42] R. C. Liu, B. Odom, Y. Yamamoto, and S. Tarucha, Quantum interference in electron collision, *Nature (London)* **391**, 263 (1998).
- [43] T. Jonckheere, J. Rech, C. Wahl, and T. Martin, Electron and hole Hong-Ou-Mandel interferometry, *Phys. Rev. B* **86**, 125425 (2012).
- [44] E. Bocquillon, V. Freulon, J.-M. Berroir, P. Degiovanni, B. Plaçais, A. Cavanna, Y. Jin, and G. Fève, Coherence and indistinguishability of single electrons emitted by independent sources, *Science* **339**, 1054 (2013).
- [45] R. Lopes, A. Imanaliev, A. Aspect, M. Cheneau, D. Boiron, and C. I. Westbrook, Atomic Hong-Ou-Mandel experiment, *Nature (London)* **520**, 66 (2015).
- [46] See, e.g., Ref. [4] for a first experimental realization of such a TOF spectroscopy in the case of three trapped fully spin-polarized ultracold fermions.
- [47] S. Mährlein, J. von Zanthier, and G. S. Agarwal, Complete three photon Hong-Ou-Mandel interference at a three port device, *Opt. Express* **23**, 15833 (2015).
- [48] S. Agne, T. Kauten, J. Jin, E. Meyer-Scott, J. Z. Salvail, D. R. Hamel, K. J. Resch, G. Weihs, and T. Jennewein, Observation of Genuine Three-Photon Interference, *Phys. Rev. Lett.* **118**, 153602 (2017).
- [49] A. J. Menssen, A. E. Jones, B. J. Metcalf, C. Tichy, S. Barz, W. S. Kolthammer, and I. A. Walmsley, Distinguishability and Many-Particle Interference, *Phys. Rev. Lett.* **118**, 153603 (2017).
- [50] S. Aaronson and A. Arkhipov, The computational complexity of linear optics, *Theory Comput.* **9**, 143 (2013).
- [51] M. C. Tichy, Interference of identical particles from entanglement to boson sampling, *J. Phys. B: At. Mol. Opt. Phys.* **47**, 103001 (2014).
- [52] V. Tamma and S. Laibacher, Multiboson Correlation Interferometry with Arbitrary Single-Photon Pure States, *Phys. Rev. Lett.* **114**, 243601 (2015).
- [53] S. Laibacher and V. Tamma, From the Physics to the Computational Complexity of Multiboson Correlation Interference, *Phys. Rev. Lett.* **115**, 243605 (2015).
- [54] J. Carolan, J. D. A. Meinecke, P. J. Shadbolt, N. J. Russell, N. Ismail, K. Wörhoff, T. Rudolph, M. G. Thompson, J. L. O'Brien, J. C. F. Matthews, and A. Laing, On the experimental verification of quantum complexity in linear optics, *Nat. Photon.* **8**, 621 (2014).
- [55] M. Walschaers, Signatures of many-particle interference, *J. Phys. B: At. Mol. Opt.* **53**, 043001 (2020).
- [56] R. Zitko, SNEG: MATHEMATICA package for symbolic calculations with second-quantization-operator expressions, *Comput. Phys. Commun.* **182**, 2259 (2011).
- [57] MATHEMATICA, ver. 11.3 (Wolfram Research, Champaign, IL, 2018).
- [58] P.-O. Löwdin, Quantum theory of many-particle systems. I. Physical interpretations by means of density matrices, natural spin-orbitals, and convergence problems in the method of configurational interaction, *Phys. Rev.* **97**, 1474 (1955).
- [59] M. Alvioli, C. Cio degli Atti, L. P. Kaptari, C. B. Mezzetti, H. Morita, and S. Scopetta, Universality of nucleon-nucleon short-range correlations: Two-nucleon momentum distributions in few-body systems, *Phys. Rev. C* **85**, 021001(R) (2012).
- [60] C. A. Coulson, Momentum distribution in molecular systems: Part I. The single bond, *Proc. Cambridge Philos. Soc.* **37**, 55 (1941).
- [61] A. Szabo and N. S. Ostlund, *Modern Quantum Chemistry: Introduction to Advanced Electronic Structure Theory* (McGraw-Hill, New York, 1989).
- [62] https://en.wikipedia.org/wiki/Linear_combination_of_atomic_orbitals.
- [63] <https://mathworld.wolfram.com/FourierTransform.html>.
- [64] The multiwell confining spatial potential, used in conjunction with full configuration interaction (CI) microscopic calculations, has been extensively described in the Supplemental Information section of B. B. Brandt, C. Yannouleas, and U. Landman, Double-well ultracold-fermions computational microscopy: Wave-function anatomy of attractive-pairing and Wigner-molecule entanglement and natural orbitals, *Nano Lett.* **15**, 7105 (2015), and in C. Yannouleas, B. B. Brandt, and U. Landman, Ultracold few fermionic atoms in needle-shaped double wells: Spin chains and resonating spin clusters from microscopic Hamiltonians emulated via antiferromagnetic Heisenberg and t - J models, *New J. Phys.* **18**, 073018 (2016), as well as in Ying Li, C. Yannouleas, and U. Landman, Artificial quantum-dot helium molecules: Electronic spectra, spin structures, and Heisenberg clusters, *Phys. Rev. B* **80**, 045326 (2009).
- [65] By controlling the potential barrier and the distance between the wells, small overlaps of the localized atomic orbitals (which guarantee the validity of our augmented Hubbard model also in the range of small values of U) are purposefully and routinely realized in current experiments with optical tweezers; see, e.g., Refs. [17,26].
- [66] Extensive comparisons between the full CI momentum correlations and those from the augmented Hubbard model have been carried out in Refs. [13] and [14] for double, triple, and quadruple wells. Recently available experimentally measured momentum correlation maps [5] for double wells show an excellent agreement with the theoretical results in the full range $-\infty < U < \infty$.
- [67] See Supplemental Material at <http://link.aps.org/supplemental/10.1103/PhysRevA.101.063614> for more information on the numerical values for the coefficients \mathcal{C} , \mathcal{B} , and \mathcal{A} as a function of U/J .
- [68] T. Young, The Bakerian Lecture: Experiments and calculations relative to physical optics, *Philos. Trans. R. Soc. London A* **94**, 1 (1804).
- [69] S. Fölling, F. Gerbier, A. Widera, O. Mandel, T. Gericke, and I. Bloch, Spatial quantum noise interferometry in expanding ultracold atom clouds, *Nature (London)* **434**, 491 (2005).

- [70] M. P. A. Fisher, P. B. Weichman, G. Grinstein, and D. S. Fisher, Boson localization and the superfluid-insulator transition, *Phys. Rev. B* **40**, 546 (1989).
- [71] For a clear description of this contribution, see Eq. (11) and related text in Ref. [8].
- [72] C. Yannouleas and U. Landman (unpublished).
- [73] Z. Y. Ou, *Multi-photon Quantum Interference* (Springer, New York, 2007).
- [74] Y. H. Shih, *An Introduction to Quantum Optics: Photon and Biphoton Physics* (CRC Press, Boca Raton, FL, 2011).
- [75] X. Lu and Y. Yu, Finite-temperature effects on the number fluctuation of ultracold atoms across the superfluid-to-Mott-insulator transition, *Phys. Rev. A* **74**, 063615 (2006).
- [76] S. Jin, X. Guo, P. Peng, X. Chen, X. Li, and X. Zhou, Finite temperature phase transition in a cross-dimensional triangular lattice, *New J. Phys.* **21**, 073015 (2019).
- [77] N. Spagnolo, C. Vitelli, L. Aparo, P. Mataloni, F. Sciarrino, A. Crespi, R. Ramponi, and R. Osellame, Three-photon bosonic coalescence in an integrated tritter, *Nat. Commun.* **4**, 1606 (2013).
- [78] A tritter is a device of three parallel optical fibers that are brought closer at a point and then are separated again; see the schematic in Fig. 1(b) of Ref. [77] and in Fig. 5 of G. Weihs, M. Reck, H. Weinfurter, and A. Zeilinger, Two-photon interference in optical fiber multiports, *Phys. Rev. A* **54**, 893 (1996).
- [79] It also applies for the case of a few strongly entangled fermions [20].
- [80] J. V. Gomes, A. Perrin, M. Schellekens, D. Boiron, C. I. Westbrook, and M. Belsley, Theory for a Hanbury Brown–Twiss experiment with a ballistically expanding cloud of cold atoms, *Phys. Rev. A* **74**, 053607 (2006).
- [81] R. G. Dall, A. G. Manning, S. S. Hodgman, W. Rugway, K. V. Kheruntsyan, and A. G. Truscott, Ideal n -body correlations with massive particles, *Nat. Phys.* **9**, 341 (2013).
- [82] T. Schweigler, V. Kasper, S. Erne, I. Mazets, B. Rauer, F. Cataldini, T. Langen, T. Gasenzer, J. Berges, and J. Schmiedmayer, Experimental characterization of a quantum many-body system via higher-order correlations, *Nature (London)* **545**, 323 (2017).